FINAL REPORT

Theoretical and Experimental Studies of the Underlying Processes and Techniques of Low Pressure Measurement

REPORT R-286

APRIL, 1966

This work was supported in part by the Joint Services Electronics Program (U. S. Army, U. S. Navy, and U. S. Air Force) under Contract No. DA 28 043 AMC 00073(E), and in part by the National Aeronautics and Space Administration under NASA Research Grant NsG 376.

FINAL REPORT

Required under the terms of NASA Research Grant NsG 376

"Theoretical and Experimental Studies
of the Underlying Processes and Techniques
of Low Pressure Measurement"

Principal Investigator:

D. Alpert

Other personnel contributing to the work
reported under this grant include

D. Coad
T. Cooper
A. Dallos
J. L. deSegovia
D. A. Lee
R. N. Peacock
T. Piper
F. M. Propst
W. C. Schuemann
L. Simonelli
F. Steinrisser
G. Tibbetts
H. Tomaschke

TABLE OF CONTENTS

1. TOTAL AND PARTIAL PRESSURE GAUGES

1.1 The Suppressor (Schuemann) Gauge

1.1.1 Introduction. A type of ionization gauge called the photocurrent suppressor gauge has been developed at the Coordinated Science Laboratory during the past four years. This gauge is capable of effectively suppressing the photoelectric current (x-ray current) from the ion collector, thereby considerably extending the range of ionization-type gauges. Simple suppressor gauges have a limitation similar to the x-ray limit of the Bayard-Alpert gauge at 1×10^{-13} Torr. Slightly more complicated suppressor gauges probably would not be limited by an x-ray effect above 1×10^{-16} Torr, though this has not been experimentally verified. These gauges have a higher sensitivity than typical inverted gauges, are only slightly more complicated, and can use the same power supplies and electrometers.

1.1.2 Review of X-Ray Effects in Ionization Gauges. Readings of the Bayard-Alpert gauge,[1] the most widely used instrument for measuring pressure in ultrahigh vacuum systems, are not linear with pressure in the vicinity of 1×10^{-10} Torr and lower because of a photoelectron current from the collector. This current is due to collector bombardment by soft x-ray photons released at the grid when it is struck by the ionizing electrons. Metson[2] and Dalke-Schutze[3] have designed gauges

---

[1] R. T. Bayard and D. Alpert, Rev. Sci. Instr. 21, 571 (1950).

[2] G. H. Metson, Brit. J. Appl. Phys. 2, 46 (1951).

[3] W. E. Dalke and H. J. Schutze, 20th Annual Conf. on Physical Electronics, M.I.T., Cambridge, Mass., 26 March 1960.

which suppress this photoelectron current by the utilization of a fourth electrode placed between the ionization region and collector at such a potential as to prevent photoelectrons from leaving the collector. Their gauges are limited in the measurement of very low pressures by two factors: (1) low sensitivity and (2) a photoelectric current which flows from the suppressor electrode to the collector as the result of x-ray bombardment of the suppressor electrode.

Previous papers on the suppressor gauge being developed at CSL have described the first working model[4] and a later version, the model 19 gauge.[5] Redhead and Hobson[6] have described their version of the suppressor gauge and developed methods for modulating the ion current in order to make pressure measurements in the low 10^{-15} Torr region possible. This section enumerates the important considerations in the design of suppressor gauges and describes the model 46 suppressor gauge which represents a considerable improvement mechanically and economically over previous suppressor gauges.

1.1.3 General Principles of Suppressor Gauges. The suppressor gauge consists of two regions separated by a shield as shown in Fig. 1.1. The filament and grid in the ionization region are similar in arrangement to those of a Bayard-Alpert gauge except for the addition of a small grid

---

[4] W. C. Schuemann, Transactions of the Ninth National Vacuum Symposium (The Macmillan Company, New York, 1962), p. 428.

[5] W. C. Schuemann, Rev. Sci. Instr. 34, 700 (1963).

[6] P. A. Redhead and J. P. Hobson, Fundamental Problems of Low Pressure Measurement Conference, Teddington (Middlesex) England (September, 1964).

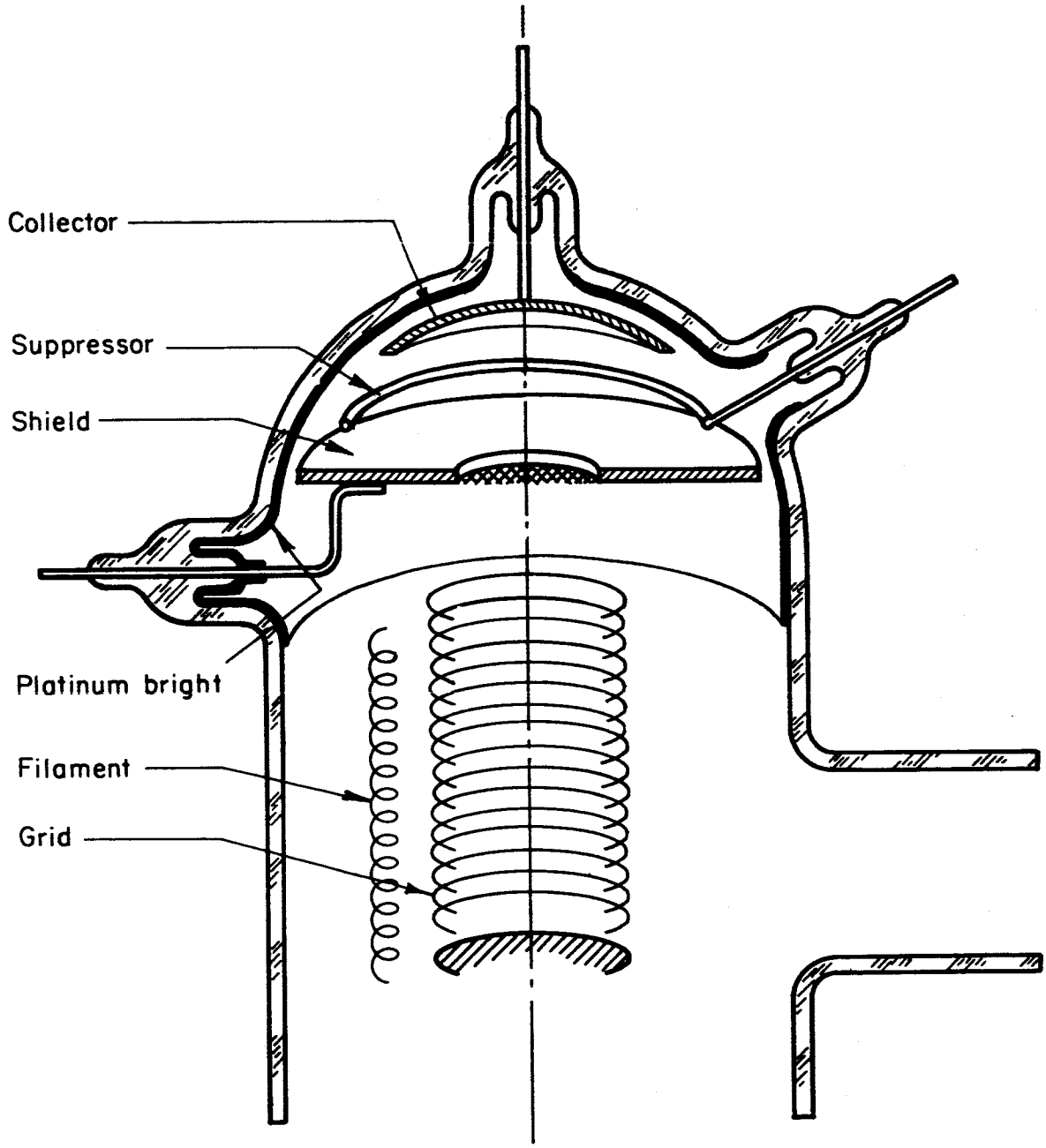

Fig. 1.1. Scale Cross-Section of the Model 46 Suppressor Gauge.

cap which closes the bottom of the grid. These electrodes are at their usual potentials of +50 and +200 volts, respectively. The shield is at ground potential and has three functions: (1) it shields the suppressor ring, which creates the retarding field for photoelectrons, from all x-rays coming directly from the grid region. Thus it prevents the creation of a large photoelectric current which otherwise could flow from the suppressor to the collector. (2) Together with the grid, the shield forms an electrostatic lens which both accelerates and focuses the ions to the collector. (3) The shield, along with the platinum bright coating on the glass, protects the ion-drift region and collector against variations in wall potential which would change the sensitivity of the gauge, or reduce its ability to suppress the photocurrents, and against pickup by the collector of electrostatic noise from the ionization region, or from outside the gauge. Operation of the gauge is accomplished using standard ionization gauge supplies plus a small battery or high voltage supply for the suppressor voltage.

1.1.4 Design Considerations for Suppressor Gauges.

1.1.4.1 Sensitivity. In a gauge intended for measuring very low pressures, it is desirable to have as high an ion current as possible while not introducing either excessive pumping speeds or ionizing electron currents. Considerations such as grid volume, grid geometry, and the collection efficiency for ions therefore become important. Tests involving the geometry shown in Fig. 1.1 showed that 50% of the ions were accelerated into a 1/4-inch circle at the center of the shield and that all of the ions were focused into a 3/8-inch

circle. After passing through the shield, the outer edges of the beam diverge rapidly, but 50% of the total ion current will still be captured inside of a 5/16-inch circle several grid diameters away from the grid, indicating a rather good collimation for half of the ions coming from the grid. As will be shown later, the rather good collimation of half of the ion current makes possible the design of a suppressor gauge which would probably be able to measure much lower pressures than the gauge being described here.

1.1.4.2 Primary and Reflected X-Ray Effects. We will define the ejection of photoelectrons from the collector by photons coming directly from the ionization region as the primary x-ray effect. The ejection of photoelectrons from the suppressor ring by photons, reflected from the collector and parts of the shield and which subsequently impact on the suppressor ring, will be referred to as the reflected x-ray effect. The primary photoelectron current from the collector, when the suppressor is grounded (no suppression), corresponds to a pressure of 7×10^{-11} Torr for the gauge in Fig. 1.1. This unsuppressed x-ray current varies with the size of the hole in the shield, distance of the collector from the grid, distribution of electron impacts on the grid, etc. The reflected photoelectric current, with the suppressor negative, corresponds to about 1×10^{-13} Torr. This current varies with the size of the hole in the shield; the size, shape, and distance from the shield of the collector; and the size, shape, and position of the suppressor ring. In most designs the surface area of the suppressor is the most important parameter. The primary x-ray effect

will result in a negative current from the collector, adding to the positive ion current flowing to the collector, while the reflected x-ray effect will result in a negative current to the collector, subtracting from the ion current.

The major feature of this type of gauge is that the primary x-ray current can be suppressed to a value small compared to the ion current by means of a retarding field in front of the collector. The effectiveness of the suppression is a function of the size, shape, and distance from the shield of the collector; of the size, shape, position, and voltage of the suppressor ring; and of any electric fields which either penetrate into the collector region from the grid region or originate on the glass walls of the collector region due to charging of the glass. In the model 46 gauge, the opening in the shield is covered with a fine mesh to isolate the collector region from fields originating in the grid region, and all glass surfaces in the collector region are covered with platinum bright which is grounded to the shield, thereby eliminating the effects of any stray electric fields. It is also necessary to realize that the suppression field is defocusing for ions, and that the collector must be large enough to capture all ions even at the highest suppressor voltages.

The majority of photoelectrons from the collector probably have energies of less than 10 volts. The number of photoelectrons which have higher energies decreases rapidly with increasing energy, though the exact distribution is not known. Since it is not necessary to suppress all of the photoelectric current but only a sufficient fraction

such that the photoelectric current remaining is small compared to the ion current being measured, it should be obvious that the suppression field and hence the suppressor voltage necessary for sufficient suppression will become larger as the pressure and hence the ion current is reduced. For the model 46 suppressor gauge, if it is specified that the photoelectric current must be less than 5% of the ion current at a given pressure, this voltage is about -1000 V at 1×10^{-13} Torr, -500 V at 1×10^{-12} Torr, and -200 V at 1×10^{-11} Torr. Of course, the voltage does not have to be varied with pressure but merely chosen sufficiently large to guarantee suppression at the lowest anticipated pressures. About -600 V has been found to be optimum.

1.1.4.3 Oscillations in Suppressor Gauges. The model 19 suppressor gauge, in use at our laboratory for several years, showed a strong tendency toward oscillation, characterized by a negative collector current when the pressure was below 10^{-11} Torr. The oscillation was very persistent, was enhanced by making the suppressor voltage more negative, and showed time constants for the growth or decay of the oscillation after the suppressor voltage was changed. This strange behavior was found to be due to wall potentials in the grid region going negative with the suppressor voltage, thereby making the potential distribution in the grid region very favorable for electron cloud oscillations. The train of events started at a small exposed wire lead for the suppressor potential. In the model 19 gauge, the exposed lead is adjacent to the grid and hence was bombarded by soft x-rays. The majority

of the resulting photoelectric current, of about 1×10^{-11} A, from the lead went to the glass walls of the gauge where it was neutralized by ions made outside the grid. When the pressure fell into the low 10^{-11} Torr region, the ion current became smaller than the photoelectric current, and the glass walls were then driven negative to near the potential of the suppressor. This allowed strong electron cloud oscillations to exist which were able to give large numbers of electrons enough energy to penetrate through the shield opening and the suppression field to the collector. Since the glass walls went negative with the suppressor voltage, the oscillations became stronger as the suppression was increased. This explains why the electrons coming from the grid region could not be prevented from reaching the collector by making the suppressor more negative. Obviously, the solution to this problem is to place the suppressor lead above the shield as shown in Fig. 1.1, thereby removing it from the grid region.

As a side experiment it was observed that the wall potentials in Bayard-Alpert gauges at 10^{-10} Torr and lower would vary anywhere from 10 volts negative with respect to the filament voltage, to several volts negative with respect to the collector voltage. In the latter case, the Bayard-Alpert gauge collector current went negative. Changes in residual magnetic field, pressure, temperature, and electron emission current sometimes caused large immediate variations in the wall potential. Negative collector currents were always eliminated by making contact with the metallic film on the glass wall and making it positive with respect to the collector.

1.1.4.4 Data from Suppressor Gauges. Two types of data (other than pressure measurements) can be obtained from a suppressor gauge. The first is illustrated in Fig. 1.2. This figure shows curves of collector current versus suppressor voltage. The data were taken at 10 mA emission current and each individual curve represents data taken at a constant pressure. These curves illustrate that as the suppressor voltage is increased, the photoelectric component of the collector current is gradually suppressed until the collector current becomes constant. This final constant collector current is the ion current to the collector. As described earlier, it can be seen that lower pressures require higher suppressor voltages for complete suppression.

The second type of data is illustrated in Fig. 1.3. This figure shows curves of collector current versus the voltage between the grid and filament. All of these curves were taken at the same pressure of 1.3×10^{-11} Torr and at 10 mA emission current. Each individual curve corresponds to data taken at a constant suppressor voltage. With the suppressor voltage at zero we see that the common x-ray curve, of the type familiar from measurements on Bayard-Alpert gauges, is obtained. For very large suppressor voltages we can eliminate the photoelectric current from the collector and are left with something resembling a probability of ionization curve. For intermediate values of suppressor voltages, we see that the suppression of the photocurrent can be maintained until the energy of the x-rays and, hence, the energy of the photoelectrons becomes sufficiently large that the photoelectrons are able to penetrate the suppression field and escape from the

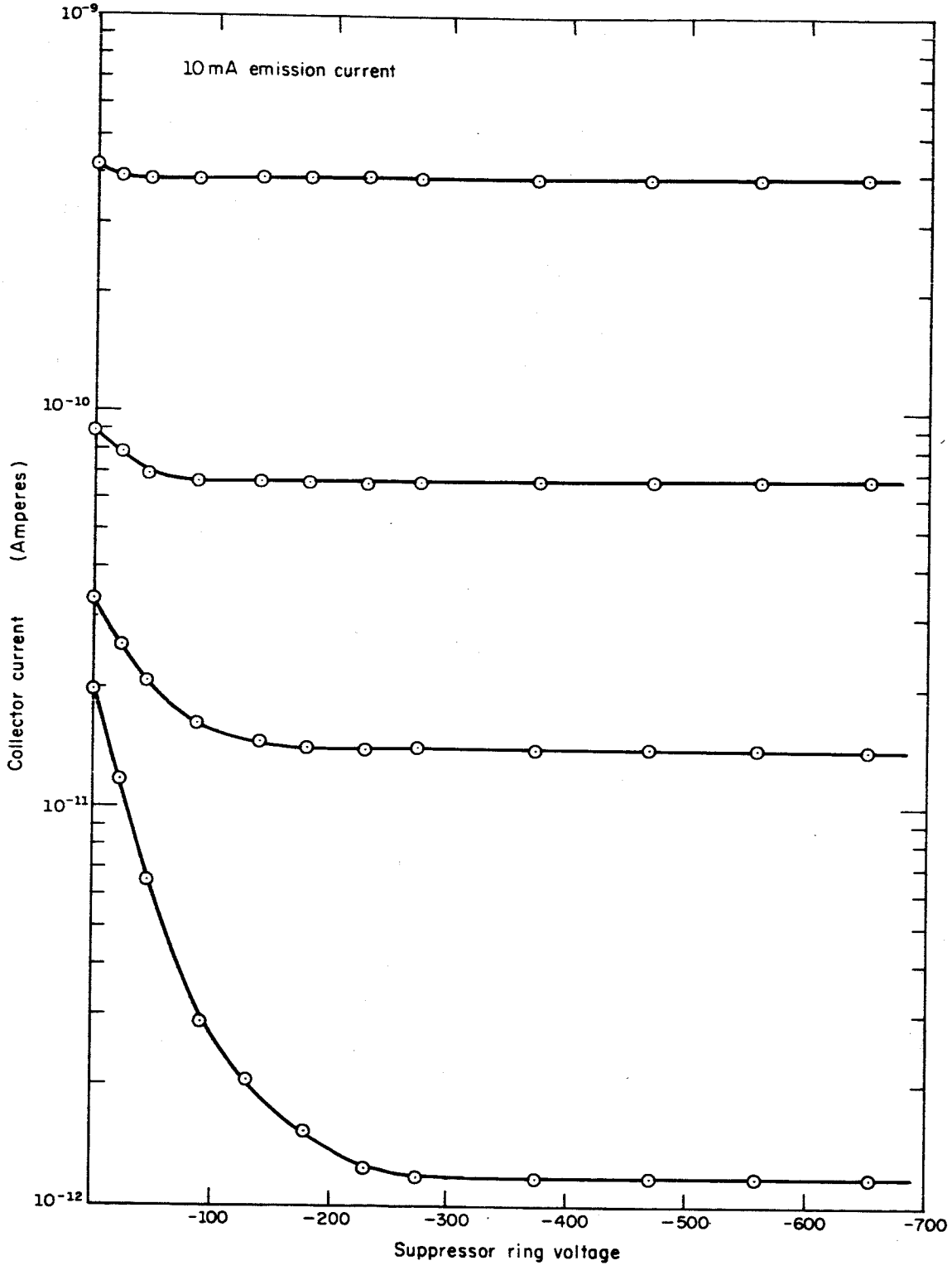

Fig. 1.2. Collector Current versus Suppressor Voltage, at Several Pressures, for the Model 46 Gauge.

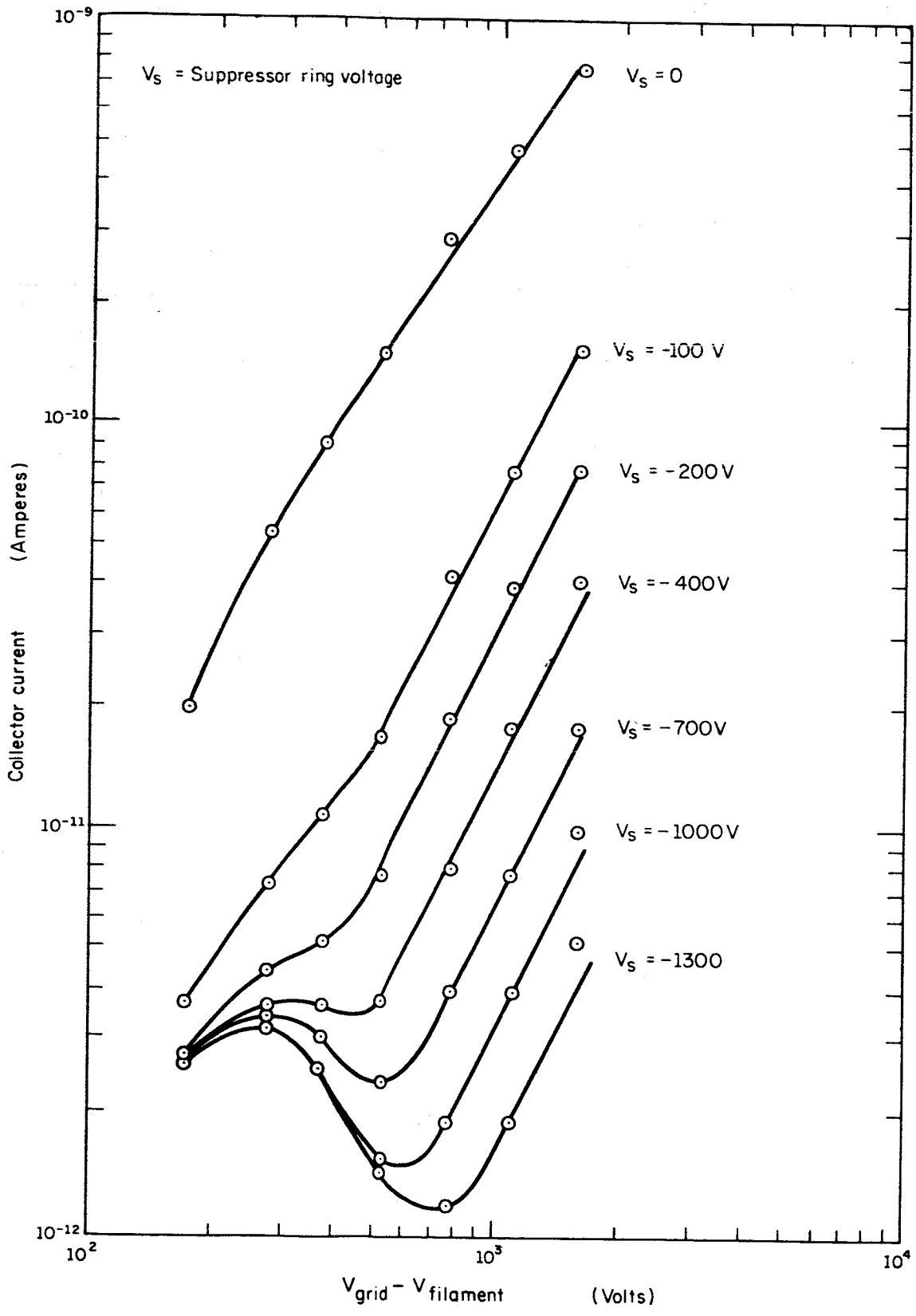

Fig. 1.3. Collector Current versus Grid Voltage, at Several Suppressor Voltages, for the Model 46 Gauge.

collector in sufficiently large numbers to cause the collector current to increase rapidly with grid voltage.

The type of curve shown in Fig. 1.2 is easy to obtain and is an excellent way of determining if the gauge and its associated electronics are performing properly. This data cannot be obtained if strong Barkhausen oscillations exist in the gauge. When they exist it is possible for electrons from the grid region to reach the collector when the suppressor voltage is less than about 100 volts. This is not normally a problem since the suppressor is always more negative than this in normal operation.

The main value of the curves shown in Fig. 1.3 is that for each suppressor voltage, the curve can be extrapolated back to normal grid voltage to determine at what pressure that particular suppressor voltage will begin to exhibit marginal suppression characteristics.

1.1.5 Model 46 Design Features. The gauge shown in Fig. 1.1 was evolved after it was decided to make a suppressor gauge that was easier and cheaper to manufacture than the model 19 gauge and which would eliminate the oscillation problem. The gauge in final form is simply a modification of a commercially available Bayard-Alpert gauge. The sensitivity of the gauge for N_2 is 27 $Torr^{-1}$. The low pressure limit of the gauge is in the low 10^{-13} Torr region. The high pressure linearity is probably due to the lack of any high ion space charge such as exists in an inverted gauge around the collector at high pressures. This gauge also has the desirable feature that the collector is completely

surrounded by a grounded conductor which considerably simplifies the ion current measuring problems due to the elimination of electrostatic noise.

1.1.5.1 Model 46 Construction Outline. Construction starts by opening up a commercial Bayard-Alpert gauge near the press. The original collector is removed from the envelope and two additional openings are made in the top of the envelope--one for the suppressor and one for the shield. The platinum bright coating is then painted on and fired to 650°C for a few minutes. The collector and suppressor ring are then inserted into the envelope and their feedthroughs sealed in. The shield with a small wire finger for making contact with the platinum bright is then inserted and its feedthrough sealed in. The bottom of the gauge's grid is then closed by spotwelding a small circular grid to the grid's four support wires. The tube is then sealed back together and is ready for service.

1.1.5.2 Operation of Suppressor Gauges. In normal operation, the shield is always grounded, the filament is at approximately +50 V and the grid is at approximately +200 V. During outgassing of the grid, the shield is left grounded and the pressure in the gauge can be monitored if the suppressor voltage is high enough to keep electrons from reaching the collector. Normal operation in our laboratories is at 3.7 mA emission current while an outgas is performed at between 100 and 150 watts. It has never been found necessary to outgas either the shield or collector to reach low pressures. They are

apparently sufficiently outgassed by thermal radiation during the grid outgas.

Tesla coils used for leak checking should not be touched to the shield feedthrough as the connection between the shield and platinum bright may be burned away.

If oscillations are present in the tube, the collector current may become negative if the suppressor is near ground due to electrons gaining enough energy in the grid region to go through the hole in the shield and impact on the collector. At normal suppressor voltages, this effect is never seen, becuase the electrons are unable to penetrate through the retarding field formed by the suppressor.

1.1.6 Outline for a Super Suppressor Gauge. In a gauge as outlined above, the reflected x-ray limit is approximately one thousandth of the unsuppressed primary x-ray limit. As long as the reflected photons reach the suppressor after one reflection, the lower limit of the gauge cannot be improved without adversely affecting one of the other characteristics of the gauge. Any geometry which would lower the reflected x-ray limit would also have to incorporate improved primary x-ray current suppression in order to keep the suppressor voltage within reason at lower pressures. The gauge shown in Fig. 1.4 satisfies both conditions, though the sensitivity will be reduced to 5 $Torr^{-1}$. By thinking about all the possible paths photons from the grid could follow, it will be seen that the only place on the suppressor where a photon can impact after one reflection is on the half of the suppressor near the shield. Any resulting photoelectron can only go the the shield and

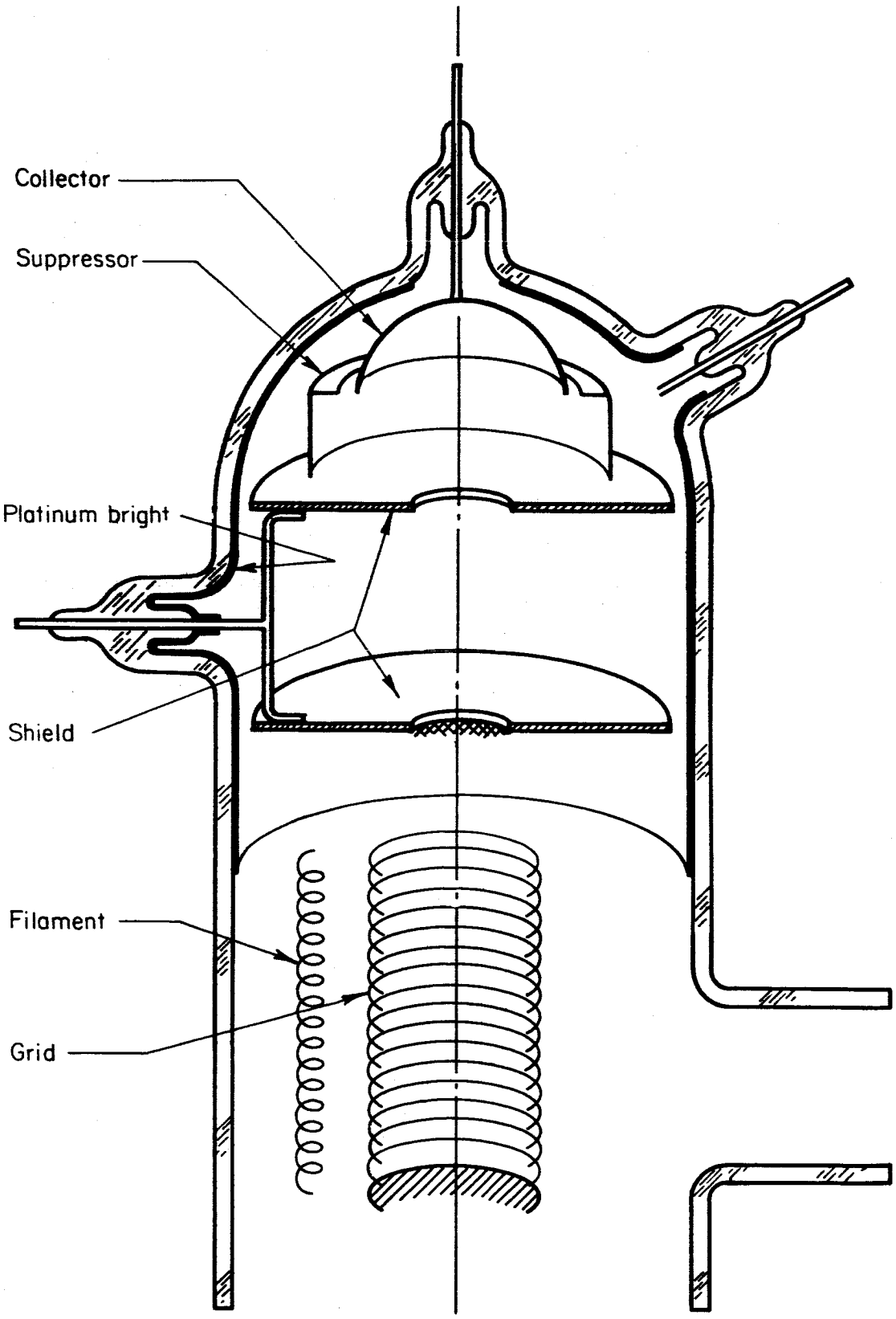

Fig. 1.4. Scale Cross-Section of the Model 45 Suppressor Gauge.

therefore never affects the collector current. The half of the suppressor near the collector can only be struck by photons after two reflections and therefore the reflected x-ray current, which can reach the collector in this case, should be approximately one millionth of the unsuppressed primary x-ray current. It should also be noted that the suppressor in this geometry is much larger than in the model 46 gauge and hence able to exercise considerably more control over the primary x-ray current. Several gauges of this type have been built and their characteristics are better than simpler suppressor gauges. At the present time our laboratory is unable to measure their ultimate x-ray limitation and has no plans to develop this version of the gauge.

1.1.7 Detailed Construction Information for the Model 46 Suppressor Gauge.

The model 46 suppressor gauges made at CSL have been converted from Westinghouse type 5966 Bayard-Alpert gauges and are shown in Fig. 1.5. These tubes are opened by our glassblower at the base of the tube where the press was originally sealed in. The press is then removed and the opening at the lower end of the envelope is widened to make it possible to insert the shield later. The original collector is then removed from the envelope and a short 12 mm glass tube glassed on to make it possible to install the collector feedthrough later without heating the main envelope. At a point 45° down and another at 90° down from the collector, holes are blown and additional short 12 mm glass tubes are added to take the suppressor and shield feedthroughs. At this time we usually change the pumping lead from 1/2 inch to 1 inch. A coating of platinum bright

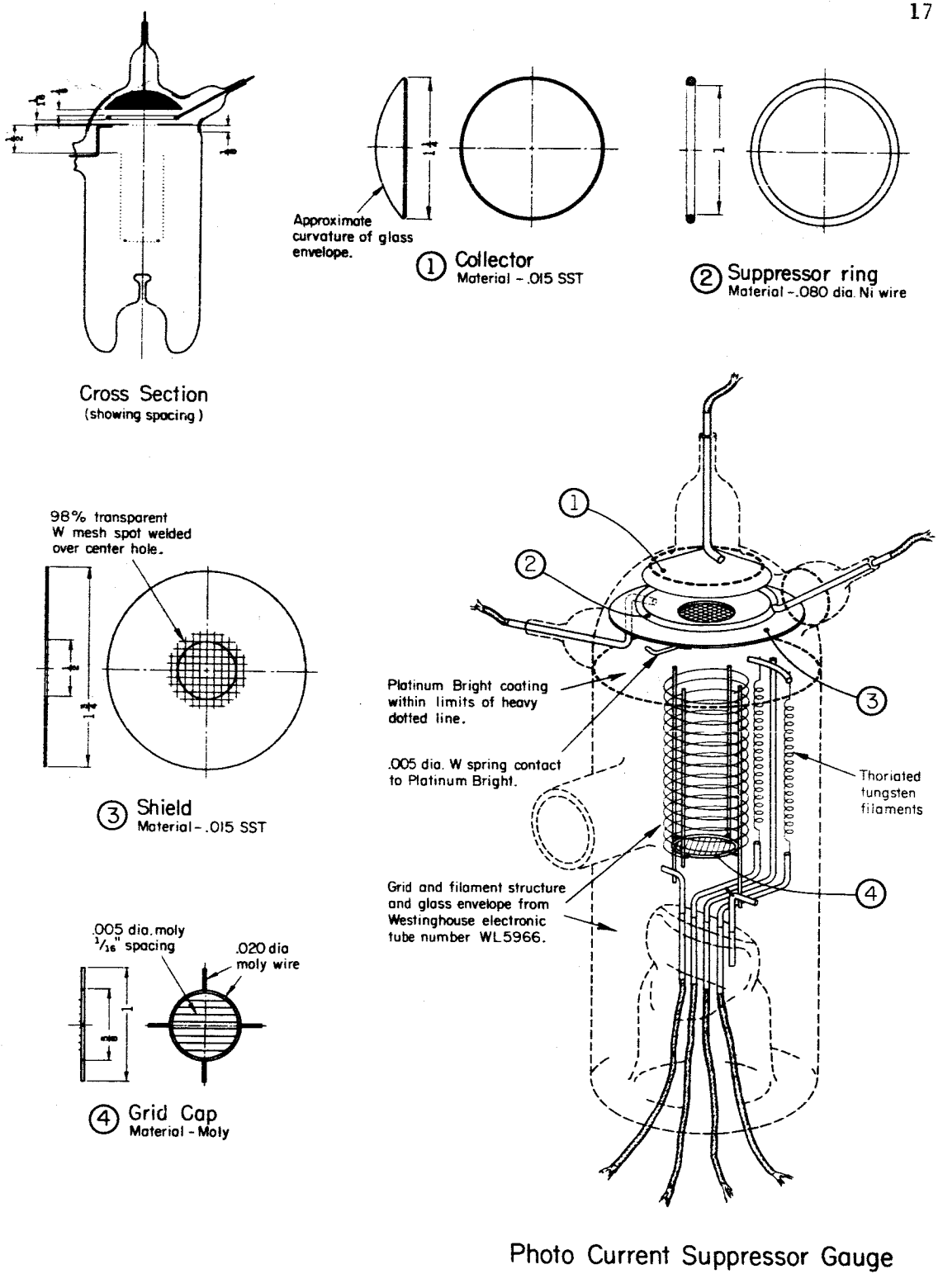

Fig. 1.5. Assembly Drawing of Model 46 Photo Current Suppressor Gauge.

is then painted on the inside of the hemisphere, which forms the end of the envelope, and 1/4 inch into the hole which will hold the suppressor. The coating should go under the edge of the collector but no closer to the collector lead than necessary to minimize any possibility of a leakage resistance between the platinum bright and the collector. The envelope is then annealed at 650°C which also fires the platinum coating. This unusually high annealing temperature is necessary in order to prevent the platinum coating from subsequently being lifted off the glass by condensed water vapor during glass blowing.

The collector is made from a disc of .010-inch stainless sheet 1-3/8 inch in diameter. It is made concave by pressing it into a lead block with a formed aluminum bar. The suppressor ring is a .080-inch nickel wire formed into a 1 inch I.D. circle. The shield is a 1-3/4 inch disc of .015-inch stainless sheet with a 1/2-inch hole in the center. Across the hole is spot-welded a 98% transparent woven tungsten mesh. On the outer perimeter of the shield, a 3/4-inch piece of .005 tungsten wire is spotwelded and bent in such a way as to make a light contact with the platinum bright coating on the envelope when the shield is installed. The feedthroughs for the collector, suppressor, and shield are standard .040-inch nickel to .030-inch tungsten to kool-grid wire type. The feedthroughs are appropriately formed and spotwelded to each piece.

An aluminum bar has been machined which fits loosely into the envelope, its top resting against the hemispherical end, which holds the collector in position for sealing in its feedthrough. A second aluminum

bar, which rests against the collector, positions the suppressor for sealing in its feedthrough. The collector has a 1/16-inch gap between it and the envelope and the top of the suppressor is 1/8 inch from the plane defined by the edge of the collector. The shield is then installed and positioned by the flat end of another machined aluminum bar a distance of 1/16 inch from the lower edge of the suppressor by a small pin which extends from the bar through the mesh to touch the collector. This completes the work on the envelope.

The circular grid is constructed of a .020-inch molybdenum wire circle with a 5/8-inch O.D. Across this are spotted .005-inch molybdenum wires on 1/16-inch spacings. Then, four .020-inch molybdenum wires are weld 90^{o} apart on the ring which extend out radially for 3/16 inch. This ring is then welded to the four support wires on the 5966 grid just at the lower end of the grid winding. The reason why all four support wires are tied together is to prevent the unsupported two from warping the grid out of shape during a hard outgassing. If this happened, then the x-ray characteristics or sensitivity of the gauge might change. Some 5966 grid support wires extend above the upper end of the grid winding a considerable distance, and they should be clipped off close to the winding. All that remains to be done is to position the grid 1/2 inch from the shield, center the grid on the hole in the shield, and close up the envelope.

1.1.8 Summary and Conclusions. A relatively simple ionization gauge for measuring down to 10^{-13} Torr has been developed. The gauge has been used successfully by several experimenters both in CSL and other

laboratories in the low 10^{-12} Torr region. Its cost in quantity would be little more than a standard inverted gauge while it can measure pressures hundreds of times lower. Because of the compatability of existing ion gauge supplies, electrometers, and measurement techniques, it is believed that the suppressor gauge offers the most promise for making it possible for vacuum research people, the vast majority of whom now use Bayard-Alpert gauges, to develop the know-how for reliably obtaining pressures in the 10^{-11} and 10^{-12} Torr region. The results of Section 1.1.4.1 (Sensitivity) indicate that the ion source used in this suppressor gauge could be applied to other instruments, such as mass spectrometers, or to still other types of gauges.

1.2 Modification of the Bayard-Alpert Gauge by the Addition of a Second Collector

With the development of the inverted ionization gauge by R. T. Bayard and D. Alpert[1] the production of low pressures was so stimulated that pressures of the order of 10^{-10} Torr are commonplace today.[7,8] Further advances in attaining even lower pressures have been hampered by the lack of a simply constructed gauge which is capable of reading pressures below the usually accepted x-ray limit of the Bayard-Alpert gauge. This section describes a modification of the inverted gauge in which the effective x-ray limit has been substantially reduced.

In this modification, a second collector has been added to the gauge and is biased at a potential below that of the first collector (see Fig. 1.6). With a bias of 60 V the ion current from the biased collector was found to be twice that of the unbiased collector. On the other hand, the x-ray currents from these collectors are approximately equal due to their similar construction and symmetric placement of the collectors within the gauge. Thus, if the collector currents are subtracted, the x-ray currents nearly cancel, and the net current is to first order due only to ions. Since the ion current to the biased collector is approximately twice that to the unbiased electrode, the difference current corresponds to that of a gauge with a sensitivity one-third that of a standard gauge, but with a greatly reduced x-ray current.

---

[7] D. Alpert, "Production and Measurement of Ultrahigh Vacuum," Handbook of Physics, ed. by S. Flugge (Springer-Verlag, Berlin, 1958), p. 609.

[8] H. A. Steinherz and P. Redhead, Sci. Am. 206, 78 (1962).

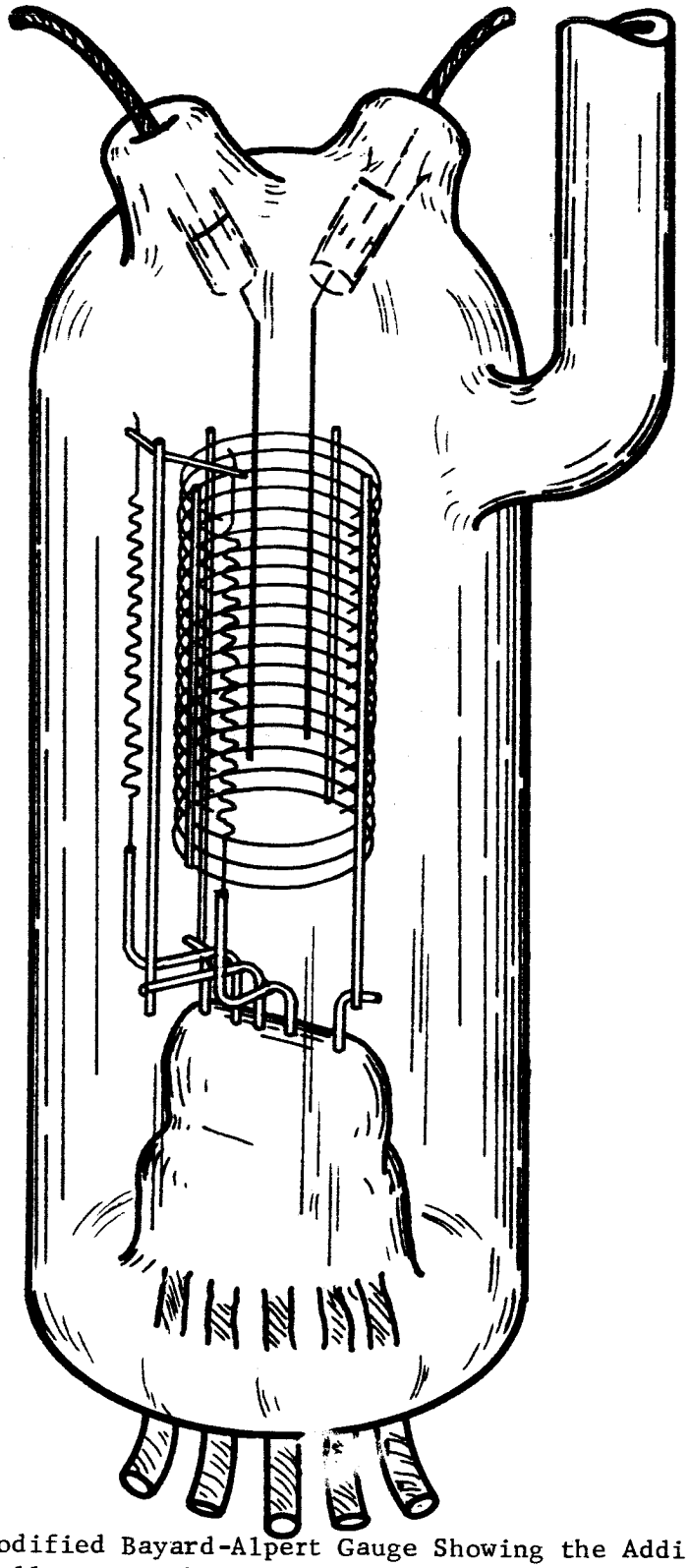

Fig. 1.6. Modified Bayard-Alpert Gauge Showing the Addition of a Second Collector. The second collector is used to cancel the x-ray component of the current.

A modified gauge was constructed by a simple alteration of a commercial version of the Bayard-Alpert gauge. The bias voltage typically used is 60 V, though this is not critical. The design of the biasing circuit is, however, quite important, since leakage currents can easily be as large as the ion currents to be measured. However, it has been found that, with the proper use of guard-ring potentials on the gauge as well as on the biasing device, the leakage currents may be reduced to tolerable values. The use of low noise coaxial cable was also found to be necessary. A Keithley differential electrometer (model 603) is ideally suited to perform the subtraction of the two collector currents.

The modified gauge was tested on an ultrahigh vacuum system capable of attaining gauge readings corresponding to a few times 10^{-11} Torr. In order to ascertain the effective x-ray limit, the net current was measured as a function of the energy of the ionizing electrons. Figure 1.7 indicates the results of two typical runs. Curve (1) was obtained by biasing one collector, while curve (2) was obtained by interchanging the electrometer leads and thus biasing the second collector. The small remaining contribution of the x-ray current is evidenced by the slowly increasing tail in curve (1) and the slowly decreasing tail in curve (2). (The subtraction process causes the change in sign of the contribution of the x-ray current upon interchanging the leads.) Since the contributions are of opposite sign, the x-ray effect can be further reduced by the summation of curves (1) and (2). Curve (3) is this sum and is characteristic in shape of an ionization probability curve for electron energies up to 400 eV.

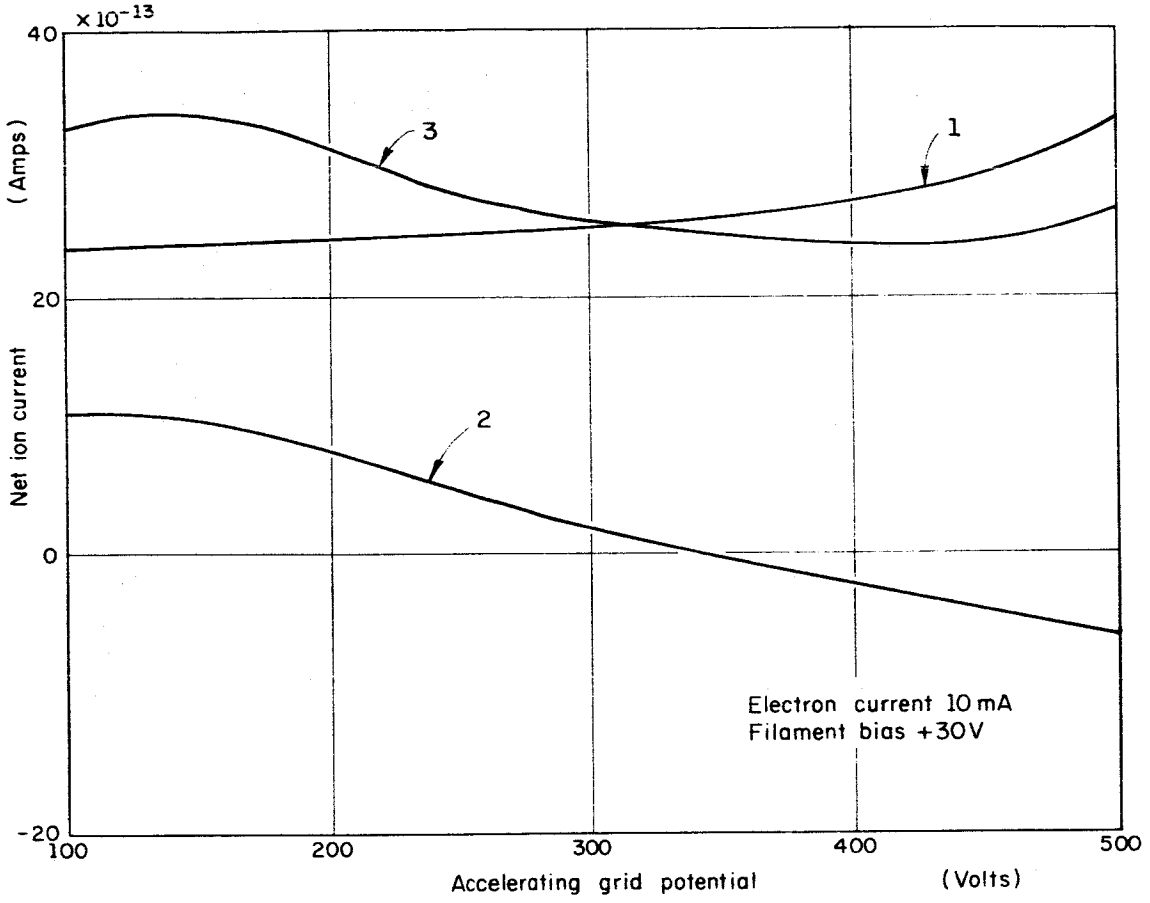

Fig. 1.7. X-Ray Current Characteristics of the Modified Gauge.

The insertion of the second collector allows this gauge to be used in the Redhead mode of operation; that is, the second collector may be used to modulate ion current using an ac voltage.[9] The x-ray limit as measured in this mode of operation is approximately the same as that observed in the differential mode. However, the differential mode of operation is free of troublesome transients introduced in switching or modulation. Furthermore, the differential mode provides continuous pressure readings with a response time characteristic of the electrometer (a few seconds), rather than some multiple of the switching time (approximately 30 sec).

The modified gauge has an effective x-ray limit at least one, and possibly two, orders of magnitude below that of a standard inverted ionization gauge. Since the gauge is a simple modification of the original Bayard-Alpert design, it can be operated with standard power supplies. The ultimate pressure measurable with the modified gauge is limited by the quality of the differential microammeter and by the ability of the experimenter to eliminate stray dc leakage currents. Since quality differential microammeters are available commercially, this gauge represents an attractive solution to the problem of reading pressures into the 10^{-12} Torr pressure region.

---

[9] P. Redhead, Rev. Sci. Instr. 31, 343 (1960).

1.3 A Simple High-Sensitivity Mass Spectrometer

The additional information about system conditions that can be obtained with the help of a mass spectrometer made it increasingly obvious that a useful addition to vacuum instrumentation would be a relatively inexpensive, easy to operate mass spectrometer which could be placed on any vacuum station much as Bayard-Alpert gauges are now applied. Such a device should preferably have a sensitivity of 10^{-1} amps/Torr without an electron multiplier at the output.

Toward the above end a type of mass spectrometer utilizing a magnetic field was investigated theoretically and one model of such an instrument was tested briefly.

In a mass spectrometer utilizing a magnetic field where a high sensitivity without an electron multiplier is desired it becomes necessary to eliminate fine slits and small cylindrical beams of electrons (magnetic deflection and omegatron mass spectrometers, respectively). The fine slits reduce the transmitted ion beam, and fine beams of electrons suffer from large space charge problems at milliampere-sized currents. The mass spectrometers briefly described here are a partial solution to the above problems in that a sheet beam of electrons is used and only one slit for ions is required. The slit is at the ion collector and has a negligible effect on sensitivity. Two forms of the instrument are possible. The more complicated one gives higher resolution while the less complicated one simplifies the electron space charge neutralization problem.

The more complicated instrument is shown in the first schematic (Fig. 1.8). A sheet-beam of electrons (shown by the x'ed line), perpendicular to the paper, ionizes molecules which are accelerated in the crossed E and B fields toward the grid. The path of each individual ion is a cycloid. Upon passing through the grid the trajectory of the ion becomes circular and finally passes through the slit to the collector. It can be shown that good focusing can be obtained from such an instrument.

The less complicated instrument is shown in the second schematic (Fig. 1.9). Again the x'ed line represents the sheet of electrons. The ions produced within the beam are accelerated in the crossed $\vec{E}$ and $\vec{B}$ fields. At the point where the ion has reached its maximum distance from the plane of the electron beam, there exists a collector. Due to the nature of the ions' cycloidal path at this point, all ions change their x coordinate very little for a rather large change in their y coordinate. This allows ions formed in all parts of the electron beam to be approximately focused onto the collector.

The instrument built was of the form shown in Fig. 1.8 and was operated in a magnetic field supplied by a permanent magnet. It had a sensitivity of 10^{-2} amps/Torr and a resolution of about 10. The expected resolution was 30; the lack of sensitivity was attributed to the slit passing only a fraction of the ions through to the collector due to poor ion focusing. The resolution did not change with electron current, so it is assumed that the non-uniform magnetic field was primarily responsible for the loss in resolution. The final instrument turned out to be sufficiently complicated so that it offered little more in economy or

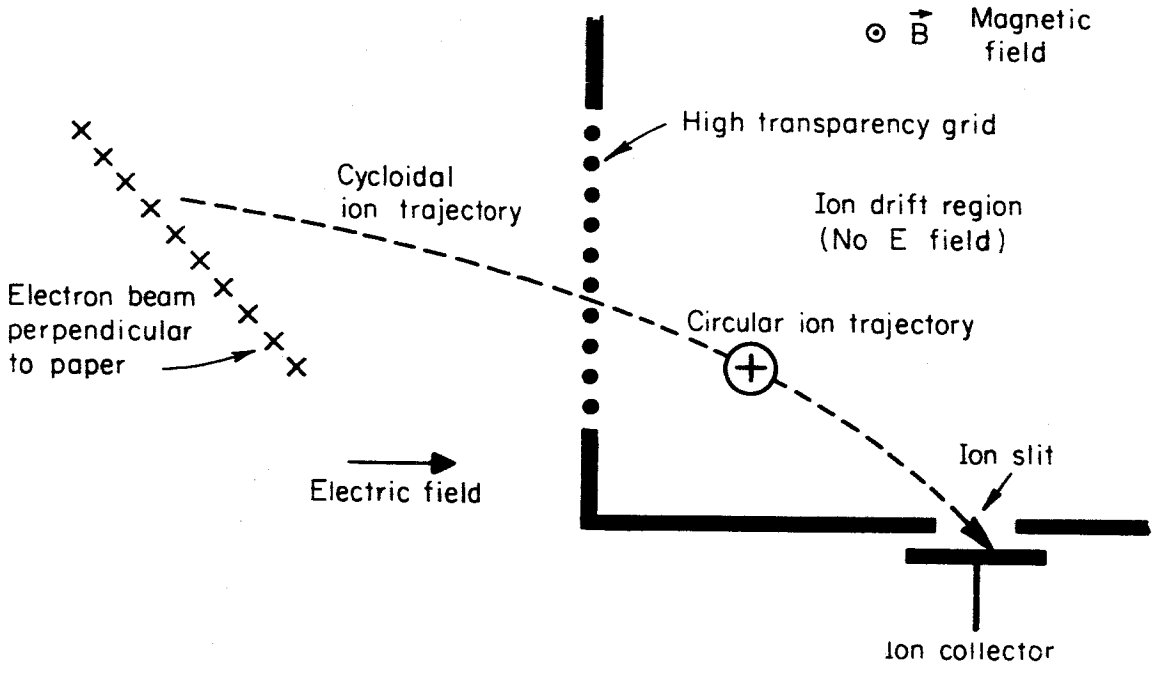

Fig. 1.8. Schematic of High Sensitivity, High Resolution Mass Spectrometer.

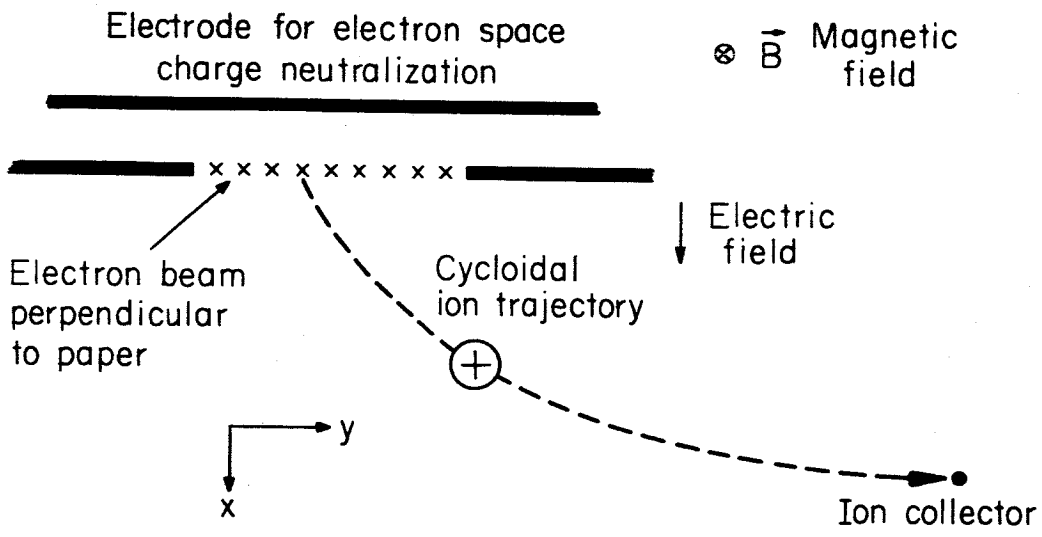

Fig. 1.9. Schematic of a Simple High-Sensitivity Mass Spectrometer.

performance over normal deflection-type mass spectrometers. A number of reasonably simple residual gas analyses have appeared on the market recently. One, produced by Varian Associates, offers high current sensitivity combined with moderate resolution to mass 70. It therefore has been decided to discontinue work on the instruments described in this section.

1.4 Effects of Electron-Surface Interaction in Ionization Gauges, Including O_2 to CO Conversion.

1.4.1 Introduction. In 1962, several experimenters reported an anomalous behavior of ionization gauges which was characterized by a departure from proportionality between the ion collector current and the electron current to the grid. Since this behavior may result in serious errors in pressure measurement, particularly when gauges are operated at low grid currents, the discovery and interpretation of the effect is of major significance in the field of ultrahigh vacuum. The effect was reported by Ackley, Lothrop and Wheeler[10] in a paper given at the 1962 Vacuum Symposium. They demonstrated that the anomalous readings were related to the condition of the grid surface and that the effect could be greatly reduced either by electron bombardment of the grid or by operating the gauge at relatively high electron currents ($I_g > 3$ mA). Redhead[11] independently reported a similar effect and showed that it was unusually large after oxygen was introduced into the system. Other workers have reported related observations.[12,13]

---

[10] J. W. Ackley, C. F. Lothrop and W. R. Wheeler, 1962 Vacuum Symposium Transactions (The Macmillan Company, 1963), 452.

[11] P. A. Redhead, Vacuum 12, 267 (1962).

[12] In a paper which has received little attention Y. Mizushima and Z. Oda reported such an effect in 1959 but did not put forth a plausible interpretation (Rev. Sci. Instr. 30, 1037, 1959).

[13] T. E. Hartman, Rev. Sci. Instr. 34, 1190 (1963).

Early conjectures as to the physical processes responsible for the anomalous effect have been replaced by a new explanation put forth independently by the present authors[14] and by P. A. Redhead.[15] In this picture the observed discrepancies are attributed to electron impact ionization of gases adsorbed or chemically bound at the grid surface of the gauge. The present paper describes experiments which indicate the nature and magnitude of the anomalous effects, gives evidence for the impact ionization hypothesis, and describes auxiliary effects of significance in pressure measurement.

1.4.2 Experiments with the Redhead Modulator Gauge and the Schuemann Suppressor Gauge.

In his original investigation[11] of the anomalous effect, Redhead used the modulator method.[9] After oxygen was introduced into the system, he found a very large increase in the so-called "residual current," i_r. Such a large increase in i_r could be interpreted either as an increase in the positive ion current to the collector or an increase in the "x-ray" or electron current from the collector. In our first attempts to reproduce these effects we utilized a modulator gauge of somewhat different design but similar principle to that of Redhead. As was true for all gauges used in our experiments, the grid material was molybdenum. With oxygen present and under conditions in which we expected to observe a substantial increase in i_r we actually found a decrease. In fact, a

---

[14] D. Alpert, Physics Today 16, 23 (1963).

[15] P. A. Redhead, Vacuum 13, 253 (1963).

negative "residual current" was observed. That is, when the modulator electrode was made more negative in voltage, the current to the collector actually increased! Furthermore, it was observed that the sum of the currents to the collector and to the modulator increased when the potential of the modulator was made more negative.

These unexpected results with the modulator gauge have not been pursued in detail. They are reported here because they led to some interesting conclusions. First, the modulator method itself is not fully understood under such conditions and may give misleading results. Second, these results suggested that in the presence of oxygen, the collection efficiency of the Bayard-Alpert gauge might vary in an unexpected way as a function of the potential of the ion collector. Third, it seemed desirable to study the effect with a Schuemann suppressor gauge,[5] which unambiguously distinguishes between ions arriving at the collector and electrons leaving it.

The results with the Schuemann gauge are shown in Fig. 1.10. Shortly after oxygen was introduced and maintained at approximately 10^{-8} Torr in a previously outgassed system, the suppressor gauge gave indications of anomalous readings comparable to those in a Bayard-Alpert gauge when it was operated at low emission currents. It was observed that both the ion and electron components of the current rose sharply, but that the ion component was at least 10 to 20 times higher than the electron component, and approximately 10 times higher than that given by a monitor gauge on the system. Since most of the electrons could be accounted

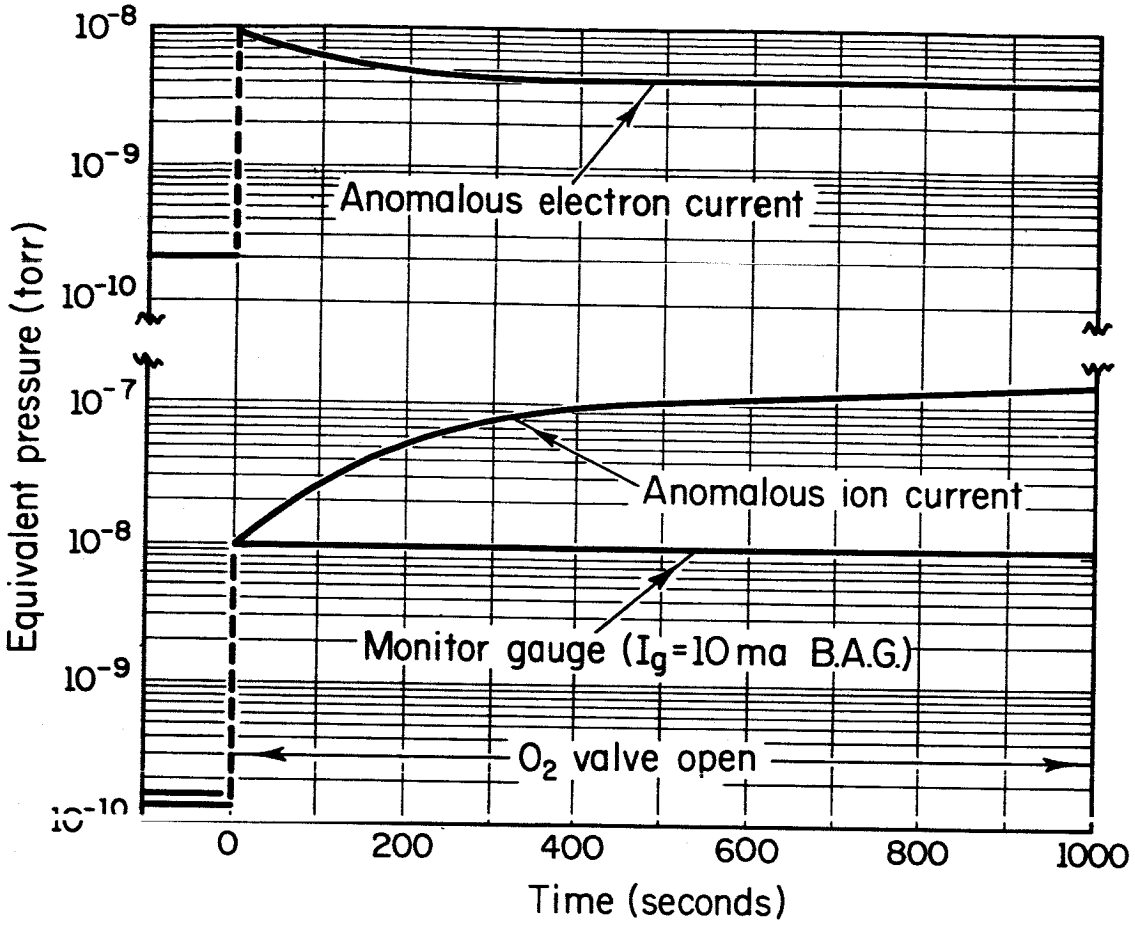

Fig. 1.10. Anomalous Ion and Electron Currents in a Suppressor Gauge Exposed to Oxygen

for as due to secondary ejection[16] by the impinging ions it was evident that the primary component in the enhanced or anomalous reading was due to ions arriving at the collector. These results immediately suggested the new interpretation of the anomalous effect based on the production of ions by electron impact at the surface of the grid.

1.4.3 Evidence for the Surface Impact Ionization Hypothesis

To gain further insight into the nature of the anomalous behavior, an experiment was carried out to measure the collection efficiency of a single collector Bayard-Alpert gauge as a function of collector voltage. For gases which do not exhibit the effect (noble gases, nitrogen, etc.), the ion current to the collector, I_c, is attributable to ions formed within the grid structure of the gauge. I_c is expected to be a slowly varying function of voltage applied to the collector, V_c, on the basis of the following argument: in view of the electrical potential well formed by the negative collector within the positively charged grid there is a high probability that a given ion will ultimately strike the collector even if it misses the collector many times in the course of an oscillatory trajectory. Hence the curve of collector current versus the collector voltage normally saturates at a value of approximately 150 to 200 volts. I_c falls off at somewhat more negative values of collector voltage due to the increasing repulsion of the ionizing electrons and a corresponding reduction of the volume where ions are formed.

---

[16] F. M. Propst, "A Study of the Ejection of Electrons from the Surface of Tungsten by Low Energy Ions," Ph.D. thesis, University of Illinois, 1963.

Experimental data for nitrogen are shown in the dashed curves of Figure 1.11; the lower curve for I_g = 10 mA, the upper for I_g = 0.1 mA. The potentials of the filament and grid were maintained at their normal operating values of +45 v and +180 v. The collector potential was varied as shown to negative values. The abscissa gives the potential difference between collector and grid. It is seen that the experimental results verify the expected behavior.

In the presence of oxygen, a substantially different dependence of ion collector current on collector voltage was observed. As shown in the solid curves, the dependence of ion current on collector voltage differs markedly for different values of electron current: for I_g = 10 mA, the shape of the curve is similar to those for nitrogen, whereas for I_g = 0.1 mA there is a sharp increase of the collector current with collector voltage. Our interpretation of the above behavior is as follows. When oxygen is present, many ions are formed by electron impact[17] of the chemisorbed gas on the grid of the ionization gauge. Such ions are formed at the very edge of the potential well. If one of these ions misses the collector on its first trajectory through the gauge it has a very high probability of emerging on the opposite side and then being captured at the negatively charged envelope of the gauge. If the ions are ejected from the surface with an initial kinetic energy,[15] the probability of such escape is further enhanced. Thus the collection efficiency for ions formed at the grid is lower than that for ions formed in the volume at

---

[17] G. E. Moore, J. Appl. Phys. 32, 1241 (1961).

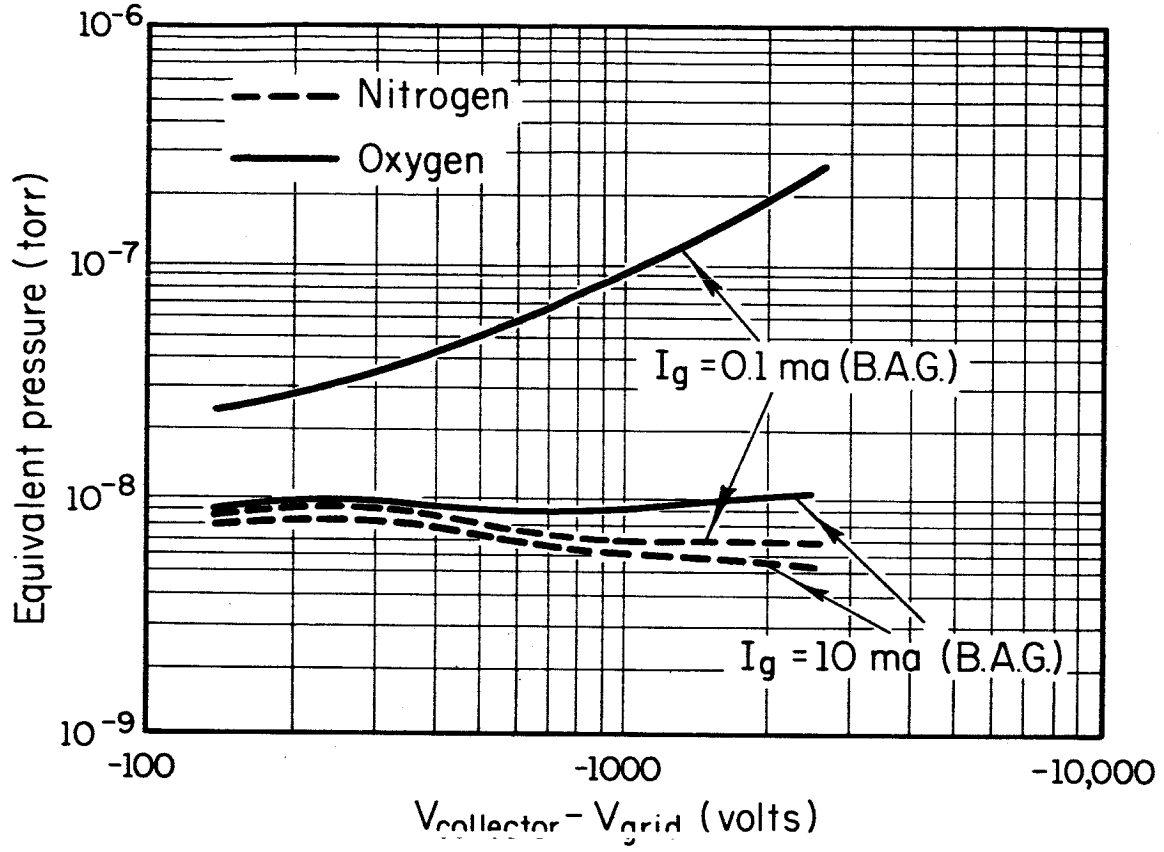

Fig. 1.11. Bayard-Alpert Gauge Reading vs. Collector Voltage.

normal operating voltages. Under these circumstances the probability of capturing an ion is increased if the potential difference between collector and grid is increased, and I_c goes up rapidly with V_c.

If the Bayard-Alpert gauge structure is surrounded by a metallic cylinder at or near collector potential, the currents to the inner and outer collector can be measured and the above picture verified. Such a gauge has been constructed and the following results obtained. In the presence of nitrogen, the inner collector captured approximately 12 per cent of the total number of ions produced; the remainder were collected at the outer cylinder. In the presence of oxygen a similar ratio was observed with the emission current to the grid held at 10 mA. When the grid current was reduced to 0.1 mA, the total number of ions per electron increased, but the fraction captured at the inner collector was reduced to approximately 2-1/2 per cent of the total current. Thus the anomalous reduction in collector efficiency is seen to be correlated with the enhanced rate of production of ions. Both effects are consistent with the picture of ion production at the grid surface.

Further support for the hypothesis of surface ionization by electron impact is provided by observation of the ions produced in a Davis and Vanderslice magnetic deflection mass spectrometer. In the presence of oxygen, a large double peak is observed with one component displaced from the expected mass 16 position. The magnitude and separation of the

peaks indicate a high probability of the dissociative ionization of O^+ at the surface of the ionization enclosure.[18,19]

1.4.4 Comparison of Ionization Gauge Readings in the Presence of O_2 and CO.

Although the above results together with those of other experimenters give good evidence for the interpretation of the effect and a qualitative estimate of the possible errors in gauge readings, we undertook a systematic series of runs under controlled conditions to verify the magnitude of the effect and its dependence on the grid current of the gauge.

The system used was a standard glass oil-pumped, zeolite-trapped system with provision for introducing various gases. Three gauges were utilized and compared: (1) a 5966 Bayard-Alpert gauge, (2) a photocurrent suppressor gauge, and (3) a Philips omegatron.[20] The conductance between the gauges was approximately 1.5 ℓ/s. The omegatron was used as a monitor of the pressure; it exhibited no anomalous effects and gave a reliable indication of the partial pressures of the gases in the system.

The results of a series of runs is shown in Figure 1.12. After a bakeout of the system and outgassing of the gauge (background gas,

---

[18] See also W. D. Davis (1962 Vacuum Symposium Transactions).

[19] J. L. Robins (private communication) has also made a detailed study of the anomalous O^{16} peak in a Davis and Vanderslice instrument.

[20] A. Klopfer and W. Schmidt, Vacuum 10, 363 (1960).

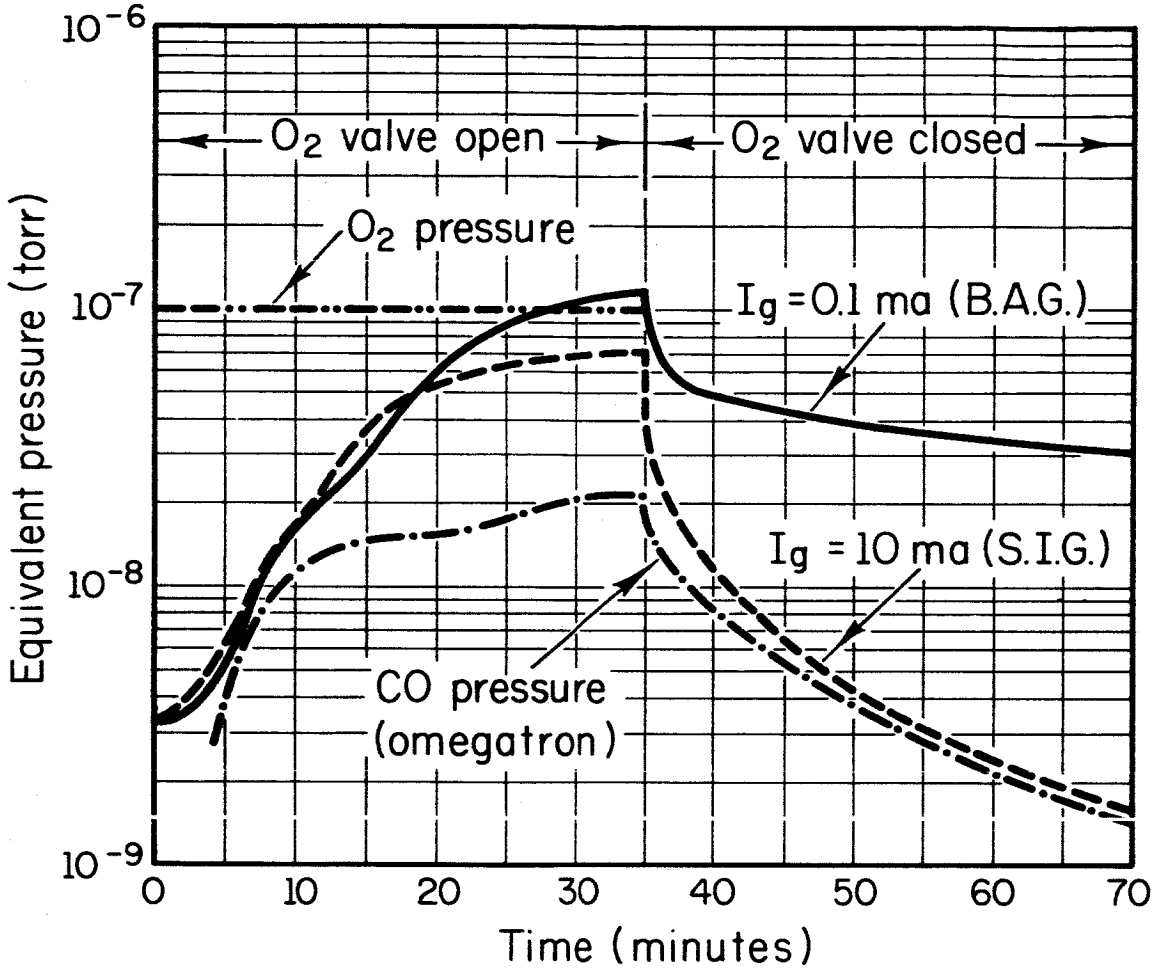

Fig. 1.12. Effect of Grid Current on the Pressure Measurement of Oxygen (I_g varied in Bayard-Alpert Gauge).

mainly CO at 7×10^{-11} Torr) oxygen was introduced into the system at time t = 0. The oxygen was continuously flowed through the system for 35 minutes and maintained at a pressure of 10^{-7} Torr as read on the omegatron. Then the O_2 valve was closed. In the case shown, one of the two ionization gauges, in this case the suppressor gauge (SIG), was maintained at 10 mA while the other, the Bayard-Alpert gauge (BAG) was run at an emission current of 0.1 mA. As will be shown in the next series of runs, interchange of the currents in the two gauges showed that they behaved in a similar manner; hence the important parameter to be observed here is the electron emission current. The following significant features were noted:

(1) Although pure O_2 was being introduced into the system, there was a very large rate of production of CO in the presence of oxygen. During the initial period both ion gauges were in error, apparently due to the large pumping speed of the gauges for O_2 and CO, as well as to the surface effect. The pumping speeds for these gases was evidently large compared to the conductance between the gauges.

(2) When the O_2 valve was closed, the oxygen peak as read on the omegatron fell to less than 10^{-10} Torr in a few seconds. The predominant residual gas remaining thereafter was CO, which was gradually removed but at a rate far slower than the characteristic pumping time for the system.

(3) In the period following the removal of O_2 the gauge operating at 10 mA approached the omegatron reading within a few minutes and read pressure correctly thereafter.

(4) In the same period, the gauge operating at 0.1 mA departed significantly from the "true" pressure as read on the omegatron and the SIG. The maximum error observed was at least an order of magnitude on the high side.

Figure 1.13 shows the results of a similar series of runs for five different values of emission current. In these runs the BAG was operated at 10 mA and the SIG at values of 10, 3, 1, 0.1 and 0.01 mA. To simplify the drawing, only the curves for I_g = 0.1 mA are shown for the initial interval during which oxygen was present.

From these curves the following observations can be made.

(1) There is a monotonic increase in the size of the anomalous effect with decreasing electron grid current. For I_g = 10 mA, the error in pressure reading is small and disappears within a few minutes; for $I_g \leq 0.1$ mA, the error is large.

(2) The size of the effect decreases with time for all values of I_g although the change is not perceptible for the smallest value of I_g. The time constant for the decay of the effect varies approximately inversely with the electron current.

Figure 1.14 shows results for CO similar to those above for oxygen. Note that the effect is significantly smaller. For I_g = 0.1 mA the maximum error in the reading of the gauge is less than a factor of

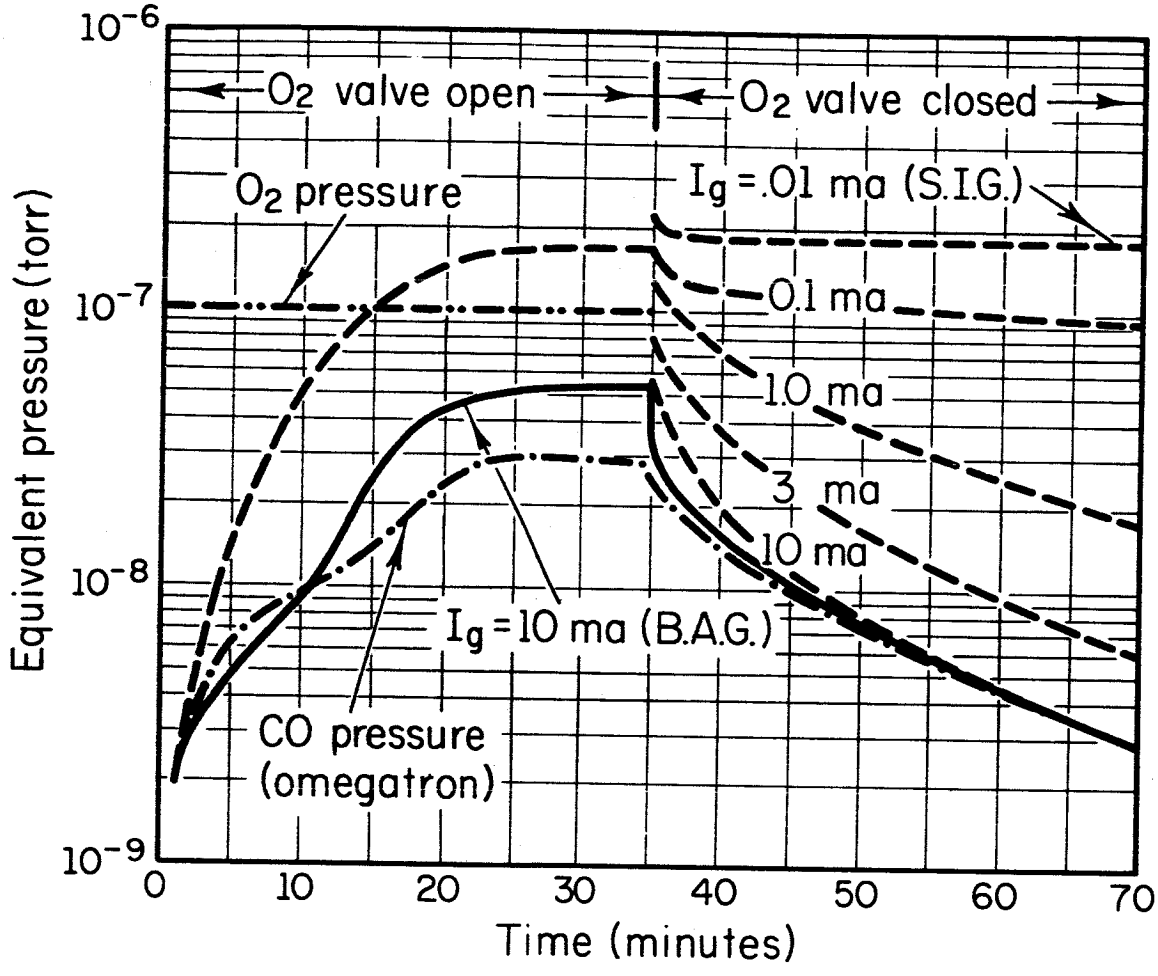

Fig. 1.13. Effect of Grid Current on the Pressure Measurement of Oxygen (I_g varied in Suppressor Gauge).

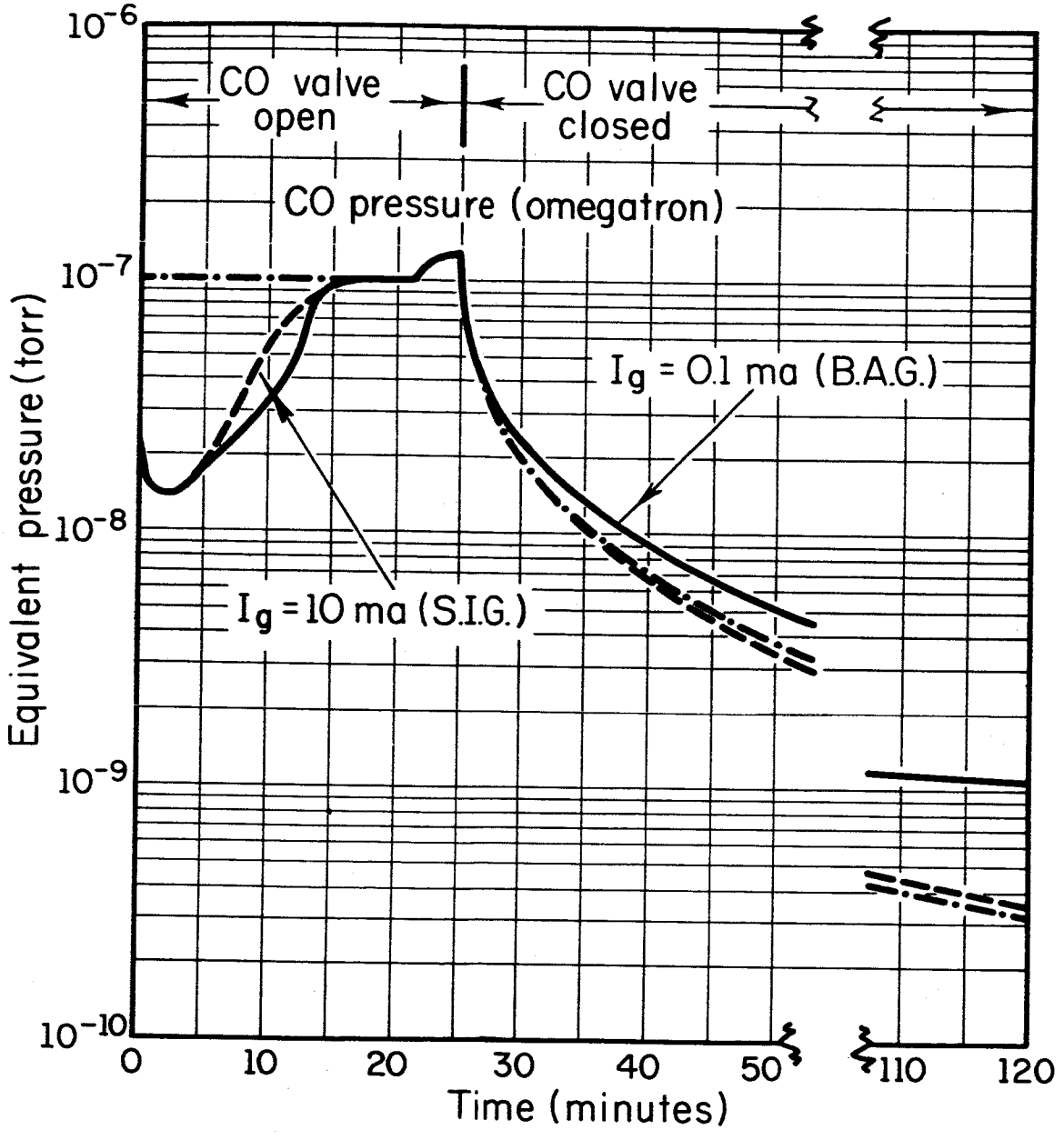

Fig. 1.14. Effect of Grid Current on Pressure Measurement of Carbon Monoxide (I_g varied in Bayard-Alpert Gauge).

four. This result is rather surprising in view of the large cross section for ionization reported by Moore, and further study of CO is called for. Another feature of these curves is the large departure of the readings of both gauges from the omegatron readings in the early part of the runs. This is attributable to a large pumping speed of each gauge for CO and explains in part the similar curves in Figure 1.12.

While significant qualitative conclusions from these results can be made, a quantitative analysis of the dependence of the time constants awaits further experimentation. Such an analysis is difficult in the case of oxygen because within a short period of time a very large fraction of this gas was converted into CO and the effects of the two gases were not readily separated. This result is in itself worthy of careful note. Further observations which are not reported here showed that while the hot tungsten filament is responsible for a sizeable fraction of the conversion of oxygen to carbon monoxide, other physicochemical processes may be even more significant. A preliminary experiment demonstrated that oxygen is also converted into CO in a process which involves the electron bombardment of adsorbed gas at the surface of the grid. This could result from the chemical recombination with carbon of atomic oxygen released at the grid.

1.4.5 Mechanism of Surface Ionization and Gas Removal. A detailed quantitative picture for the electron impact ionization process is not easy to arrive at since it must vary with the composition of the gas and with the grid surface of the gauge. The observation of a large O^+

peak in the presence of oxygen is suggestive of a process of dissociative ionization of the adsorbed gases as studied by Moore for CO in molybdenum. In fact, Moore observed a large O^+ peak in the presence of O_2. He measured a cross-section for the process as high as 10^{-4} ions per incident electron for oxygen-covered molybdenum. Redhead[15] has measured a maximum cross section of about 10^{-5} ions/electrons for O_2 on molybdenum and has proposed that in addition to the release of O^+ ions a large quantity of neutral oxygen atoms is also desorbed by electron bombardment. In typical vacuum systems, however, molecular oxygen is one of the least likely components of the residual gas. It is therefore likely that other adsorbed or chemically bound gases play a contributing role. For example, the metallic oxides formed on the surface of the grid may also be dissociated and ionized by electron bombardment to give a major effect. Young[21] measured maximum ionization efficiencies of 10^{-5} ions/electrons (also O^+) for 90 eV electrons impinging on oxidized surfaces of copper, nickel, molybdenum, and tungsten. This process may therefore be a significant factor in the high readings observed in an ionization gauge immediately following bakeout of the vacuum system but before outgassing the gauge.

As was indicated in Figures 1.12-1.14, the anomalous production of ions at the surface is decreased in the process of measuring it, due to the electron impact removal of the adsorbed or chemically bound gases. The effect may be more rapidly reduced to a negligible value by thoroughly

---

[21] J. R. Young, J. Appl. Phys. 31, 921 (1960).

outgassing the grid by electron bombardment. Thereafter, the onset of erroneous readings can be prevented by operating the gauge at sufficiently high electron currents, the minimum current depending on the amount and composition of the background gas in the system. For typical ultrahigh vacuum conditions at 10^{-9} Torr or lower, no anomalous effects have been reported when gauges are operated at values of I_g of 5 mA or greater.

1.4.6 Summary and Conclusions

1. A systematic study of an anomalous non-linearity in ionization gauges has been made, indicating the magnitude of possible errors in ionization gauge readings. The errors are particularly enhanced after oxygen has been introduced into the system.

2. Evidence has been provided for the interpretation of the effect as due to dissociative ionization by electron impact at the grid surface. At low values of grid current, there is an enhanced rate of production of such ions accompanied by a reduced rate of collection in a Bayard-Alpert gauge.

3. The anomalous readings in ionization gauges can be greatly reduced by thorough outgassing of the grid by electron bombardment. Thereafter, operation at electron currents of 5 mA or greater gives reliable readings.

4. In the presence of O_2 a number of other effects may be present to give erroneous ionization gauge readings; in particular, the composition of the gas may be altered, both by chemical reactions at the hot filament

and by electron bombardment of adsorbed gases. Additional recent information on O_2 to CO conversion is given in Section 5.

5. Studies of these effects have brought valuable insight into very interesting physical and chemical processes which take place not only in ionization gauges and mass spectrometers, but wherever electrons are incident on solid surfaces.

1.5 An Evaluation of Thin Film Electron Sources for Use in Ionization Gauges

The presence of a thermionic cathode in mass spectrometers and ion gauges frequently alters the identity of the gases measured by these instruments. A simple and robust cold electron source inert with respect to its surroundings would be very desirable. When Mead[22] suggested the use of thin film multi-layer devices as electron sources, it looked as though a solution of this problem might be at hand. A suitable source for use in modern vacuum techniques should not be damaged by bakeout at temperatures up to at least 400°C, nor should it contribute "dirt" to the system at these temperatures. For many applications a long, stable life would be a necessity.

Mead sources are three-layer devices consisting of an evaporated metal base, a thin insulating film a few hundred angstroms thick, and a thin covering metal film operated a few volts positive with respect to the base. Initial attempts to fabricate such sources in the Coordinated Science Laboratory were successful to the extent that electron emission was observed. The usual materials of the sandwich were aluminum-aluminum oxide-gold, although tin oxide was also used with several metals. It should be noted that at the insulator thicknesses used in this laboratory and also for those used by Hickmott[23] and others,

---

[22] C. A. Mead, J. Appl. Phys. 32, 646 (1961).

[23] T. W. Hickmott, J. Appl. Phys. 33, 2669 (1962).

the spacing between the metal layers is so great that the "diode" current in the insulator is not the result of quantum mechanical tunneling. Therefore, the frequently used name, "tunnel cathode," for a source of the present type is a misnomer, unless the insulator is less than about 50 Å thick. The conduction process in the thicker films is complicated and not well understood.

Electron emission currents up to several microamperes were observed in samples prepared under the present contract. The operation of a source at such currents gave at best fractional-hour life. In fact, merely bringing the device to operating voltage (about 10-12 volts) caused irreversible changes in the diode conductivity of the sample. The emission current for all samples of any materials tried was "noisy." A source of a few mm^2 area was placed several centimeters from a phosphor screen to permit examining a magnified image of the emission pattern. Most of the electrons were found to originate from a number of spots that flickered on and off, the number of spots remaining approximately constant. A small steady current component was seen.

Much better cold cathodes have been made by Cohen.[24] Cohen used cesium to lower the work function of the outer metal film and thus increased the emission of his sources by 10^5. This technique could be very useful for a permanently evacuated tube, but it would not be applicable to one baked-out or opened to air after sensitization, or to one operated under even moderate pressures of active gases.

---

[24] J. Cohen, J. Appl. Phys. 33, 199 (1962); Appl. Phys. Letters 1, 61 (1963).

Perhaps the most useful electron source could be made by combining a Mead-type cathode with a resistance strip electron multiplier. By operating the film device at very low currents it would be more reliable, and a multiplier could increase the current to a value of at least several microamperes.

2. SURFACE PHYSICS: ADSORPTION

2.1 A High Resolution Secondary Emission Spectrometer for Surface Research

2.1.1 Introduction. Secondary emission has been the object of a great deal of study since its discovery around the turn of the century. Although of great practical importance, this work has not contributed greatly to our understanding of the solid state or surfaces. The primary reasons for this are:

a) The lack of control.

It was early recognized that secondary emission is strongly dependent on the condition of the surface; however, it has only been in the past few years that the techniques of ultrahigh vacuum and surface preparation have been developed to a degree sufficiently sophisticated to allow good control over surface experiments.

b) Poor resolution.

Typically, secondary experiments have consisted of a source of electrons (a hot filament), a means for focusing these onto a target, and some type of analyzer to determine the number and energy distribution of the ejected electrons. In such an arrangement, the best resolution that can be achieved is equal to the thermal spread of the incident beam ($\gtrsim$ 0.25 eV).

(c) The lack of substantial theoretical support.

The difficulty of meaningful calculations on surface problems has in general made the field unattractive to theoreticians. There has been some change in this attitude recently, however, and hopefully this positive trend will continue.

Many difficulties have been substantially eliminated during the past few years, and it seems that secondary emission can be a very useful tool for the study of a number of processes. Some of the possibilities will be discussed briefly.

The secondary electrons leaving a surface can be divided into two broad classes: the primary electrons scattered (elastically or inelastically) from the surface, and electrons excited from the surface by the primaries. This classification is different from the normal "true secondary" and "elastic" division. The truly elastically scattered electrons constitute a small part of the total secondaries. This elastic process involves a transition in which the whole lattice takes up the momentum change in the collision, much in the same manner as in the Mössbauer effect. Grouped closely around these truly elastically scattered electrons (and with typical resolutions indistinguishable from the elastic content) are "almost" elastically scattered electrons, i.e., electrons that scatter with the emission or adsorption of a phonon (virtual or real). It would be possible, then, with a system of adequate resolution to study this second type of scattering in detail. In particular, it should be possible to study the excitation of the vibrational states of adsorbed gas specie on the surface.

In addition to vibrational states, the adsorbed atoms on surfaces have electronic transitions available for excitation. It is felt that these transitions can also be detected by secondary emission studies.

The excitation of plasmons by electron impact has been observed by numerous experimenters. In general, the measurements have suffered from the lack of good control of the surface contamination. Again, an experiment under good control and with high resolution can yield much important information concerning the intensity of the plasmon excitation as a function of the primary energy, the width of the plasma excitation as a function of the primary energy, and the influence of surface coverage and surface damage.

Other processes which can give rise to discrete energy losses are the excitations of a) optical defects, b) donor and acceptor levels in semiconductors, c) Tamm type surface states and d) inner core states. The only type of all of the above processes which has been observed and identified is the plasmon excitation. We cannot say a priori which of the mechanisms will definitely be amenable for study by this technique; however, over the entire energy range available, it seems likely that most of them can at least be observed. In particular, if the energy loss spectra shows characteristic structure for adsorbed gas specie, we will have available a quantitative tool for the study of gas-surface reactions.

All of the above mechanisms would result in electrons emanating from the surface with characteristic energy losses below the primary energy (the first class of electrons) The second class of electrons

would also be a valuable source of information concerning the interaction of electrons with electrons and with phonons.

This is a brief listing of the types of processes which we expect to observe and study. A brief description of the instrument constructed for this work follows.

2.1.2 Experimental Apparatus. A schematic of the apparatus constructed for high-resolution studies of secondary electron emission is shown in Fig. 2.1. Electrons pass from the electron source into the first energy analyzer (monochromator), the electrons from the monochromator strike the target and produce secondary electrons. Those secondaries leaving the target at the proper angle enter the second analyzer (analyzer), which determines the energy distribution of these electrons. An electron multiplier is used as the detector of the electrons leaving the analyzer, and either an electrometer or counting techniques can be used to monitor the output of the multiplier.

Figure 2.2 is a more detailed drawing of the apparatus. With this drawing in mind, several design considerations will be discussed. Since we want to work at very low energies, it is necessary that considerable care be exercised to minimize the deleterious effects of magnetic fields and space charge. To illustrate, the radius of curvature of 1 eV electrons in a 500 milligauss field is about six centimeters, and an electron density of 10^6 electrons/cm^3 changes the potential from the vacuum value by 2.25 volts in one centimeter.

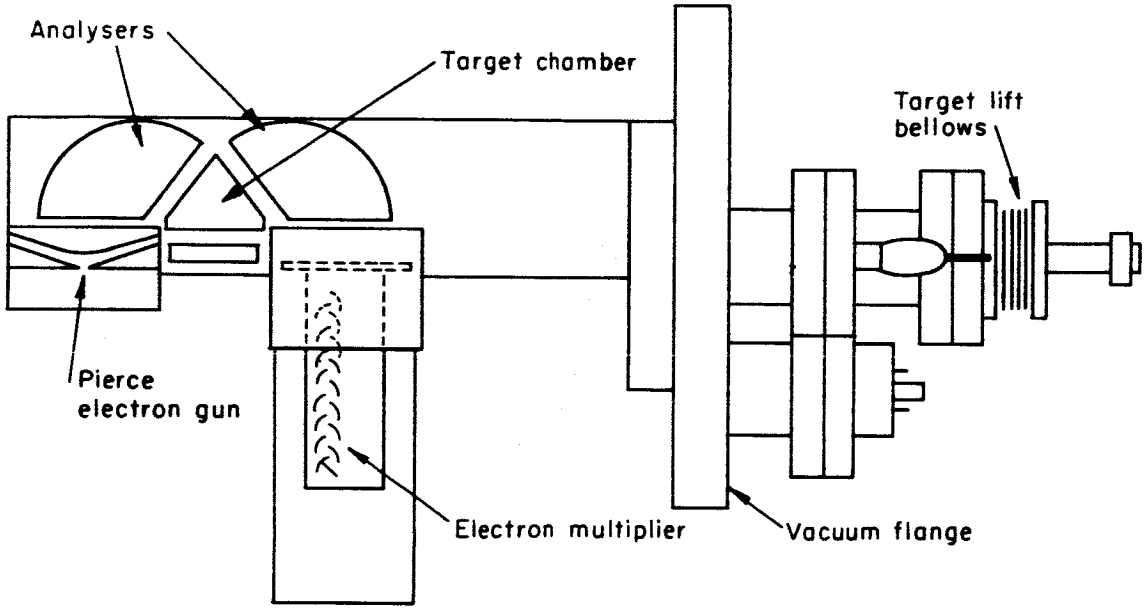

Fig. 2.1. Schematic of the Secondary Electron Experiment, showing the electron gun, the analyzers, and the electron multiplier arrangement.

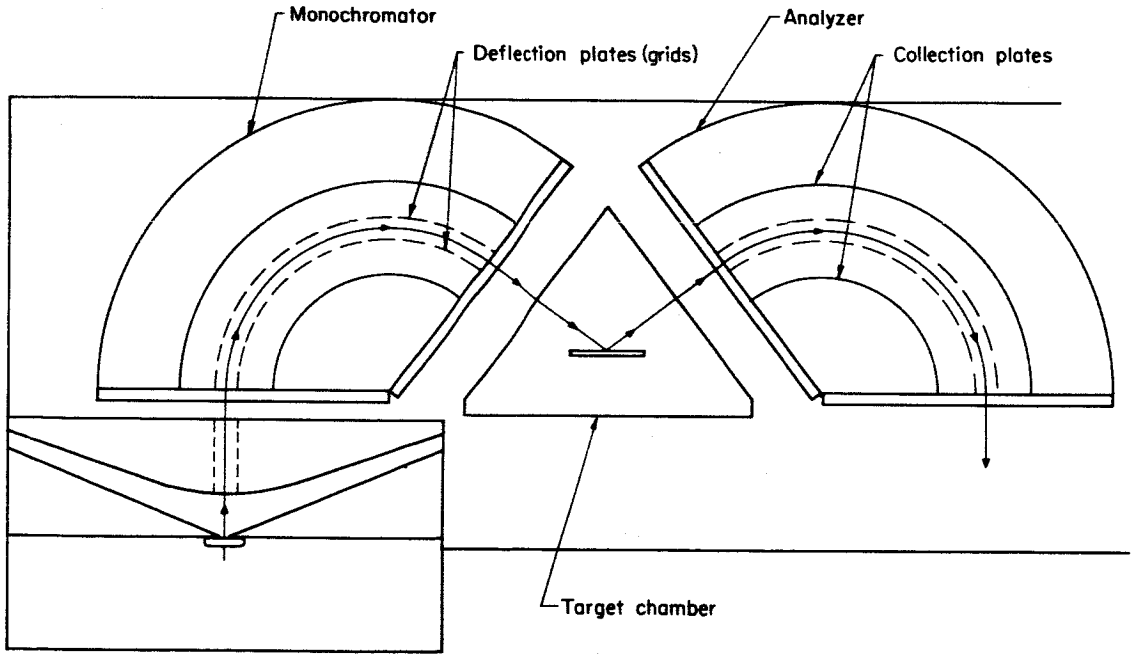

Fig. 2.2. Schematic of the Monochromator-Analyzer System, showing the deflection plate grids and the electron collection plates.

2.1.2.1 Magnetic Fields. Clearly, the earth's magnetic field must not enter the working region. A shield structure consisting of three concentric boxes constructed of high permeability CoNetic AA material prevents this from happening. Calculations, based on the radii of curvature due to magnetic fields, show that the field in the apparatus must be less than a few milligauss for one volt electrons to pass through the apparatus without consequential perturbation. The cathode heating current gives rise to a magnetic field in an extremely critical region, since the energy of the electrons is very low near the cathode. Figure 2.3 shows field versus distance for a single wire and a dipole wire each carrying 0.1 ampere. An indirectly heated cathode with a twelve-pole heater is used. The field from this heater drops off much more rapidly than that of the dipole.

2.1.2.2 Space Charge. We have taken several precautions to minimize the effects of space charge. Use of a low temperature cathode produces electrons with a substantially narrower thermal energy distribution than high temperature cathodes. (The indirectly heated cathode also prevents IR drops and the associated energy spread.) Figure 2.4 shows dI/dE for two cathodes, one with a work function three times the other. The curves are normalized so that dI/dE in both cases is the same in the region of the maximum, where the monochromator is tuned. The conclusions one can draw are: If $\varphi_1 = K\varphi_2$, T_1 must nearly equal KT_2 in order for $(dI/dE)_{1\ max} = (dI/dE)_{2\ max}$. If $T_1 = KT_2$, the total emitted current from cathode one is K times the total current from cathode two. However, the effective current, that is the value at the

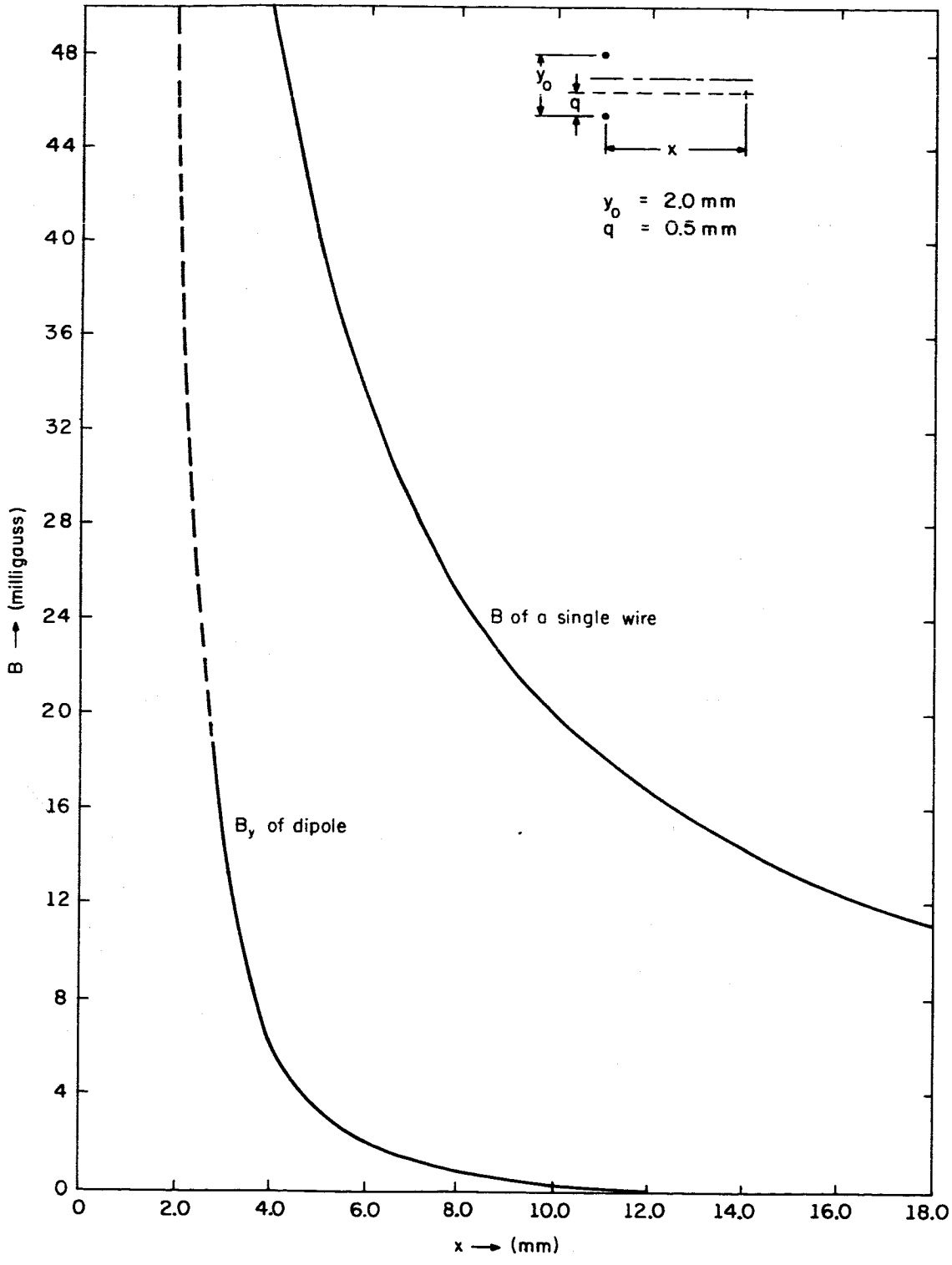

Fig. 2.3. Magnetic Field Produced by a Monopole and a Dipole as a Function of the Distance from the Axis of the Pole. The current is 0.1 amp in each case.

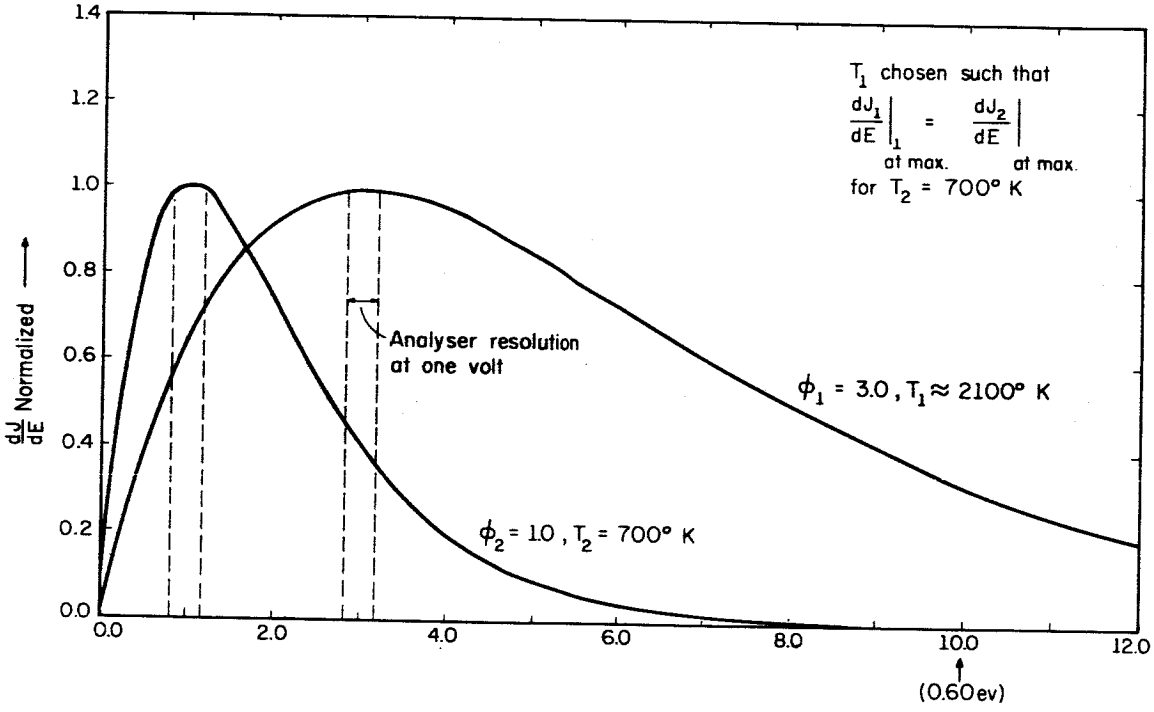

Fig. 2.4. Energy Distribution of Electron Thermally Emitted from Cathodes with Work Functions of 1.0 and 3.0 Volts.

maximum of the distribution, is the same in both cases. Since the monochromator accepts only a 20 mV slice of the total current, there is approximately K times as much unwanted current in the case of cathode two as for cathode one. Thus, the low temperature cathode is effective in reducing space charge.

As another effort to reduce space charge,[1] grids with collection plates behind them constitute several of the electrodes of the apparatus. The collection plates will attract spurious electrons which strike their surfaces, preventing the electrons from re-entering the beam region. The grid structures are incorporated as the deflecting plates in the monochromator and analyzer and in the target chamber. The use of grids as the deflection plates in the monochromator is especially important, since space charge can be especially high in this region.

Figure 2.5 illustrates why the grids should be spaced as closely as is reasonable. The potential curve is drawn assuming the two grids are at the same potential. The parabolic portion of the curve shows the variation of V across the space charge region. The sloped straight line portion is due to the E field which extends from the sheet of space charge to each of the grids. Since the E field depends only on the charge/area in the sheet, the slope remains the same as grid spacing changes. But the integral of the slope is the voltage and changes as the spacing changes. Thus, wider grid spacing allows

---

[1] P. Mermet and L. Kerwin, Can. J. Phys. 38, 787 (1960).

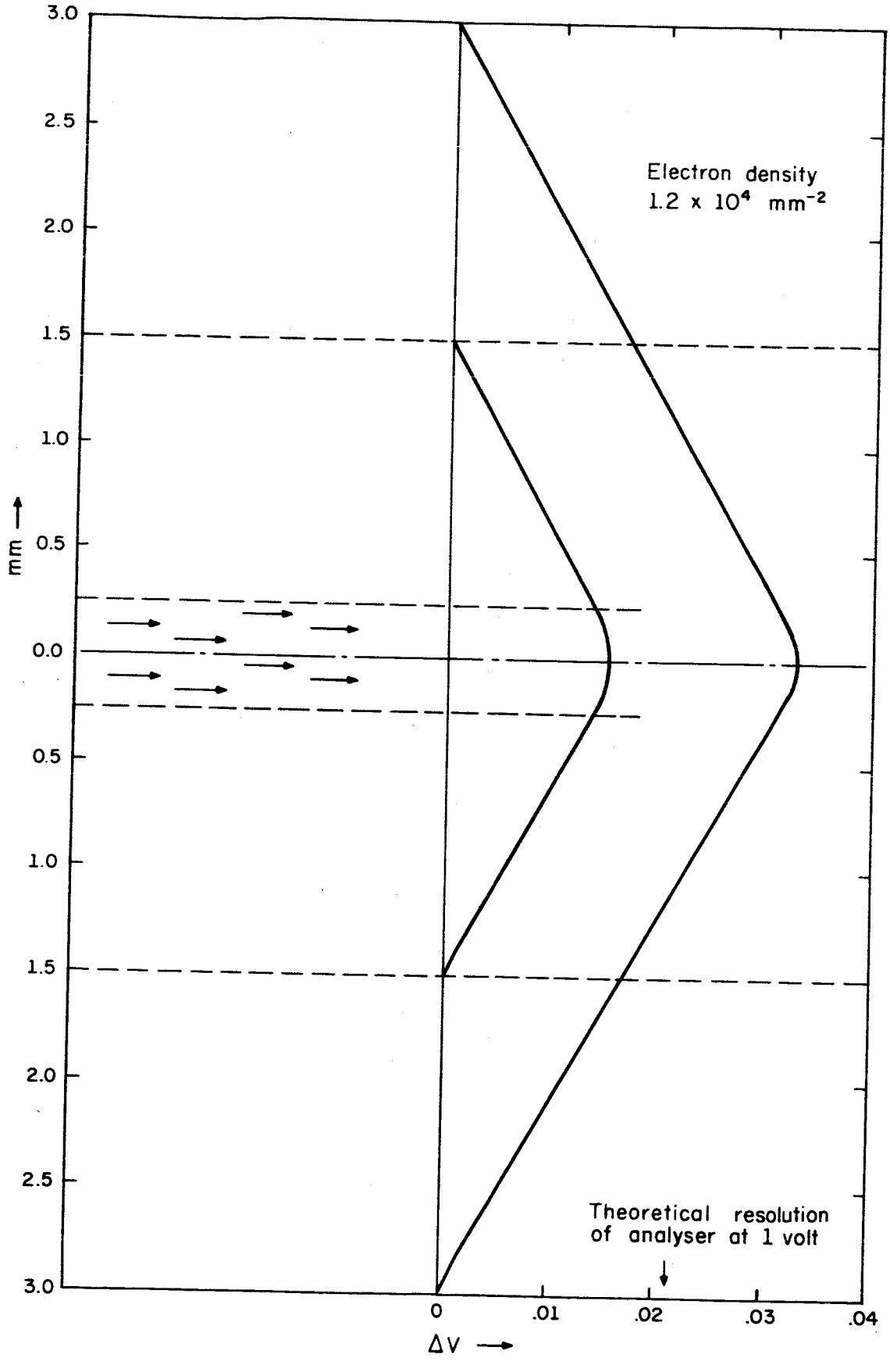

Fig. 2.5. Potential Produced by a Uniform Sheet of Space Charge.

the charge density of the beam to cause greater changes in the potential in the region of the beam. This effect causes electrons to have less kinetic energy than they would have without space-charge and can seriously affect the operation of the analyzer at low electron energies. (Note that the theoretical resolution of the analyzer at 1 volt is 0.02 volt which is the same magnitude as the space charge depression.)

2.1.2.3 Operation. There are several modes of operation of the apparatus. Figure 2.6 shows voltage connections to the system. Some typical modes are:

1) With S_1 at a and $V_{SHIFT} = 0$, one can sweep $\not{V}$ and obtain the energy distribution of electrons coming from the target for any primary energy chosen.
2) Doing the above with a positive value of V_{SHIFT} simply moves the distribution, obtained by procedure 1), over a distance V_{SHIFT} from zero.
3) With S_1 at a, $V_{SHIFT} = 0$, and $\not{V}$ set to a given pass energy, one can obtain the variation of the height of a peak (say from an Auger process) at a given energy above the vacuum level of the target as a function of the primary energy.
4) With S_1 at b and $V_{SHIFT} = 0$, varying $\not{V}$ allows one to continuously observe the height of a peak at some fixed voltage V_{Loss} below the primary energy as a function of the primary energy.

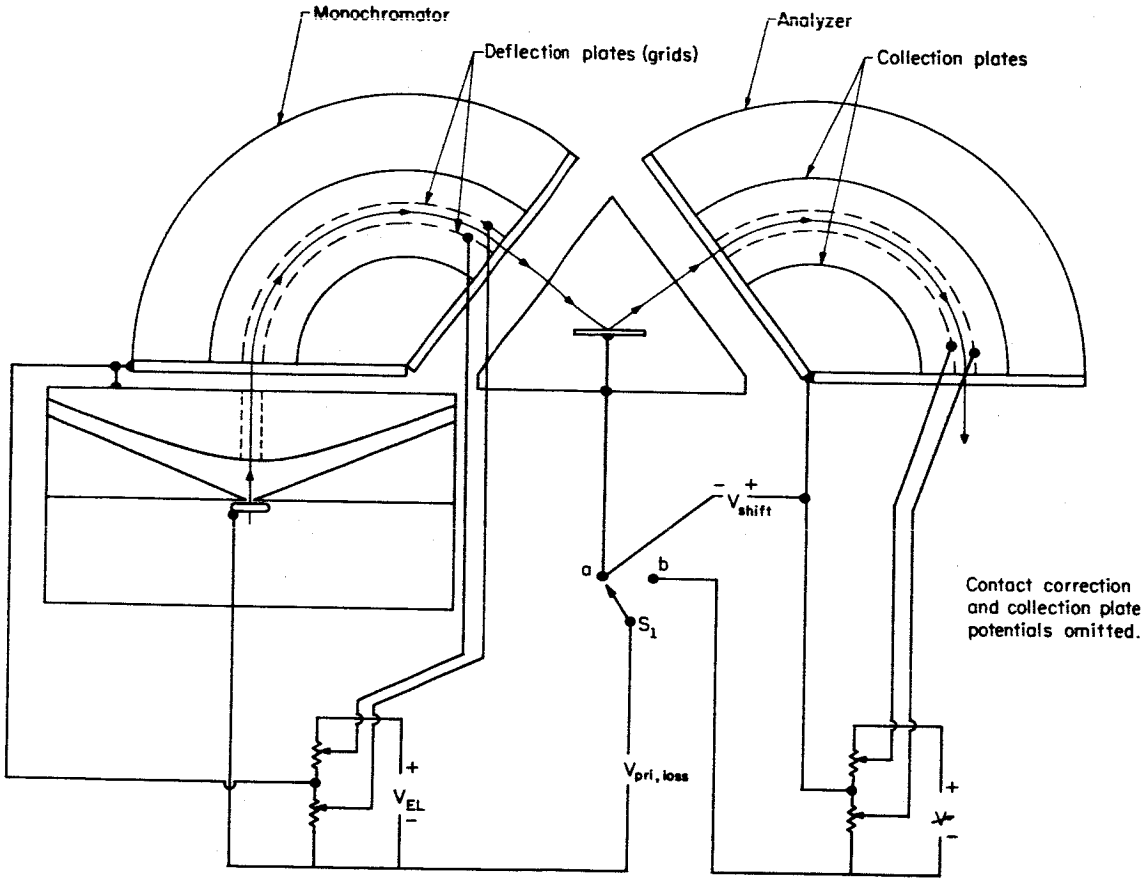

Fig. 2.6. Schematic of the Monochromator-Analyzer System, showing the electrical connections to the pertinent electrodes.

5) The energy distribution of 1) and 2) can be obtained without sweeping $\not{N}$ (and thus varying the analyzer resolution, which goes as 1/V). This is done by setting $\not{N}$ to some value and sweeping V_{SHIFT} to bring the electrons to the acceptance energy of the analyzer. This of course requires acceleration and deceleration between the target chamber and the second analyzer. A high transmission grid with wires transverse to the slit direction is placed across the exit of the target chamber. With this grid in place, the electric field is uniform where important and the electron trajectories can be calculated. A computer program was written to find the transfer ratio of electrons able to get from target into the second analyzer (with angle of entrance of less than $|\pm 3.5^{\circ}|$) for various acceleration and deceleration voltages. Figure 2.7 shows these results with the transfer ratio normalized to one for zero acceleration.

2.1.2.4 Computer Control. This experiment operates under computer control. A schematic of the control system is shown in Fig. 2.8. The basic operation is very similar to a multichannel analyzer operated in the multiscaling mode. A digital-analog converter is stepped by the computer through 128 channels, a counter is operated for a preset time in each of the channels, and the number of counts is stored in temporary memory in the computer. This data can then be analyzed by the

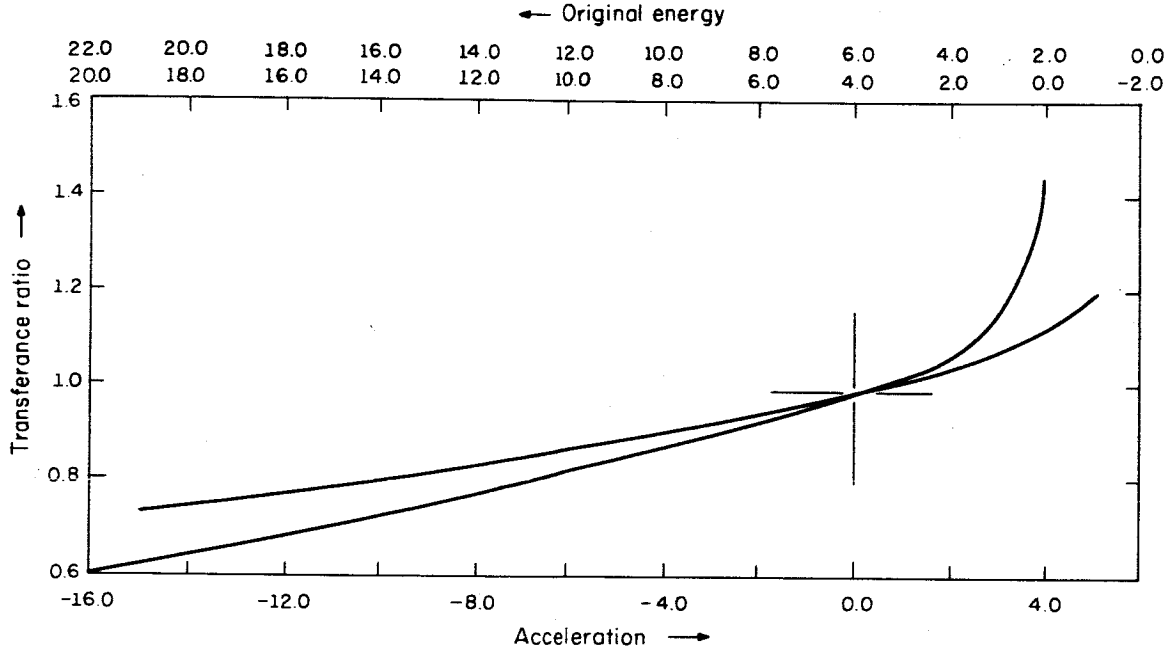

Fig. 2.7. Transfer Ratio of Current from Target Chamber to Analyzer as a Function of the Accelerating or Decelerating Voltage Applied between these Two Electrodes.

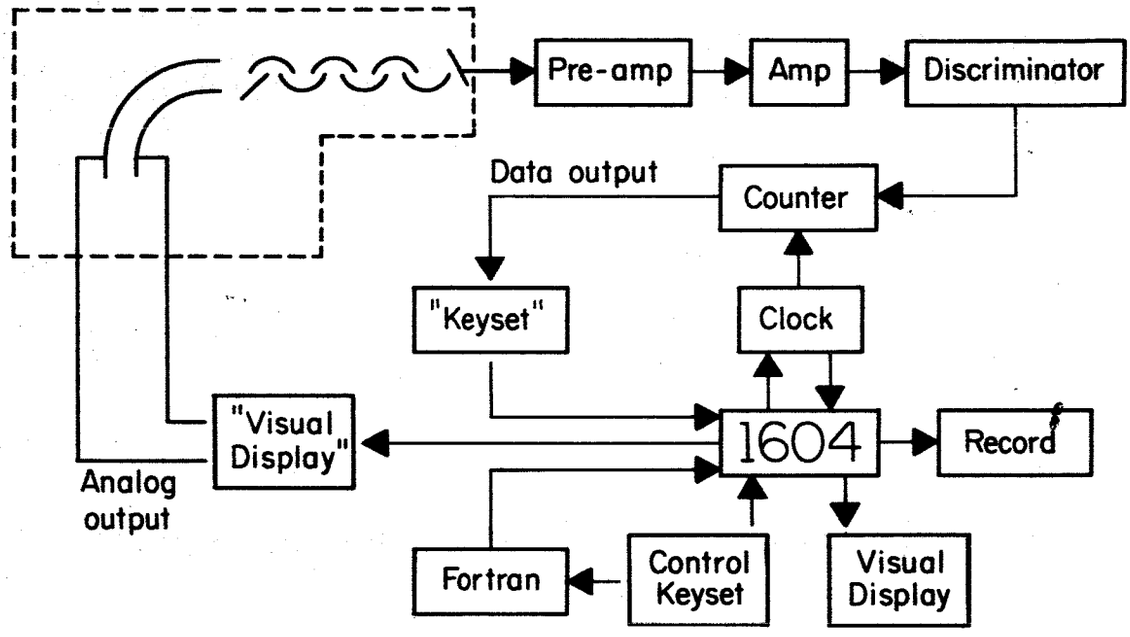

Block diagram of computer controlled secondary electron experiment

Fig. 2.8. Schematic of Computer-Controlled Secondary Electron Experiment.

computer and displayed on a television monitor at the location of the experiment. The whole operation is controlled by a teletype keyset also located at the experiment. In addition to calling to the experiment programs written previously for the analysis of the data, Fortran statements can be written on the teletype keyset for performing analysis which was not anticipated. There are a number of significant aspects to this type of experimentation. These general aspects will be studied and constitute a substantial part of this portion of the program.

The computer-control part of this experiment is being done in cooperation with the PLATO teaching machine program of the laboratory. The major portion of the buffer equipment is a part of that system. Programming and design of additional buffer equipment have been due also in large part to the PLATO group.

2.1.2.5 Performance. Figure 2.9 illustrates the total resolution that has been achieved with this instrument. The full-width at half height is approximately 50 meV. This curve was obtained by scattering the beam from the target at 5.0 eV primary energy. There seems to be essentially no spreading of the line width due to scattering. There is some evidence of inelastic scattering on the low energy side of the peak.

2.1.3 Discussion of Results. The measurements which have been made with this instrument to date have been on the (100) surface of a tungsten single crystal ribbon. Measurements have been made of the energy distribution of secondary electrons for primary energies between

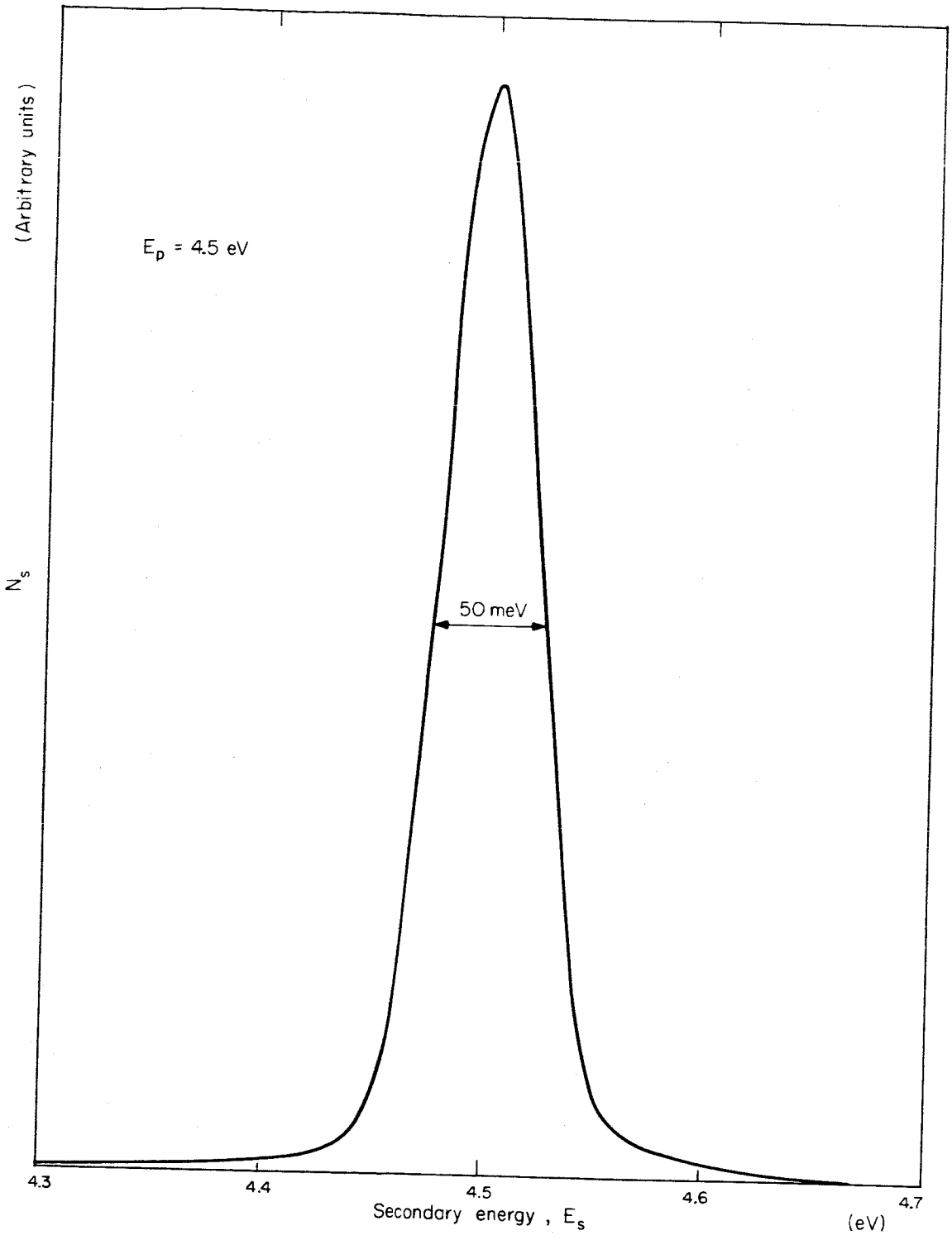

Fig. 2.9. Elastic Peak for E_p = 4.5 eV Illustrating the Resolution (50 meV) of the Electron Spectrometer System.

1 and 45 eV; the number of electrons produced with 1.0, 1.5, 2.0, 2.5, and 3.0 eV energy less than the primary energy as a function of primary energy; and the elastic reflection coefficient for primary energies between 0 and 100 eV. These measurements have been made for the target cleaned by flashing to 2300°K and with N_2, H_2, and CO adsorbed on the surface. The results indicate that several of the processes discussed above have been observed.

2.1.3.1 Discrete Loss Mechanisms. Figure 2.10 shows a logarithmic plot of the energy distribution of scattered electrons from the tungsten surface. These results were obtained after system bakeout and before any further processing of the target. The region of the distribution shown is in the "valley" just below the very strong elastic peak (the elastic peak is not shown). The peaks in the distribution are due to excitation of discrete states in the surface. They are separated by approximately 400 meV, the separation becoming somewhat less between the peaks of lower intensity. It is very likely that this structure represents the excitation of the vibrational states of gas adsorbed on the surface. The structure disappears after flashing the target. Efforts to observe the structure with N_2, H_2, and CO adsorbed on the surface have not been successful. It is possible that the system which exhibits the structure of Fig. 2.10 is the hydrogen-nitrogen bond on tungsten. The value of 395 meV observed for the surface loss is close to the N-H stretching bond in a number of systems. Figure 2.11 shows the same type of structure which resulted from exposing the clean target

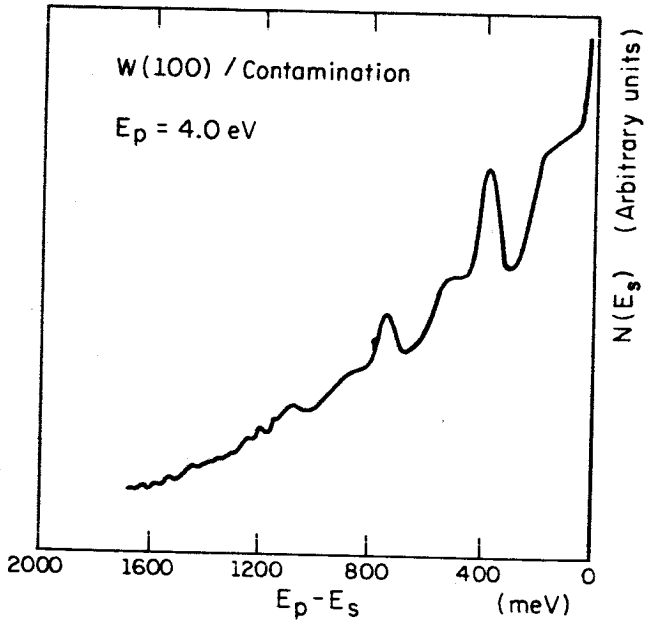

Fig. 2.10. Energy Distribution of Secondary Electrons from a Contaminated Tungsten (100) Surface, Showing the Existence of Low Energy Discrete Losses.

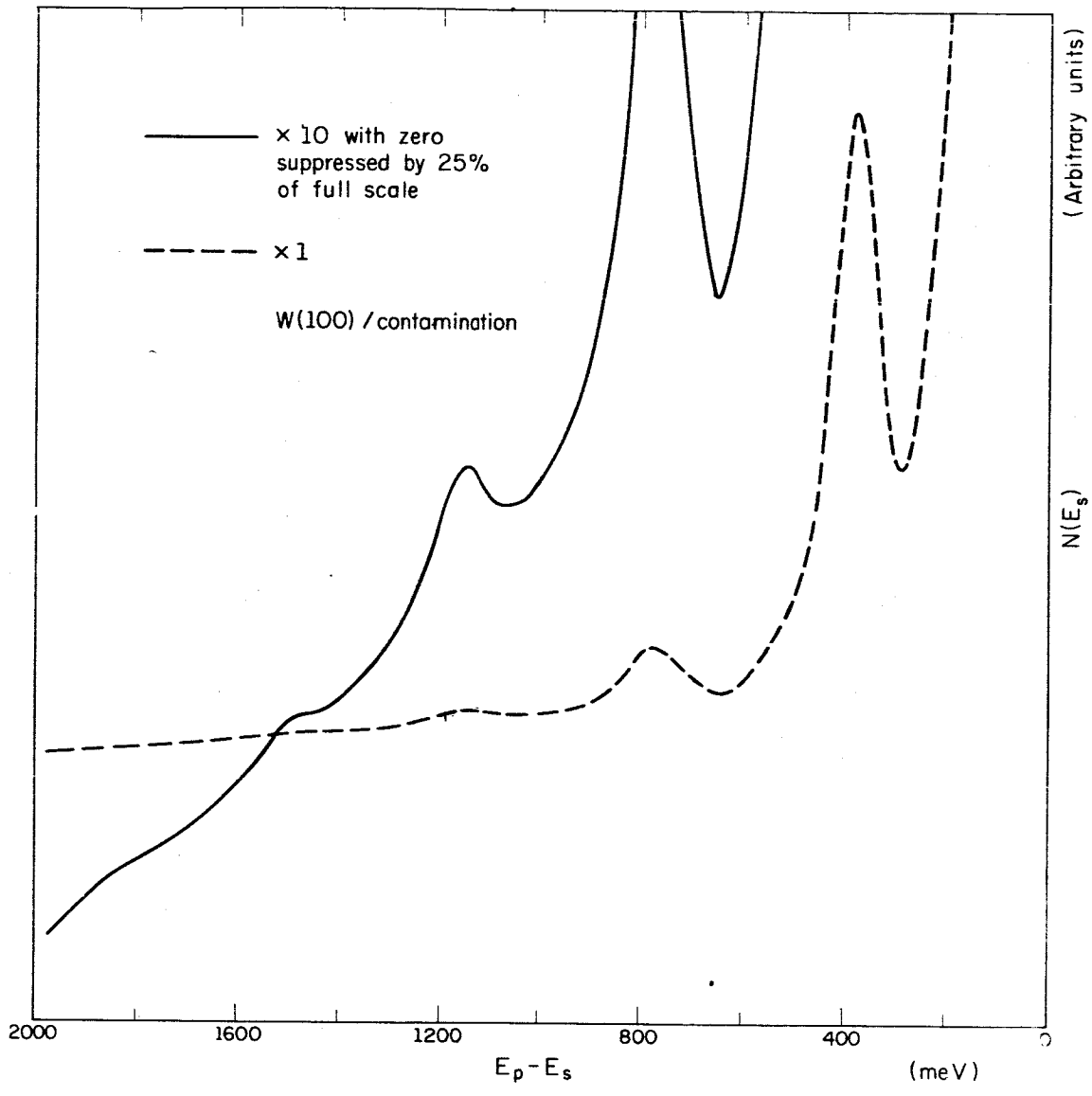

Fig. 2.11. Energy Distribution of Secondary Electrons from a Tungsten (100) Surface after Exposing the Surface to Nitrogen and the Reaction Products of the Nitrogen with an Operating Hot Cathode Ionization Gauge.

to the outgassing products of a gauge which had been exposed to O_2. The structure is very similar to that in Fig. 2.10, and again it seems likely that N-H or C-H is the source. Various vapors will be introduced directly into the system to check this hypothesis.

These results, although by no means complete, open the possibility of a technique of the analysis of surface contaminants and structure similar to infrared spectroscopy.

2.1.3.2 Energy Distributions and Inelastic Scattering Probabilities.

Figures 2.12 and 2.13 show the energy distributions for secondary electrons from clean tungsten for the primary energies indicated. There are two interesting features in these curves. First, there is a peak at approximately 1 eV below the elastic peak. This is very likely due to a peak in the density of states in the band structure of the solid at 1 eV above or below the Fermi level. The calculation of the band structure of tungsten by Mattheiss[2] indicates a peak at this energy below the Fermi level. In addition, there is structure in the low energy region of these distributions. In particular, there are small peaks at approximately 1 and 2.7 eV. These would indicate peaks in the density of states at these energies relative to the vacuum level.

Figure 2.14 shows the number of electrons leaving the target with 0.0, 1.0, 2.0, and 2.5 eV energy less than the primary energy, plotted as a function of the primary energy. Figure 2.15 shows the same data, plotted as a function of the energy of the electrons leaving the target. We note two things.

---

[2] L. F. Mattheiss, Phys. Rev. 139, A1893 (1965).

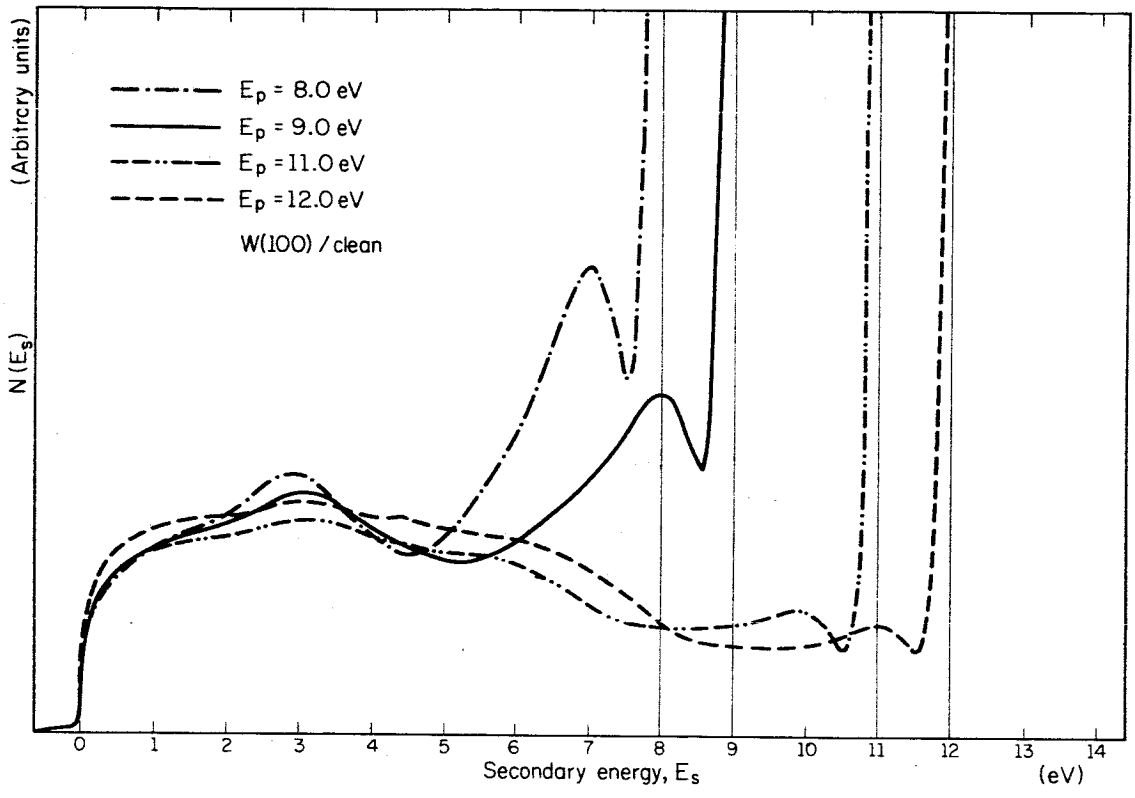

Fig. 2.12. Energy Distribution of Secondary Electrons from a Clean Tungsten (100) Surface.

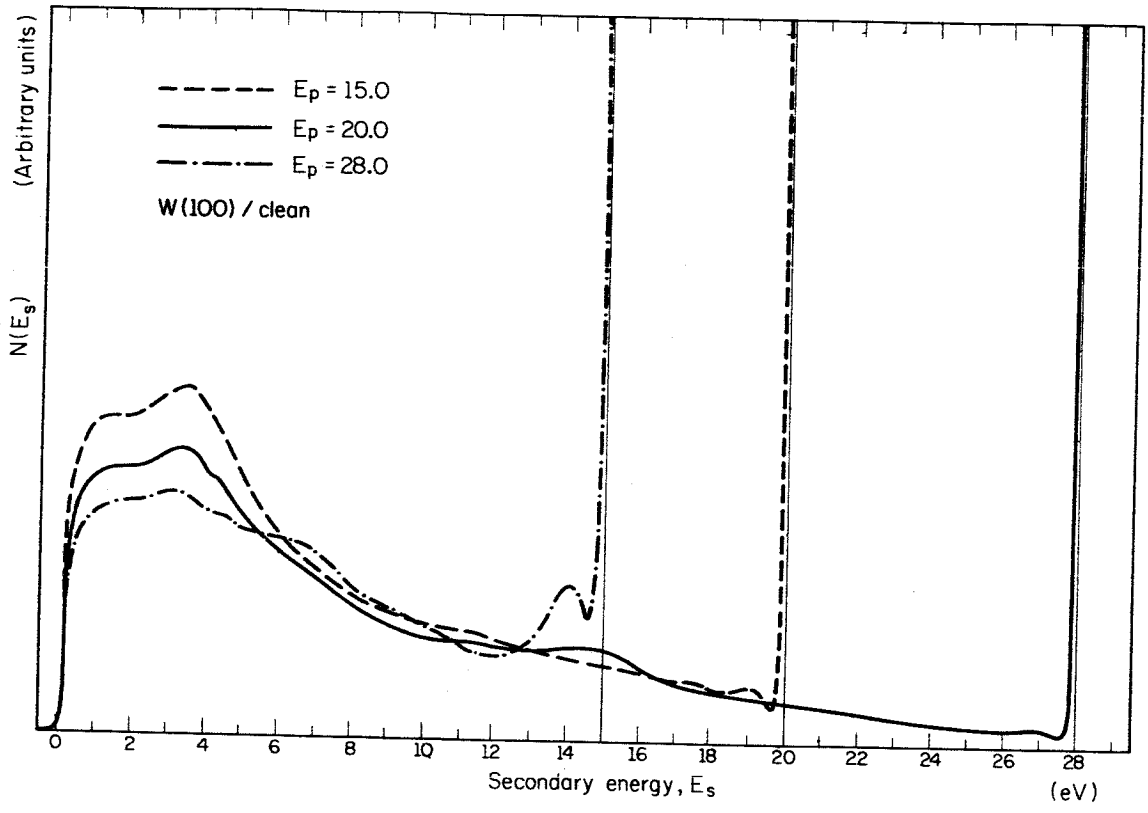

Fig. 2.13. Energy Distribution of Secondary Electrons from a Clean Tungsten (100) Surface.

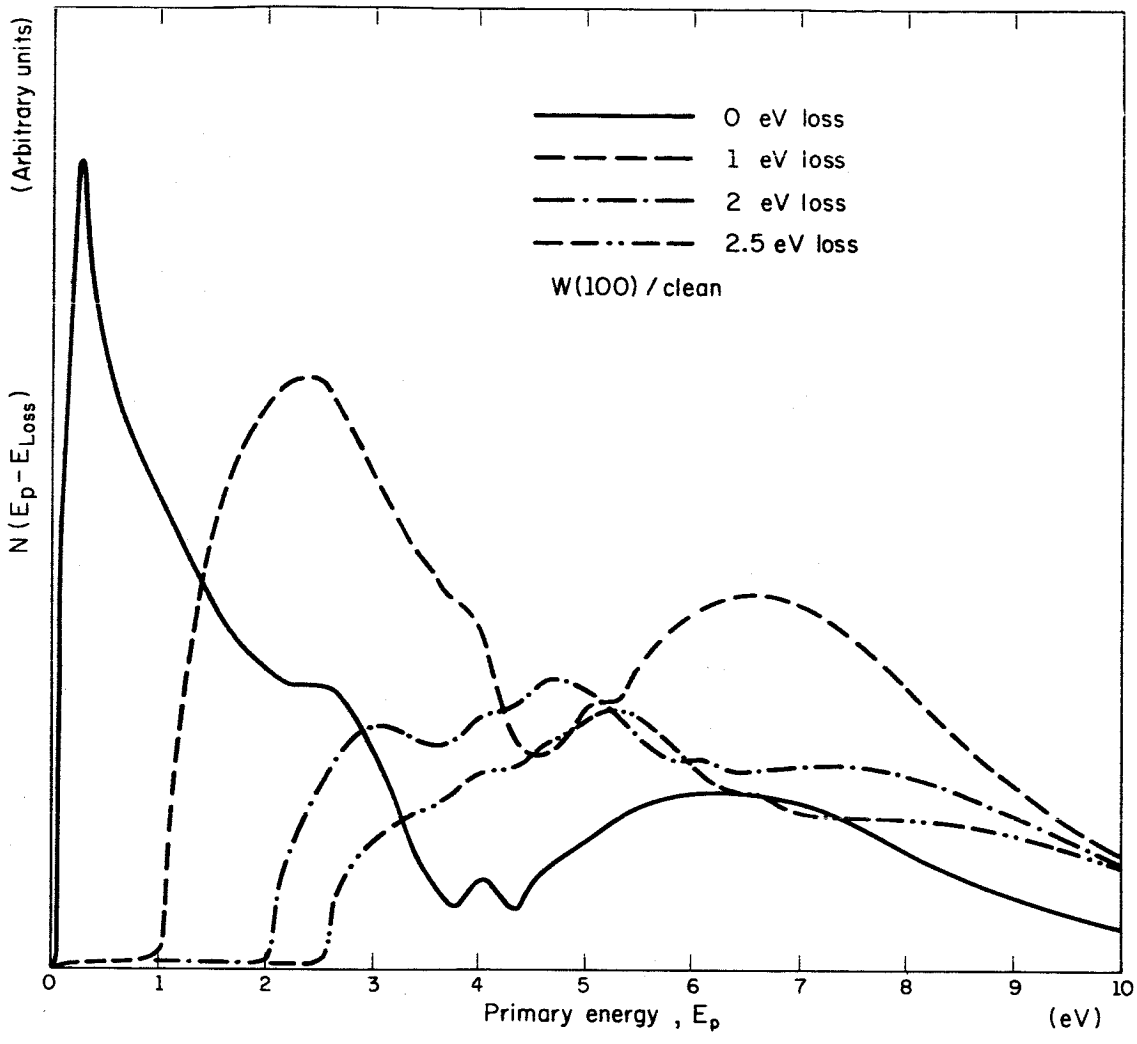

Fig. 2.14. Plot of the Number of Electrons Produced with 0.0, 1.0, 2.0, and 2.5 eV Kinetic Energy Less than the Primary Kinetic Energy Plotted as a Function of the Primary Energy. The data shown are for the clean tungsten (100) surface.

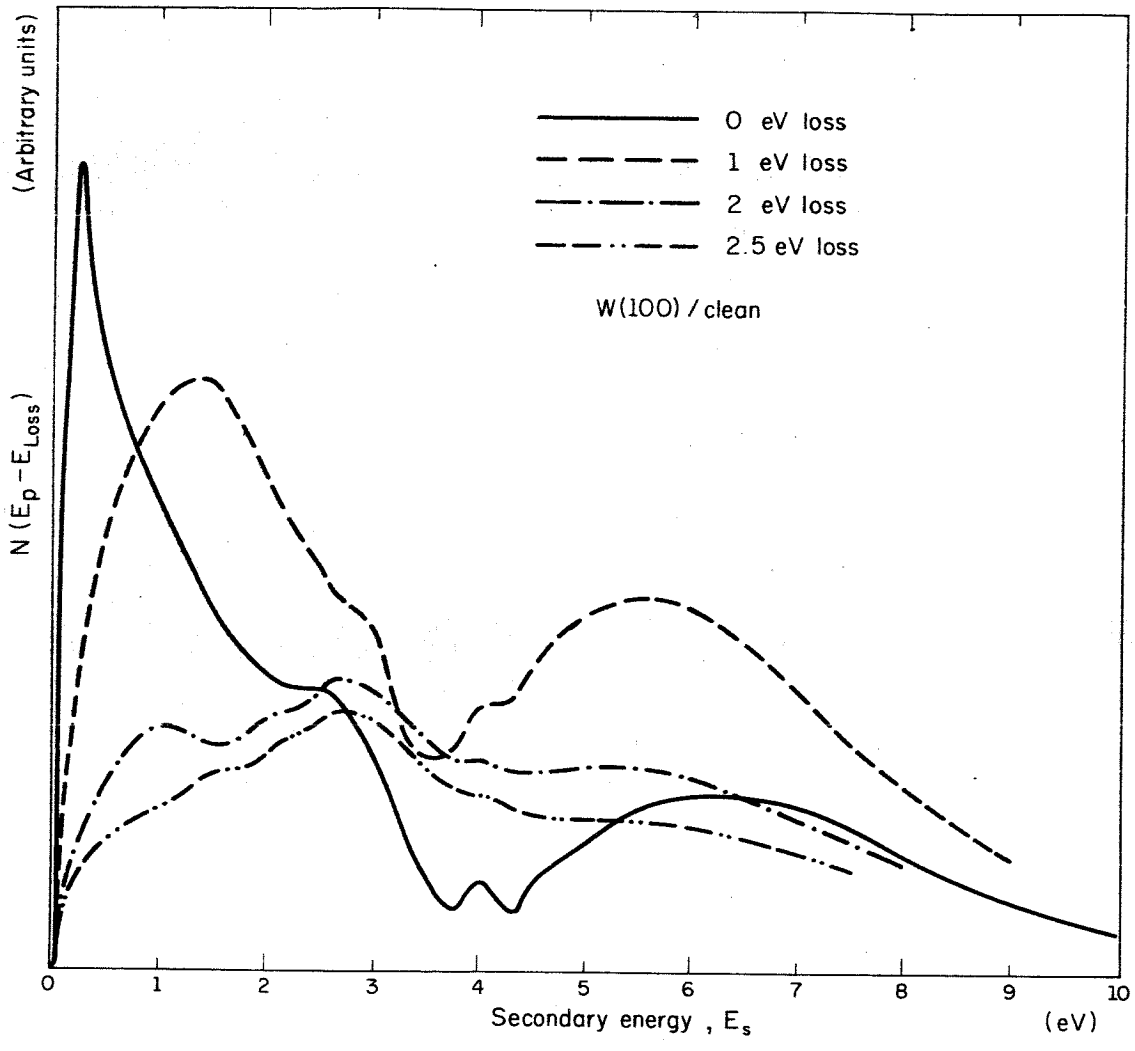

Fig. 2.15. Data of Fig. 2.14 Plotted as a Function of the Energy of the Electrons Leaving the Target.

First, in Fig. 2.14, there is a peak in each of the curves at 4 eV primary energy. (In the curves shown the electrons leave the target with 4.0, 3.0, 2.0, and 1.5 eV kinetic energy when the primary energy is 4 eV.) In Fig. 2.15, there is a peak in the number of electrons leaving the target with 1.0, 2.7, 4.0, and 6.0 eV kinetic energy regardless of the primary energy. The first of these results indicates that there is a high probability of elastic scattering of 4 eV primary electrons, followed by inelastic scattering to give the structure at 4 eV (Fig. 2.14). The structure in Fig. 2.15, being fixed with respect to the kinetic energy of the electrons leaving the target, is indicative of structure in the density of states of the metal. The first two of the peaks (1.0 and 2.7 eV) of Fig. 2.15 correspond to the weak structure at the same energy in the energy distribution of secondary electrons (Figs. 2.12 and 2.13).

The peaks at approximately 1.0, 2.7, and 4.0 eV are in reasonably good agreement with the energies of the $H_{25'}$, N_3, and H_{15} symmetry points of the tungsten band structure as calculated by Mattheiss.[2] In particular, Mattheiss gives the band structure calculated using two potentials, V_1 and V_2. These potentials are identical with the exception that the exchange potential in V_1 is reduced by 30 per cent in the case of V_2. If one assumes a linear dependence of the energy separation of these symmetry points on the strength of the exchange potential, the energies for the $H_{25'}$, N_3, and H_{15} points are 1.4, 2.7, and 4.0 eV, respectively, when the exchange potential of V_1 is reduced by approximately 20 per cent.

Figures 2.16 through 2.21 show the same type of results as above, but for the target exposed to N_2 and H_2. The main feature illustrated is that the structure (although somewhat diminished) is qualitatively the same as for the clean surface. Again, we have the indication that the structure that is observed is due to the bulk properties.

In the studies of gas adsorption, the target exposure was approximately 10^{-3} Torr·sec in each case. Flash-filament measurements indicate an extremely low sticking probability. In particular, there is probably very little N_2 adsorbed on the target for the curves of Figs. 2.16, 2.17, and 2.18 even after the very long exposure of the target.

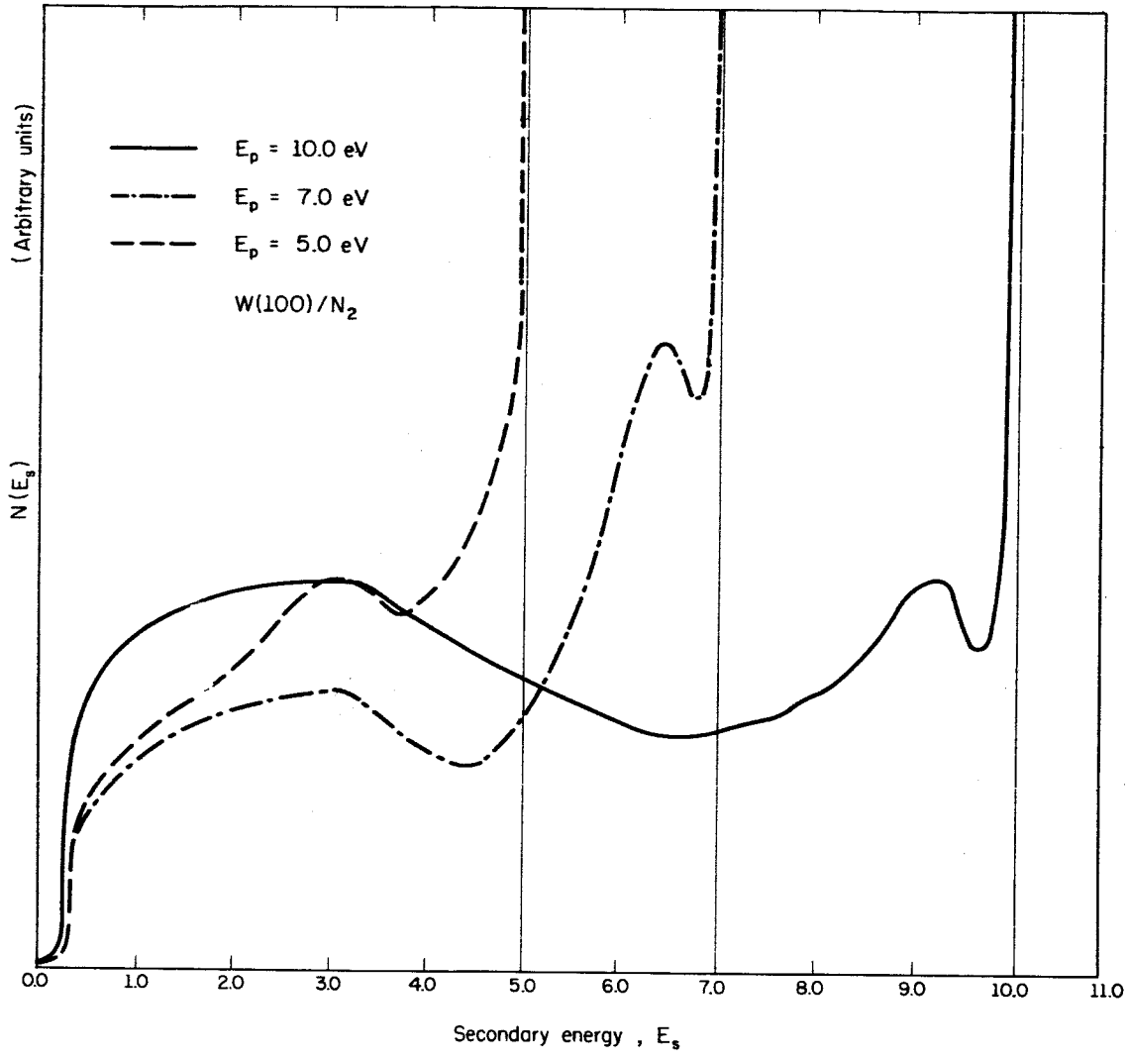

Fig. 2.16. The Energy Distribution of Secondary Electrons from the Tungsten (100) Surface after Exposure of the Surface to N_2.

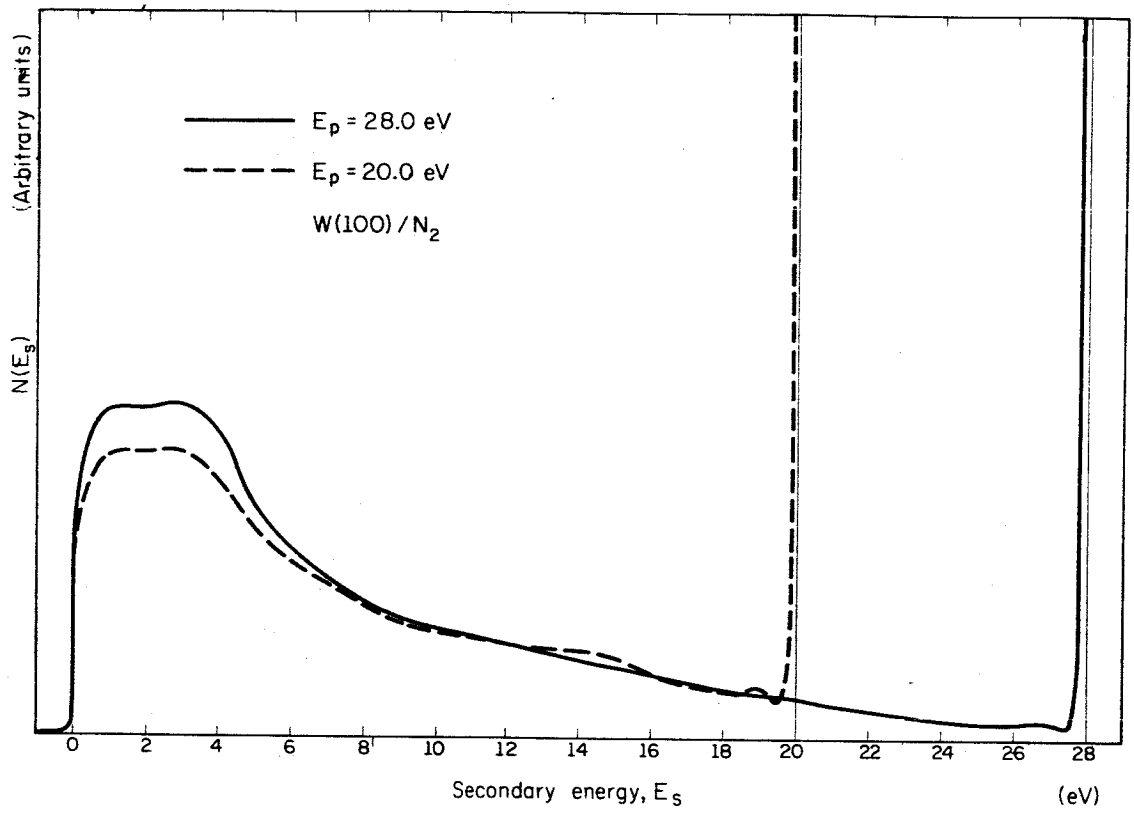

Fig. 2.17. The Energy Distribution of Secondary Electrons from the Tungsten (100) Surface after Exposure of the Surface to N_2.

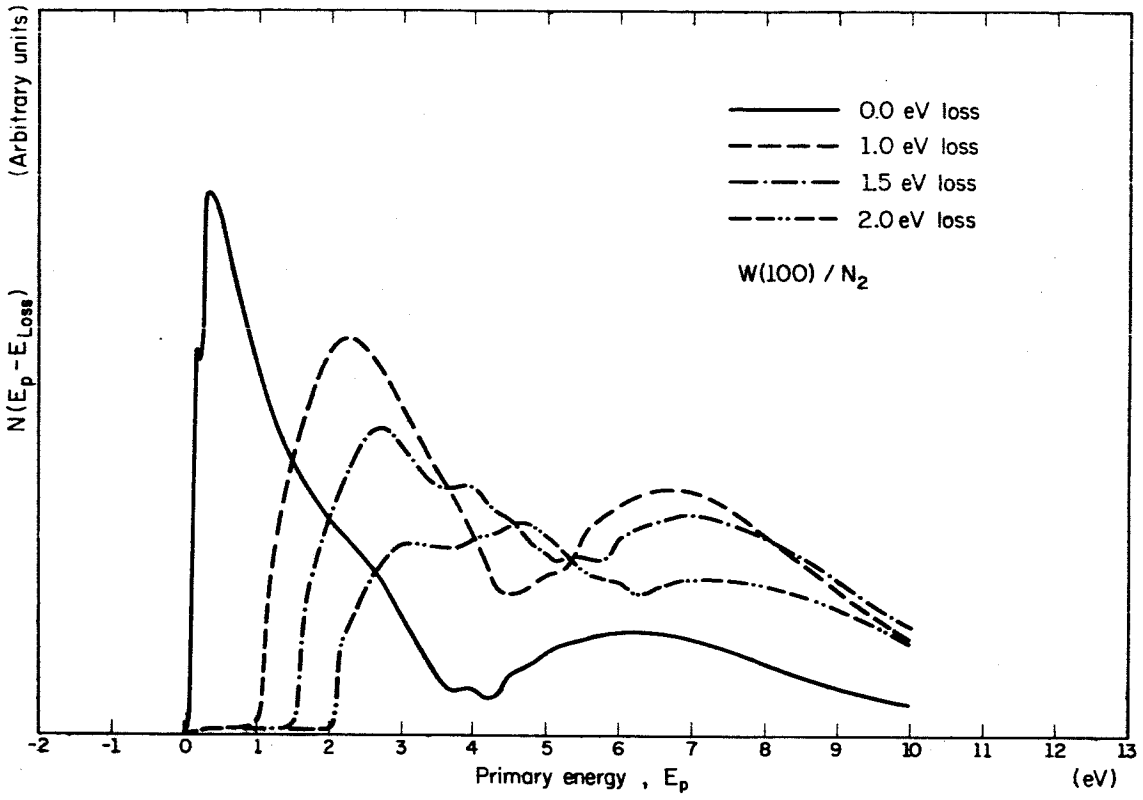

Fig. 2.18. Plot of the Number of Electrons Produced with 0.0, 1.0, 1.5, and 2.0 eV Kinetic Energy Less than the Primary Kinetic Energy Plotted as a Function of the Primary Energy. The data presented are for the (100) tungsten surface after exposing the surface to N_2.

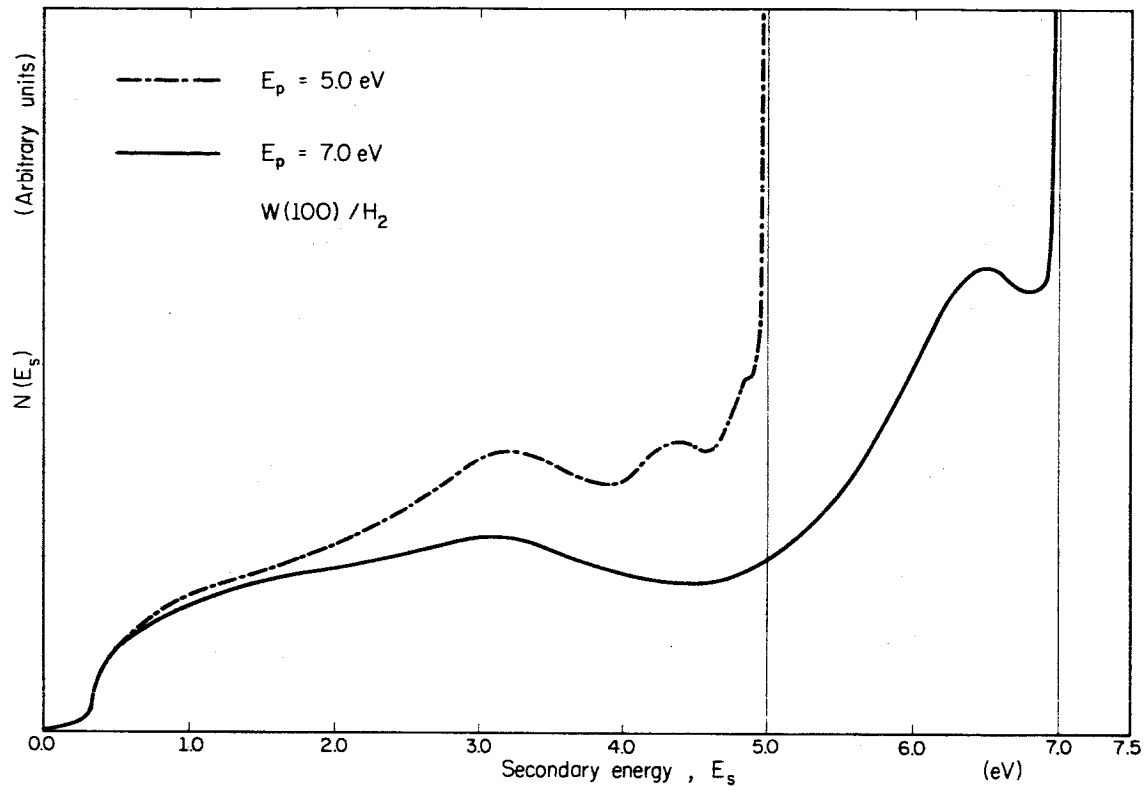

Fig. 2.19. The Energy Distribution of Secondary Electrons from the Tungsten (100) Surface after Exposure of the Surface to H_2.

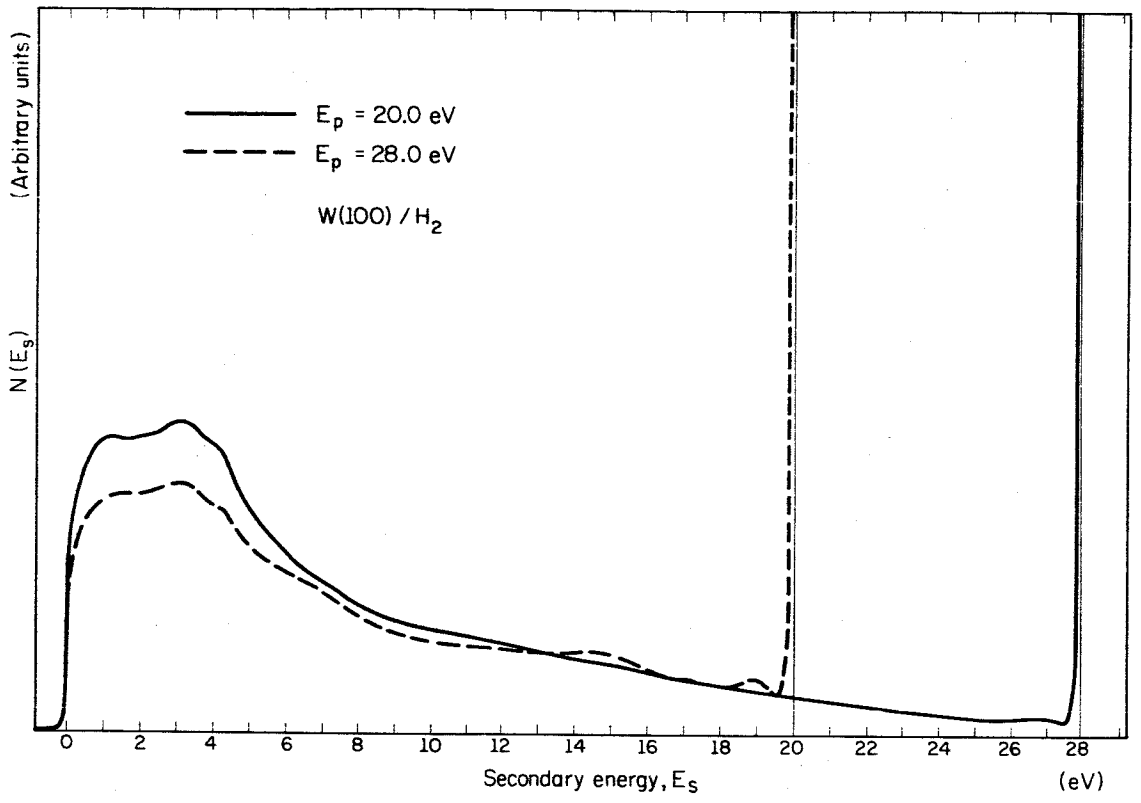

Fig. 2.20. The Energy Distribution of Secondary Electrons from the Tungsten (100) Surface after Exposure of the Surface to H_2.

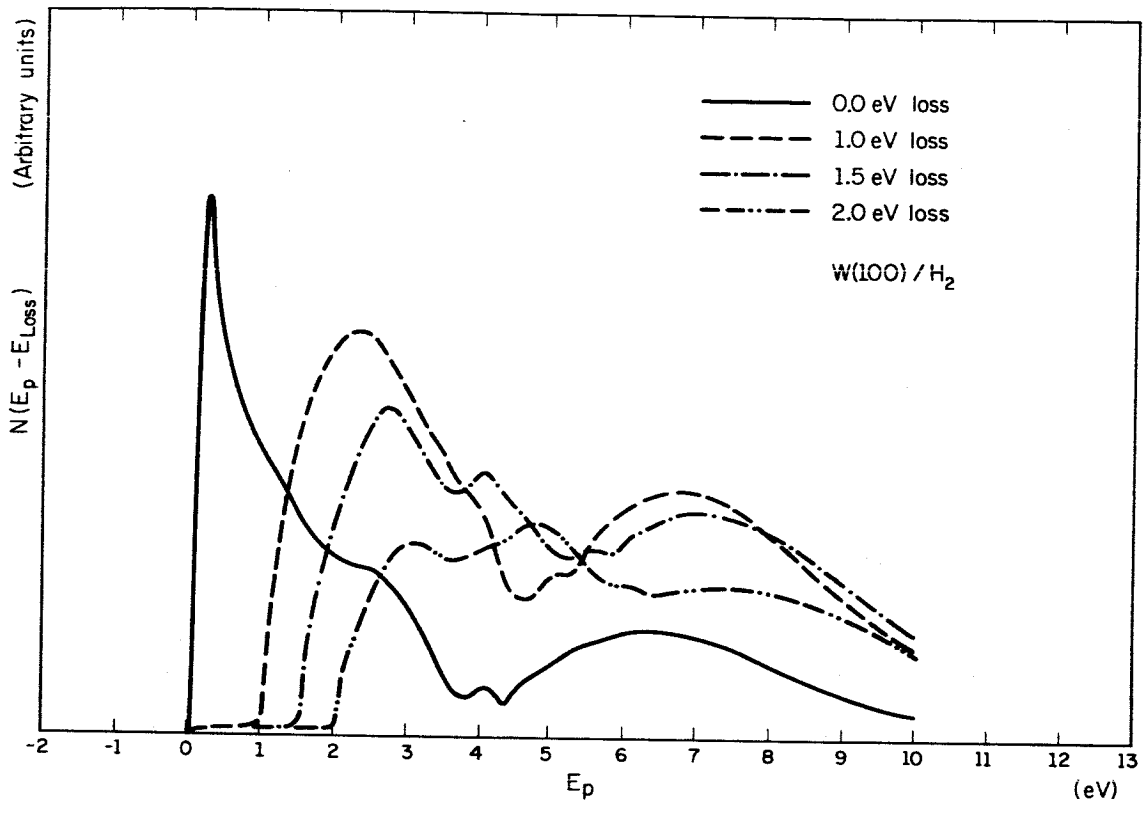

Fig. 2.21. Plot of the Number of Electrons Produced with 0.0, 1.0, 1.5, and 2.0 eV Kinetic Energy Less than the Primary Kinetic Energy Plotted as a Function of the Primary Energy. The data presented are for the (100) tungsten surface after exposing the surface to H_2.

2.2 Study of the Adsorption of Cases on Metals by the Auger Process

2.2.1 Introduction. Much of the work that has been done on the adsorption of gases on metallic surfaces has suffered from the inherent limitations of the standard methods. A technique for determining to coverage, θ, the fraction of the adsorption sites which are filled by gas atoms, is required.

When gas is adsorbed on the surface, there is a realignment of the electronic bonds on the surface metal atoms. The resulting change in work function, closely related to θ, may then be measured by many methods, all of which are rather difficult. Field emission studies have given direct, but difficult to reproduce, information about adsorbed surface atoms. Electron diffraction also has been successfully used; however, this technique fails when the scattering factor of the adsorbed species is much smaller than that of the substrate, or when the adsorbed gas replicates the crystallographic structure of the substrate.

One of the most commonly used techniques is the flashing of a metal filament to drive off the adsorbed gases and then measuring the consequent pressure rise within the system.[3] This method requires extreme precautions in relating the pressure rise to θ. Furthermore, as long, thin filaments are used, specific crystalline faces are not available. Since field-ion-microscope studies indicate that the

---

[3] Ehrlich, J. Chem. Phys. 34, 29 (1961).

adsorption of gases has different characteristics on the different crystal faces, this method leaves many questions unanswered.

Migration of the gas atoms from the end of the filament when desorptive heating has begun can also decrease the amount of gas evolved, thus decreasing the value obtained for the desorption constant.

We intend to use the Auger process (emission of electrons by low energy incident ions) to measure the degree of surface coverage. In the clean surface case, He^+ ions incident on a metal interact with two electrons from the metal's conduction band. One of the electrons drops into the empty level, neutralizing the He^+ ion, and the other adsorbs the energy released in the process, ultimately being ejected from the metal in about one-fourth of the cases. The ratio

$$\gamma = \frac{\text{electrons ejected}}{\text{incident ions}}$$

is called the "Auger yield." Propst[4] has suggested that when gases are adsorbed on the tungsten, the secondary electrons attempting to escape the metal are scattered back into the metal with a probability dependent on the coverage. Experimentally, θ is found to decrease almost linearly with increasing coverage until there is about one monolayer of adsorbed gas on the surface.

Thus, an observation of γ gives a direct and sensitive measure of θ, since the amount of high energy secondaries may decrease by a factor of three or more with adsorption of one monolayer of gas. Since

---

[4] F. M. Propst and E. Lüscher, Phys. Rev. 132, 1037 (1963).

only a small area of tungsten need be observed, it is possible to use single crystal material.

The apparatus shown in Fig. 2.22 is now under construction. Basically, we will use an electron impact helium ion source, leading to a cylindrical lens which focuses the ions onto the target. The target is a single-crystal tungsten ribbon mounted on two heating leads which pass directly into a liquid nitrogen cooling bath. If the ion current is held constant by a feedback loop to the ion source, then γ is directly proportional to the current from the collector electrode.

The simple model of desorption process is analagous to the problem of a particle vibrating with a frequency ν in a potential well of depth E_B. An approximation to the escape probability will be

$$\beta(T) = \nu e^{-E_B/kT} .$$

If there are several possible types of bonding wells available on the surface as is suspected,

$$\beta(T) = \sum_i \nu_i e^{-E_{Bi}/kT} .$$

We will illustrate the experimental technique by considering desorption of a monatomic gas from the surface. First we flash the target clean and allow it to cool at time t_o (Fig. 2.23). At time t_1 the target has cooled, so that gas can be admitted, and the target exposed until the coverage increases to θ_o and the change in yield is $\Delta\gamma_o$. The gas flow is stopped at t_2. At time t_3 the target temperature is increased to temperature T_1 or T_2 so that thermal desorption begins.

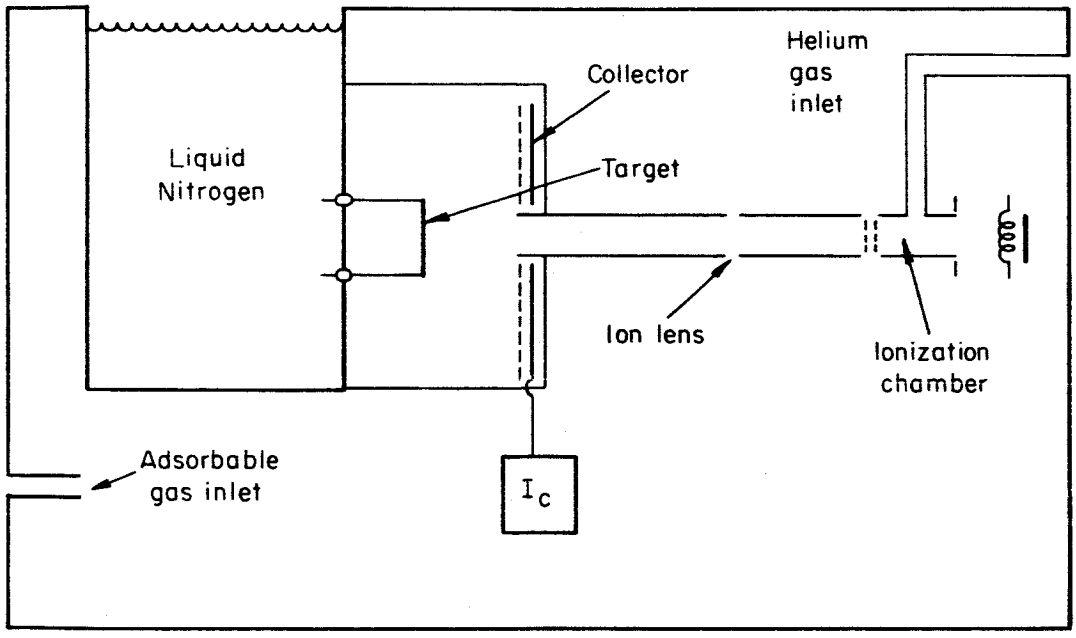

Fig. 2.22. Schematic of Adsorption-Desorption Experiment.

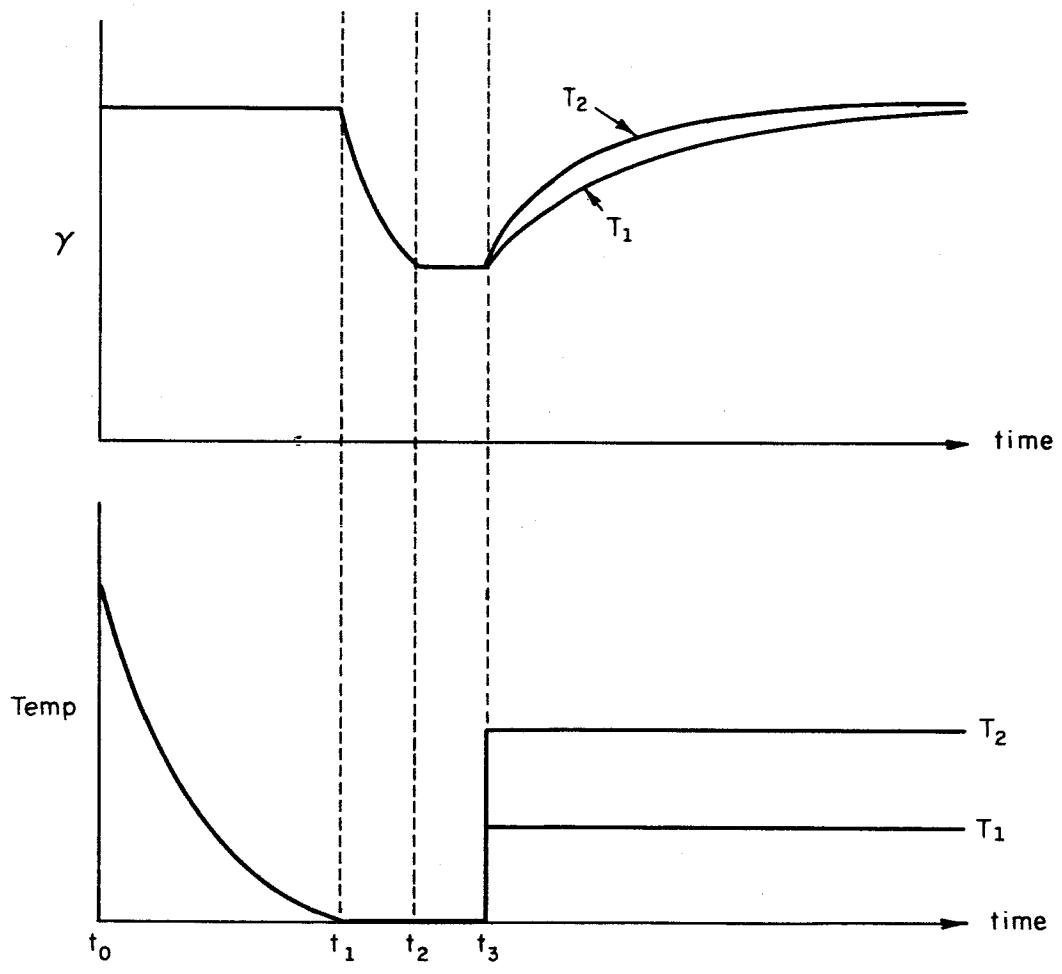

Fig. 2.23. Schematic Illustrating the Principle of One Mode of Procedure of the Adsorption-Desorption Experiment.

As desorption continues, the values of the yield in both cases approach the clean surface value. We define the desorption coefficient $\beta(T)$ in this case by the equation

$$\frac{d\theta}{dt} = -\beta(T)\theta$$

so that

$$\beta(T) = (1/t)\ln(\theta_o/\theta) = (1/t)\ln(\Delta\gamma_o/\Delta\gamma) \ .$$

Thus by plotting $\ln(\Delta\gamma_o/\Delta\gamma)$ versus t, we can find β from the slope. Non-linearities in the slope will reveal complexities in β, such as the small variation of β with θ.

This plotting procedure gives us one value of $\beta(T)$. By repeating the operation for a range of temperatures, T_1, T_2, $\cdots$, we will be able to construct the behavior of β with respect to T, and check with the simple model we have used to determine E_B and ν. We hope to be able to determine the number of bonding states and their energies from this information.

Finally, we note that this technique can be applied to various types of desorption, such as electron impact desorption, photo-desorption, and ion sputtering.

2.2.2 Experimental Apparatus. The system indicated schematically in Fig. 2.22 has been constructed and initial tests performed. An ion gun and feedback arrangement to hold the ion current striking the target has been developed. A schematic of this system is shown in Fig. 2.24. The operation is as follows.

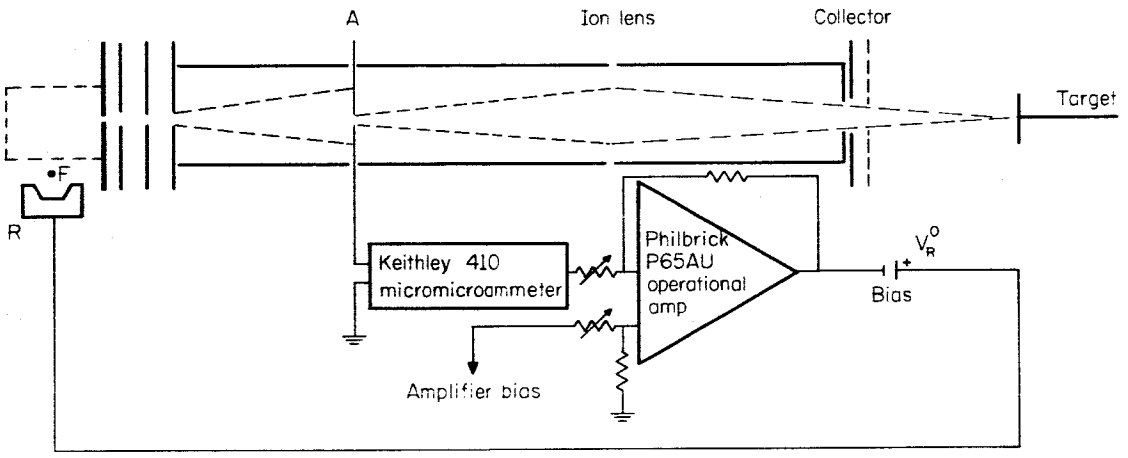

Fig. 2.24. Ion-Current Control System.

The potential V_R of the electron-focus electrode controls the emission current from the filament F and the trajectories of the electrons into the ionization region; hence, it may be used to control the total ion current. A constant freaction of these ions moving toward plate A pass through its aperture and are focused onto the target. A plot of the relationship between V_R and I is shown in Fig. 2.25.

When the system is operating in the feedback mode--say at operating point P corresponding to an ion current I^o and an electron focus potential $V_R{}^o$--a momentary increase in ion current causes an increased electrometer-output voltage. Thus, a larger voltage is applied to the negative input of the operational amplifier, pushing the amplifier out of its balanced state and giving a negative instead of a zero output voltage. This negative voltage will drop the focus-electrode voltage from its steady-state value, thereby reducing the ion current and bringing the amplifier back into balance. A momentary decrease in ion current produces the converse result.

Using this system, we have observed runs of many hundreds of seconds during which the ion current was constant to better than one per cent.

The vacuum system has achieved pressures in the 10^{-10} Torr range. A quadrupole mass analyzer was used to obtain partial-pressure measurements of the residual gases in the system. Figure 2.26 shows a typical spectrum taken after a light bakeout (250^oC) and an outgassing of both the Bayard-Alpert gauge and the analyzer. Peaks at 18 due to

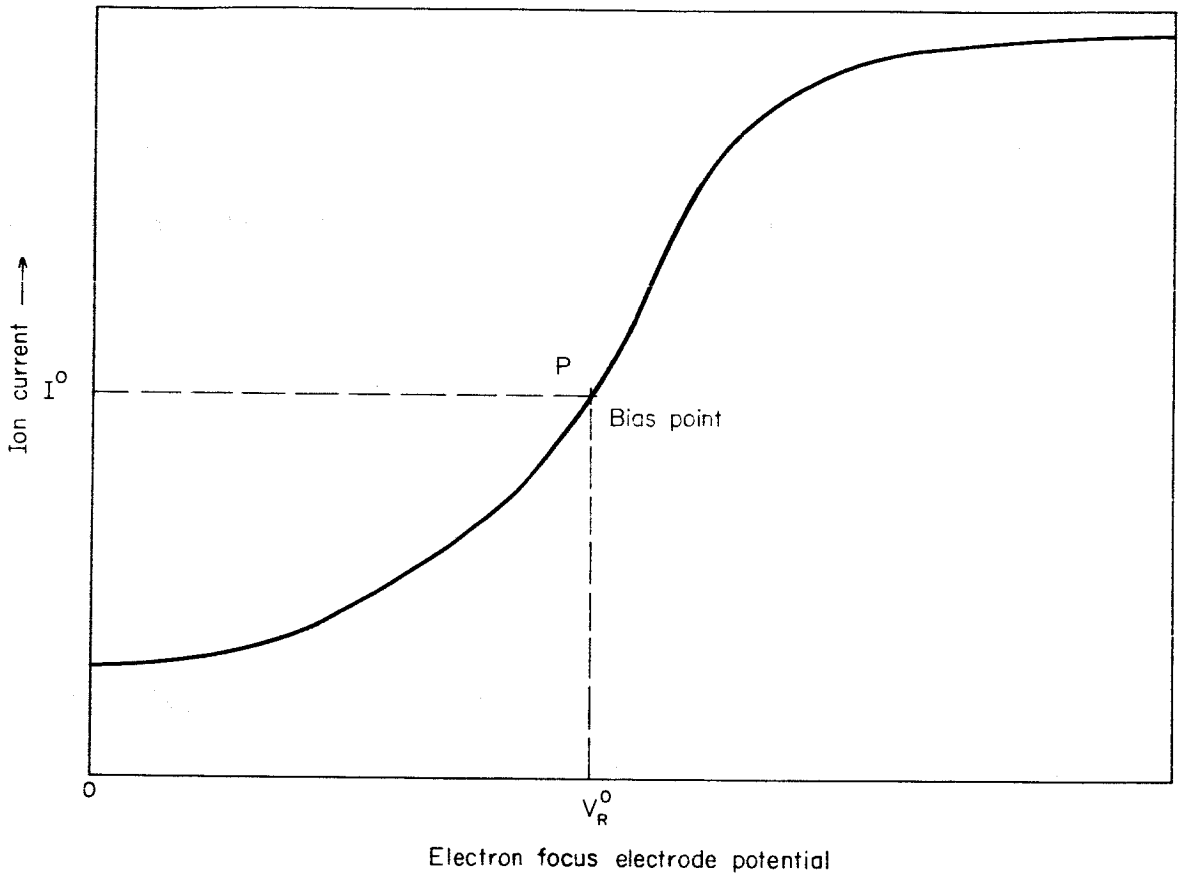

Fig. 2.25. Ion Current versus Electron Focus-Electrode Potential.

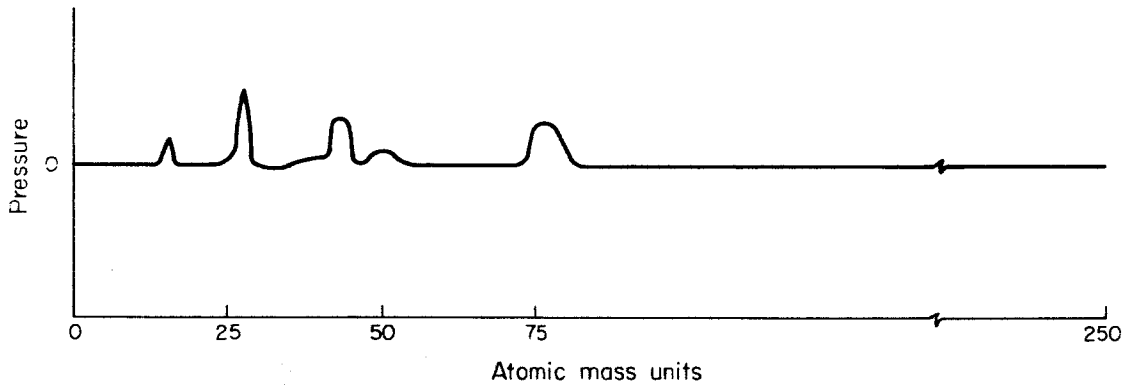

Fig. 2.26. Typical Mass Spectrum of Residual Gases.

H_2O^+, at 28 due to CO^+ and N_2^+, and at 44 due to CO_2^+ are apparent. Background pressure was about 3×10^{-9} Torr. Since our system is pumped with DC-705 oil, it is possible that the peak at 78 is due to C_6H_6, as observed by Gosselin and Bryant.[5]

After removing the mass analyzer and baking to 450°C, the system pressure went down to less than 8×10^{-10} Torr in a few days. After some weeks of operation, the pressure dropped to below 4×10^{-10} Torr.

Considerable difficulties have been encountered in the feed-through of this system. Relatively major repair and redesign has been required. Once these changes are made, initial measurements should be possible immediately.

---

[5]C. M. Gosselin and P. J. Bryant, J. Vac. Sci. Technol. 2, 293 (1965).

2.3 Angular Distribution of Auger Electrons

Although the Auger neutralization effect[6] has been studied extensively during the last few years, a number of important questions still remain unanswered. Among these are:

(1) What is the angular distribution of ejected electrons?

(2) To what degree does the interaction between Auger and conduction band electrons influence the effect?

(3) To what degree does the crystal structure influence the effect?

(4) How does the effect depend on the angle of incidence of the ion beam?

An apparatus is being designed to perform three types of surface studies on a given crystalline surface in-situ. The three measurements are:

(1) Auger neutralization

(2) Electron diffraction

(3) Secondary electron emission.[7]

It is hoped the correlation of these three types of measurements will provide definitive answers to the above questions. This study, in conjunction with the experiments described in the previous

---

[6] F. M. Propst and E. Lüscher, Phys. Rev. 132, 1037 (1963); and H. D. Hagstrum, Phys. Rev. 89, 244 (1953); Phys. Rev. 96, 336 (1954); Phys. Rev. 104, 1516 (1956); Phys. Rev. 122, 83 (1961).

[7] H. Bruining, Physics and Applications of Secondary Electron Emission (Pergamon Press, New York, 1954).

sections, should also provide a more coherent picture of surfaces and surface interactions.

The apparatus is shown schematically in Fig. 2.27. Low energy (< 200 eV) ions or electrons impinge on a single crystal, tungsten target.[8] The scattered or ejected electrons pass through a slot in the shield and are collected by a collector of the Faraday cage or other design. Two grids attached to the collector make possible the direct measurement of the energy distribution of the ejected electrons. This is accomplished by modulating the ejected electron beam and using an AC detection technique.

The azimuthal angle, φ, is varied by rotating the target. The latitudinal angle, θ, is varied by rotating the collector. In the configuration shown in Fig. 2.27, interference between the ion gun and collector makes measurement of the distribution impossible for approximately 15° of the latitudinal angle. If it is found that the angular distribution does not depend significantly on the angle of incidence of the ion beam, a second experimental configuration will be used. In this configuration the impinging ion or electron beam will be at an angle of about 15° relative to a line normal to the target surface. With this arrangement, it will be possible to measure the ejected electron intensity over the entire 2π steradians. A rotary-motion feedthrough to be used for Faraday cage and tungsten target is described under Section 5.4.

---

[8] G. Tibbetts and F. M. Propst, Rev. Sci. Instr. 34, 1268 (1963).

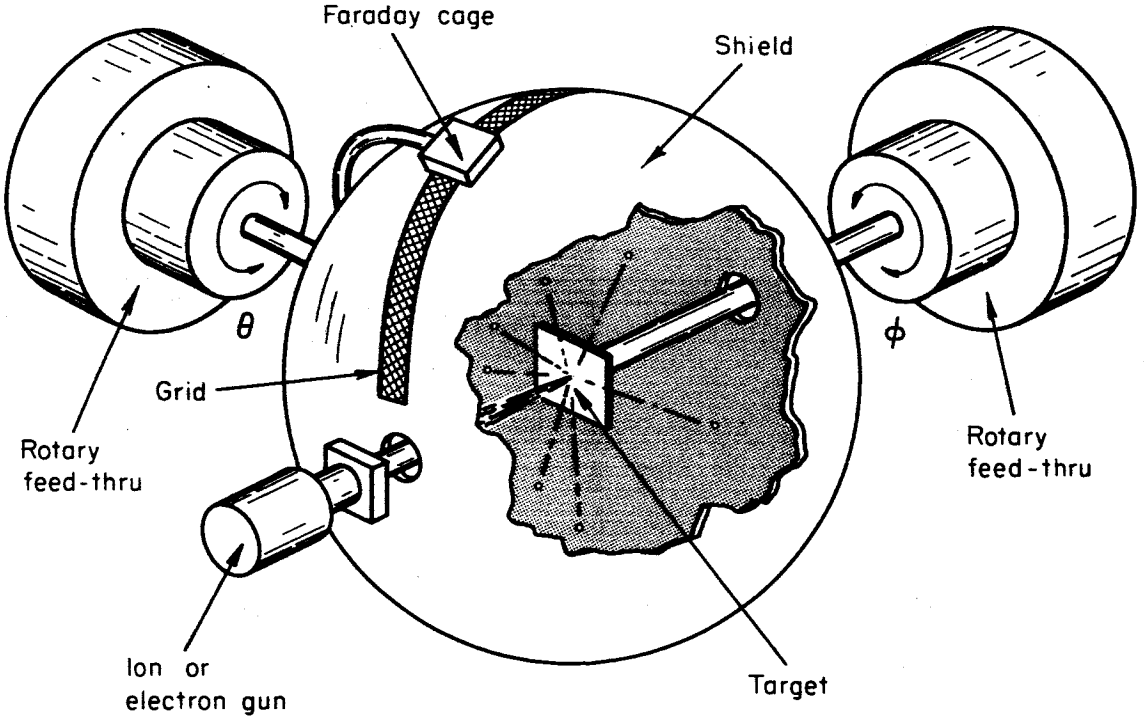

Fig. 2.27. Schematic of Angular Distribution Experiment.

The vacuum chamber, target assembly, collector assembly, and ion gun for this system have been completed. Pressures in the low 10^{-10} Torr region have been achieved. Initial tests of the complete system should be feasible in the next two months.

3. A SURVEY OF GROUPS AND INSTRUMENTATION CONCERNED WITH MEASUREMENT OF THE NEUTRAL COMPOSITION OF THE UPPER ATMOSPHERE (1963)

3.1 Introduction

One of the most important and challenging research efforts in the field of aeronomy at the present time is the measurement of the neutral and ion composition of the upper atmosphere. In the following section we shall restrict ourselves to the discussion of neutral composition measurements.

The first attempt to measure the atmospheric composition with a mass spectrometer was made by Townsend and co-workers[1] in 1953. A Bennett mass spectrometer[2] was flown in an Aerobee rocket over White Sands with the objective being to measure diffusive separation of atmospheric constituents by monitoring the N_2/A ratio as a function of height. No diffusive separation was detected, but a number of error sources made the interpretation of the data rather unreliable. Despite this shortcoming, it was the first demonstration of the use of a mass spectrometer in a rocket experiment. An improved Bennett spectrometer was flown by the same group in 1956 and 1958 over Fort Churchill.[3] In these flights evidence for diffusive separation at altitudes of 120 km was obtained, as well as qualitative data on the upper atmospheric composition.

---

[1] Rocket Exploration of the Upper Atmosphere, ed. by Boyd, Seaton, and Massey, Interscience Publishers, 1954.

[2] J. W. Townsend, Jr., Rev. Sci. Instr. 23, 538 (1952).

[3] J. W. Townsend, Jr., et al., A of the IGY 12, 431 (1960).

Around the same time (1959), similar experiments were conducted in the Soviet Union by Pokhunkov,[4] who also used a Bennett spectrometer. These flights revealed a number of typical difficulties that are encountered in the analysis of the neutral atmosphere. The following error sources can be identified:

1. No precautions were taken to discriminate against backstreaming gas entering the ionization region and becoming ionized. Consequently, it is very difficult to determine the true ambient pressure from the ion currents.
2. As a direct consequence of (1), sizeable contributions from outgassing were recorded. Some recorded mass numbers like H_2O, CO_2, and NO were attributed entirely to outgassing and secondary reactions taking place in the spectrometer.
3. No precautions were taken to prevent atomic oxygen from hitting surfaces prior to entering the ionization region. Hence, a substantial recombination of atomic oxygen might have occurred.
4. The use of low energy ionizing electrons (36 eV) introduces a considerable uncertainty in the absolute values of the neutral concentrations, because the ionization cross sections are very sensitive to energy in this range. The use of low energy ionization energies is, of course, motivated by the desire to prevent multiple ionizations. It

---

[4]Pokhunkov, Planet. Space Sci. 9, 269 (1962); Planet. Space Sci. 11, 441 (1963).

may be questionable, however, if the uncertainty in the ionization probability is not larger than the contribution of doubly ionized ions, a contribution which, moreover, can be taken into account.

The remaining part of this section will be devoted to a discussion of current efforts on the mass spectrometric measurements of neutral composition. Since most of these efforts are not yet available in the open literature, visits were arranged to the main laboratories that are actively engaged in this field or, in some cases, private discussions were conducted with scientists working in this area.

3.2 High Altitude Engineering Laboratory, Department of Aeronautical and Astronautical Engineering, University of Michigan, E. J. Schaefer

This group started to develop a mass spectrometer for use in sounding rockets in 1958. The instrument is a quadrupole mass spectrometer[5] designed to measure the neutral composition at altitudes above 100 km where no differential pumping is required. The quadrupole mass spectrometer was given preference over a magnetic one because it is lighter, simpler in construction, easier to incorporate into a payload and within generous limits insensitive to pressure and initial energy of the ions.

---

[5] W. Paul et al., Z. fur Naturf. 8a, 448 (1953); W. Paul and M. Raether, Z. fur Physik 140, 262 (1955); and W. Paul et al., Z. fur Physik 152, 143 (1958).

The main parameters of the instrument are

Length: 12.75 cm and 17.8 cm

Field radius: 0.52 cm

Aperture: 0.081 cm diameter with an acceptance angle of 5.25^{o}

Frequency: 2.39 mc

rf voltage: 500 V at mass 40

Resolution $M/\Delta M = 40$

rf power: 3 watts.

The ion source operates with an electron emission current of 0.4 and 4 ma at 45 V. 45 V is also the acceleration potential for the ions. The filaments are rhenium; the electrical structure of the ion source is gold-plated to reduce as much as possible the recombination of atomic oxygen.

The separated ion current is detected with an electrometer of 10^{-12} amp sensitivity at a 5 ms time constant. In conjunction with the ion source this corresponds to a partial pressure of 10^{-7} Torr. The scan rate is 1/sec and 2/sec. Two modes of scanning are employed. In the first mode, the rf voltage is varied, keeping the ratio of dc-to-ac voltage, and thus the width of the stable region constant. This results in a line-type mass spectrum. In the second mode, the dc voltage is switched off. This results in an integrated mass spectrum in the sense that for a given rf voltage all masses greater than M_o reach the collector.

In order to keep contamination from the rocket to a minimum, the mass spectrometer package is ejected from the rocket at an appropriate altitude. Most of the previous failures during firings were due

to a malfunctioning of this ejection mechanism rather than to a failure of the mass spectrometer itself.

To date, two successful flights have been performed in 1962 and 1963.[6] In the first flight data were collected on the neutral composition for 100-130 km; in the second flight, the range was increased to 190 km. For the evaluation of the data on the atomic oxygen concentration it was assumed that the cross section for ionization of atomic oxygen is the same as that for molecular oxygen.[7] Some uncertainty existed as to the exact energy of the ionizing electrons. There was reason to suspect that the actual electron energy was somewhat lower on 45 V due to space charge effects. The contribution of dissociative ionization of O_2 to the O^+ ion current was determined experimentally in the laboratory, and a value of four per cent O^+ from O_2 for 45 V was obtained. In view of the low electron energy of 45 V and the uncertainty in this value, the comments made earlier on the use of low electron energies for the ion source apply.

---

[6] Schaefer and Nichols, COSPAR IV. International Space Science Symposium, Warsaw, Poland (June 1963); Schaefer, J. Geophys. Res. 68, 1175 (1963).

[7] W. L. Fite and R. T. Brackmann, Phys. Rev. 113, 815 (1959); E. W. Rothe, et al., Phys. Rev. 125, 582 (1962).

3.3 Space Physics Laboratory, Department of Electrical Engineering, University of Michigan, G. R. Carignan, Nagy, Niemann, Taeusch

Among various other projects that lie outside the scope of this survey, a very interesting method has been designed to measure the temperature of the neutral gas in the upper atmosphere.

This method uses an omegatron tuned to N_2. From the shape of the mass-line, the temperature of N_2 can be deduced. The same information could, of course, be obtained from the line shapes in magnetic deflection instruments and actually reaction energies between molecular species have been measured in this way, but this would be much more difficult in a rocket experiment than by using an omegatron. Since only one mass number is monitored, the usual difficulties associated with the use of omegatrons as mass spectrometers or partial pressure analyzers are to a great extent eliminated.

It is planned to use the omegatron, however, for the measurement of neutral gas composition in the lower atmosphere, but no flights have been performed so far.

3.4 Bell & Howell Research Center, Pasadena, California, W. M. Brubaker

Two quadrupole mass spectrometers have been developed which will be referred to as BH I and BH II. BH I is a small spectrometer designed for A. F. C. R. L. in cooperation with R. Narcisi for the measurement of neutral and ion composition in the region from 70 km up. The high ambient pressure in the D region necessitates the use of differential pumping techniques to maintain a low enough pressure in the

mass spectrometer ($\sim 10^{-4}$ Torr). This is achieved by the use of a liquid nitrogen-cooled zeolite trap that acts as a cryogenic pump with an equivalent pumping speed of the order of 100 liters/sec at 10^{-4} Torr and 50 liters/ sec at 10^{-3} Torr.

The instrument itself has the following characteristics

Length: 7.6 cm

Field radius: 0.38 cm

Aperture: 0.038 cm diameter

rf voltage: 310 V at mass 44

Frequency: 6 mc

rf power: 4.5 watts

Acceleration voltage: 125 V

Resolution: 10% between peaks at mass 16

Ion source: Current 0.5 ma; Voltage 235 V.

The choice of a higher acceleration voltage for the ionized electrons makes the cross section for ionization much less sensitive to the electron energy than in Schaefer's design.

The electrometer has a logarithmic response from 10^{-12} to 10^{-7} amps with a time constant of 10 milliseconds. The ion source is designed to have a high sensitivity to incoming molecules, but a very low sensitivity to backstreaming gas. The instrument has had one successful flight so far.

BH II is a quadrupole mass spectrometer for use in satellites. It is 25.4 cm long and has a field radius of 1.52 cm. It is designed as an ion mass spectrometer; no ion source is provided in flight. No actual flights have been performed.

3.5 Consolidated Systems Corporation, Monrovia, California, L. Hall

Three different mass spectrometers for neutral composition measurement have been designed or are under design at CSC:

1. A double focusing magnetic spectrometer that is presently being flown on Explorer XVII;
2. A quadrupole spectrometer for use in sounding rockets;
3. A quadrupole spectrometer for the measurement of the martian atmospheric composition.

1. The double focusing instrument uses magnetic and electric deflection techniques in order to focus ions of different energy onto the collector. In this instrument transverse energies of 12 eV can be accepted. The ion source operates at a voltage of 45 V and 0.5 ma emission current. The minimum detectable partial pressure is of the order of 10^{-11} Torr. This high sensitivity is achieved through the use of long integration times in the electrometer. The scan rate is thus limited to 1/min which is short enough for satellites. Preliminary results for Explorer XVII indicated that excessive amounts of O_2 were detected, an effect which was tentatively attributed to an outgassing of the titanium electrodes used in the ion source.

2. The quadrupole spectrometer is still in the developmental stage. The main characteristics are

Length: 20.2 cm

Field radius: 0.75 cm

Aperture: 0.05 cm diameter

rf voltage: 400 V

Frequency: 1.3-3.0 mc

Resolution: 1% between peaks at mass 20

Acceleration voltage: 20 V.

The ion source has a sensitivity of 10^{-4} amp/Torr and operates with an emission current of 0.5 ma. Contrary to the previously described quadrupole spectrometers, this instrument utilizes a frequency scan rather than a voltage scan. The frequency is varied in steps, corresponding to discrete, preselected mass numbers. This requires that the rf voltage is kept constant during the scan and feedback regulation must be provided. Great care has been taken to assure that the mass peaks are flat-topped, so that abundance ratios can be measured reliably. This condition is realized for entrance angles of $\pm 3^{o}$.

3. The martian atmosphere instrument is similar to the previous one, except that it is six inches long and has a field radius of 0.5 cm. The discrete frequency scan has a great advantage for this model, because it results in a considerable saving in telemetry bandwidth, which is an important factor in the transmission of data over interplanetary distances.

3.6 Geophysics Corporation of America (GCA), Bedford, Massachusetts, R. F. K. Herzog, F. F. Marmo

A helium mass spectrometer is being developed which utilizes two 90^{o} magnetic deflection sectors in order to reduce scattered ion currents and make the measurement of extremely low helium concentrations feasible. The objective of this instrument is to measure the

helium-to-argon abundance ratio in order to determine accurately the diffusive separation. The instrument is to be flown in an Aerobee rocket, but no actual flight has been performed so far.

3.7 University of Minnesota, Minneapolis, Minnesota, A. O. Nier.

A small double focusing magnetic mass spectrometer was developed at the University of Minnesota for possible use in rocket flights.[8] This instrument, together with a small 90° magnetic spectrometer, was flown successfully in June, 1963.[9] A vac-ion pump is incorporated into the payload to provide differential pumping. Although the filament of the double focusing instrument failed in flight, the single focusing instrument gave a wealth of data. Although the results have not yet been published, the preliminary data presented at the Aeronomy Conference in Urbana indicated that these are probably the best data obtained so far in the range 95-200 km.

3.8 Conclusions

As indicated earlier, this activity must be considered an attempt on the part of this laboratory to become directly familiar with the many efforts in this field. Most of the activity in this direction consisted of reviewing the literature and making visitations to a number of the most active programs in this country's aeronomy effort. It was

---

[8] A. O. Nier, et al., Rev. Sci. Instr. 31, 1127 (1960).

[9] A. O. Nier, et al., Conference on Direct Aeronomic Measurements in the Ionosphere, October 1963, Urbana, Illinois.

our experience that the visits and conversations had a beneficial effect well beyond the collection of information. Most of the scientists visited seemed to welcome the opportunity to exchange views as well as information and found it easy to do so with a group whose objectives were in no sense competitive or directly overlapping their own. Thus, in an important sense, an integration and exchange process seemed to be taking place in the course of this acquisition of information.

It is apparent from the previous discussion that a number of difficulties are encountered when mass spectrometers are used for the measurement of the neutral composition in rockets and satellites. Several of these difficulties can be avoided or eliminated by a careful design of the mass spectrometer and the payload. The measurements by Nier are probably a good example of the elimination of problems through careful engineering.

There are, however, more basic problems that require additional work in the laboratory. Some of these are

1. More data are needed on ionization cross sections, in particular for low energies and atomic species. Cross sections for double ionization are needed for almost all atmospheric constituents.
2. More information is needed on the interaction of atomic oxygen with surfaces.
3. Data on the interaction of high energy neutral molecules with surfaces should be obtained in order to get more reliable values for the accommodation coefficients.

4. Theoretical and experimental studies on the hypersonic flow around rockets and its influence on the sampling of neutral particles and ions are necessary for the proper interpretation of data at low altitudes.

4. PUMPING SPEEDS OF GETTER-ION PUMPS AT LOW PRESSURES

4.1 Introduction

Getter-ion pumps have been used for about 10 years to obtain low pressures. It is well known that the pumping speed of these pumps is fairly constant over the pressure range from 10^{-4} to about 10^{-8} Torr. For small pumps, no data have been published on their pumping speed below 10^{-8} Torr. Rutherford[1] measured discharge intensities I/P (I = pump current, P = pressure) down to 10^{-11} Torr. From the assumption that the number of molecules or atoms pumped per electric charge (PS/I) is a basic property of the pump and independent of pressure, he calculates the pumping speed, S, from the discharge intensity I/P. Klopfer[2] and Davis[3] estimated S from the pressure rise after turning off the pump at very low pressures.

Saturation in getter-ion pumps has been observed by several authors.[4,5] We know of no work in which pumping speeds at constant pressure have been measured as a function of time. Under non-equilibrium

---

[1] S. L. Rutherford, Trans. AVS Vac. Symp. 10, 185 (1963).

[2] A. Klopfer, Vacuumtechnik 10, 113 (1961).

[3] W. D. Davis, Trans. AVS Vac. Symp. 9, 363 (1962).

[4] N. Milleron and F. S. Reinath, Trans. AVS Vac. Symp. 9, 356 (1962).

[5] W. A. Grant and G. Carter, Vacuum 15, 477 (1965).

conditions, e.g., pumpdown of a system, it is difficult to separate the influence of the rest of the system from that of the pump.

The first goal of this work was to measure S and I/P for a small getter-ion pump down to very low pressures for different gases. The second goal was to study saturation effects by measuring the pumping speed as a function of time at constant pressures for a diode- and a triode-type pump.

4.2 Method and Apparatus

The pumping speed was measured with the two-gauge method[6] (pressure drop along a known conductance). Figure 4.1 shows the apparatus schematically. The formulas are:

$$S_m = G_1 \cdot \frac{P_1 - P_2}{P_2 - P_0} \simeq G_1 \cdot \left(\frac{P_1}{P_2} - 1 \right) \quad \text{if } P_2 \gg P_0 \,, \tag{4.1}$$

$$\frac{1}{S} = \frac{1}{S_M} - \frac{1}{G_2} \tag{4.2}$$

where S_M = measured pumping speed at Gauge Two (P_2),

S = pumping speed of getter-ion pump taking into consideration conductance G_2,

G_1 = conductance between Gauge One and Gauge Two,

G_2 = conductance between Gauge Two and pump,

P_1, P_2 = pressures in Gauge One and Gauge Two, respectively,

P_0 = ultimate pressure of pump as measured by Gauge Two.

---

[6] L. A. Landfors and M. H. Hablanian, Trans. AVS Vac. Symp. 5, 22 (1958).

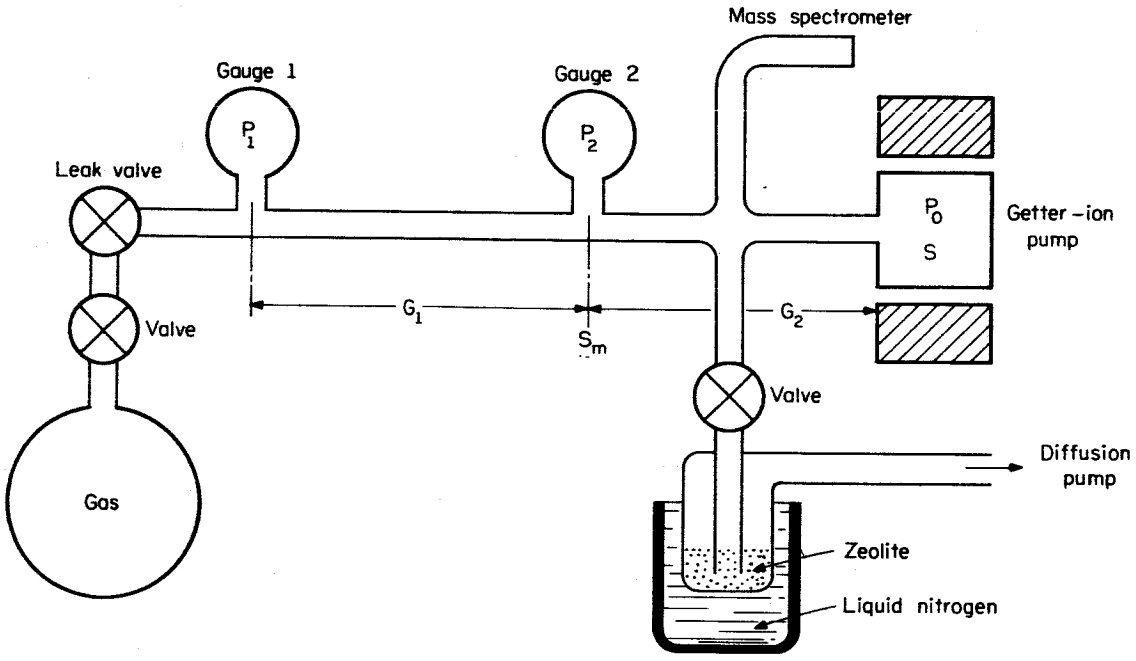

Fig. 4.1. A Schematic Representation of the Vacuum System Used for Pumping Speed Experiments.

The pumps used in this experiment were commercial diode and triode getter-ion pumps. The diode, which was rated at 15 ℓ/sec for nitrogen, was operated at 7.2 kV in a magnetic field of 1400 Gauss. The triode was rated at 8 ℓ/sec. The voltage for the triode was 5 kV, the magnetic field 1350 Gauss.

The vacuum system (Fig. 4.1) was made from Pyrex glass (Corning 7740) and had a volume of about two liters. A two-stage fractionating oil-diffusion pump (CVC GF-20), filled with Monsanto OS-124 oil, pumped the system to very low pressures before the getter-ion pump was started. An optically dense zeolite trap filled with Linde 13 X molecular sieve at liquid nitrogen temperature prevented backstreaming oil from getting into the system. A one-half inch Granville-Phillips valve separated the trap and diffusion pump from the rest of the system during the pumping speed measurements. This valve was also necessary for proper system processing (see below). With this valve closed, it was possible to open the rest of the system up to air with the diffusion pump running. Total pressure measurements were made with Bayard-Alpert gauges (WL-5966) and, in some cases, with Schuemann photocurrent suppressor gauges.[7] Partial pressure measurements were made with a 90° magnetic deflection type mass spectrometer.[8] Gas was admitted from one liter Linde flasks through a one-half inch Granville-Phillips valve and a leak valve. The latter was

---

[7] W. C. Schuemann, Rev. Sci. Instr. 34, 700 (1963).

[8] W. D. Davis and T. A. Vanderslice, Trans. AVS Vac. Symp. 7, 417 (1960).

operated by a Granville-Phillips automatic pressure controller which kept the pressure constant within a few percent.

System processing followed the procedure described by Singleton and Lange.[9] After any glassblowing, the part of the system which was exposed to air was first roughed with a forepump. When the system was at $\sim 10^{-3}$ Torr, the pump was sealed off and the valve to the diffusion pump was opened for a few hours. Then the valve was closed again and the trap baked for about four hours at 350°C. The valve and the glass tubing between valve and trap were kept at 150°C. After bakeout, the trap was immersed in liquid nitrogen, the valve opened, and the system baked for half a day at 350°C. The gauges were then outgassed at 50 watts grid bombardment power for about six hours. Again the valve was closed, the trap baked as before and then cooled again. The pressure dropped to the low 10^{-11} Torr range within an hour after opening the valve. The getter-ion pump was finally started and the valve to the diffusion pump closed.

Pumping speeds at constant pressure were recorded over a period of one day. After every measurement, the system was processed. The whole pressure range ($\sim 10^{-11}$ Torr to 10^{-6} Torr) was investigated by changing the pressure in steps of a factor three or four.

In general, no attempt was made to regenerate the pump before a pumping speed measurement except to bake it. When pumping helium for one day at pressures of 10^{-7} Torr or higher, however, strong

---

[9] J. H. Singleton and W. J. Lange, J. Vac. Sci. Technol. 2, 93 (1965).

saturation was found. After the pumping speed measurement with helium, the pump was bombarded with nitrogen for one hour at a pressure such that 50 watts power was dissipated. During this bombardment the valve to the diffusion pump was kept open. After this discharge cleaning followed by bakeout, the re-emission of helium was seen to be very low even during pumping of another gas. The cleanup process and the behavior of the pump afterward was followed with the mass spectrometer.

Current measurements for the diode pump were made on the ground return side. A shielded box with batteries provided 7.2 kV. The cable to the pump was double shielded Under low humidity conditions, the leakage current with the pump electrically connected was below 1×10^{-12} A. For currents larger than a few microamperes, a regular pump power supply was used.

Field emission currents in the triode pump reached values of a few hundred microamperes. It was impossible to subtract these currents because they changed rapidly. The diode showed field emission up to a few microamperes, but only when pumping nitorgen, and even in this case only occasionally. A straight line on a Fowler-Nordheim plot was considered a clear indication of field emission. In the diode pump the whiskers responsible for field emission could be flattened by application of an overvoltage of 20 to 25 kV. To get still lower field emission currents, nitrogen was admitted at 10^{-5} Torr with the overvoltage applied. Short starting times in the presence of field emission were observed at low pressures due to the abundance of electrons.

The two-gauge method requires only pressure ratios to be measured. No absolute pressure calibration was therefore made. Gauge Two was our standard, and the sensitivity of Gauge One compared to Gauge Two was determined with helium over a wide pressure range. The difference in sensitivity never exceeded 10 per cent and was taken into account for the pumping speed calculations. The conductance to the gauges was increased to about 15 ℓ/sec for nitrogen by attaching a one inch tubulation to them. Ion currents in the gauges were measured with Keithley micromicroammeters which were accurate within a few per cent as compared with a constant current source. The difficulties of measuring hydrogen pressures with hot filament ionization gauges are enumerated in several papers by Hickmott.[10] An enhanced pumping rate for hydrogen was observed in the presence of a hot filament ($T > 1100^{o}K$) due to dissociation of hydrogen. The pumping speed of glass or metal walls for atomic hydrogen is very large. To avoid dissociation, low temperature filaments have to be used in gauges. Unfortunately, the ion gauges used for these measurements had only regular tungsten filaments. The emission current in the gauges was held at 1 mA for the hydrogen measurements compared to 10 mA for nitrogen and helium. Pumping speed measurements for the clean system with the pump current off showed values of about one ℓ/sec for hydrogen and .15 ℓ/sec for nitrogen for times up to one day and at different pressures. These values were

---

[10] T. W. Hickmott, J. Vac. Sci. Technol. 2, 257 (1965). This article gives a number of references.

subtracted from the results obtained with the pump current on. The system was allowed to reach an equilibrium before measurements were made.

The conductance G_1 was .5 ℓ/sec, and G_2 about 15 ℓ/sec for nitrogen. The error in determining these values is less than 10 per cent for G_1, less than 20 per cent for G_2. As can be seen from formula (4.2), errors in G_2 have an influence on S if S_M is of the same order of magnitude as G_2. This is the case only for nitrogen. The overall error in the calculation of S is estimated to be less than 30 per cent.

4.3 Results

The values for pressure, P, and pumping speed, S, in this paragraph always mean the values inside the pump.* Pressures are the actual pressures for the different gases (not nitrogen equivalent).

In Fig. 4.2, I versus P curves for the diode pump are given for the gases hydrogen, helium, and nitrogen. The slope is practically the same for the different gases at the same pump current. Above $\simeq 10^{-7}$ Torr for nitrogen, $I \propto P$. Between 10^{-9} and 10^{-8} Torr, there is a transition region. No bistable operation was found, i.e., the pump current at a given pressure was always the same whether one was increasing or decreasing the pressure. Below the transition region, $I \propto P^{1.2}$.

---

*Pumping speeds are generally given as speeds at the pump flange. In this section, however, P and S are correlated to I. This should be done at the same point, i.e., inside the pump.

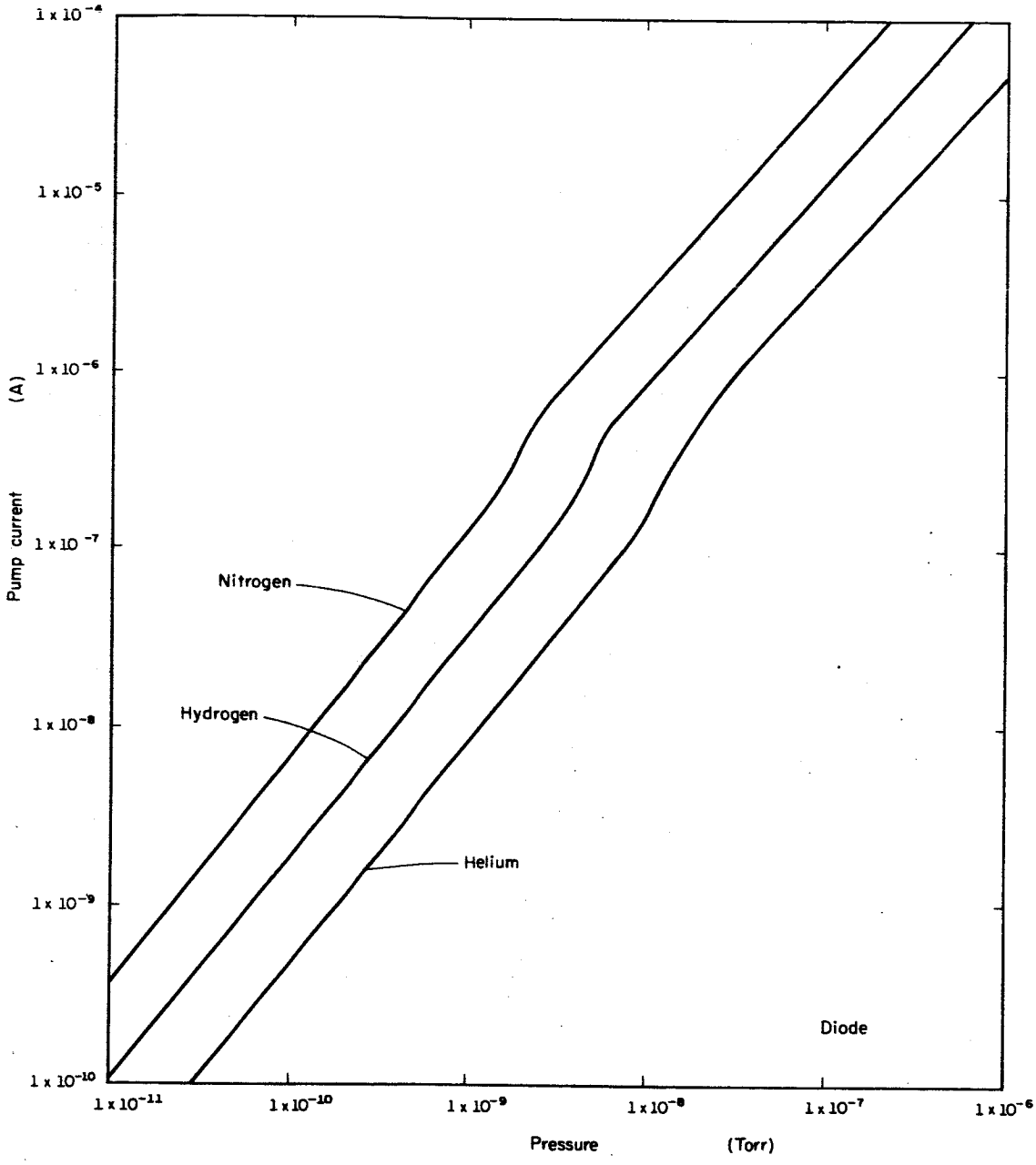

Fig. 4.2. I vs. P in the Diode Pump for the Gases Hydrogen, Helium, and Nitrogen.

The pump was found to go out regularly when the pump current dropped below 2×10^{-11} A. This current corresponds to a nitrogen pressure of $\simeq 1\times10^{-12}$ Torr. To reach this condition, the valve to the diffusion pump had to be opened and the gauges shut off.

For short pumping times, the number of molecules or atoms pumped per electric charge was found to be independent of pressure within the accuracy of our measurements. The values for hydrogen, helium, and nitrogen are, respectively, 0.5, 0.6, and 0.2. Over a period of one day, these values decreased significantly at pressures above 10^{-8} Torr for all gases investigated, the decrease being especially high for helium. One exception is the case of hydrogen in the triode pump above 10^{-7} Torr. Here, the pumping speed increased with time. The same effect has been ovserved in the diode pump at pressures of $\sim10^{-5}$ Torr after pumping for two days.[11] It is believed that this results from a cracking of the titanium cathode after prolonged hydrogen pumping which increases the permeability of the metal for the gas.

Figure 4.3 shows pumping speed, S, and discharge intensity, I/P, plotted versus pressure in the diode pump for different gases and pumping times T = 0 and T = 1 day. The dependence of I/P on pressure for nitrogen is practically the same as reported by Rutherford[1] for the same magnetic field and geometry. Our absolute values of I/P are larger by a factor of 2.7 due to the larger voltage (7.2 kV instead of 3 kV). Figure 4.4 shows the pumping speeds for the triode for similar conditions.

---

[11] S. L. Rutherford and R. L. Jepsen, Rev. Sci. Instr. 32, 1144 (1961).

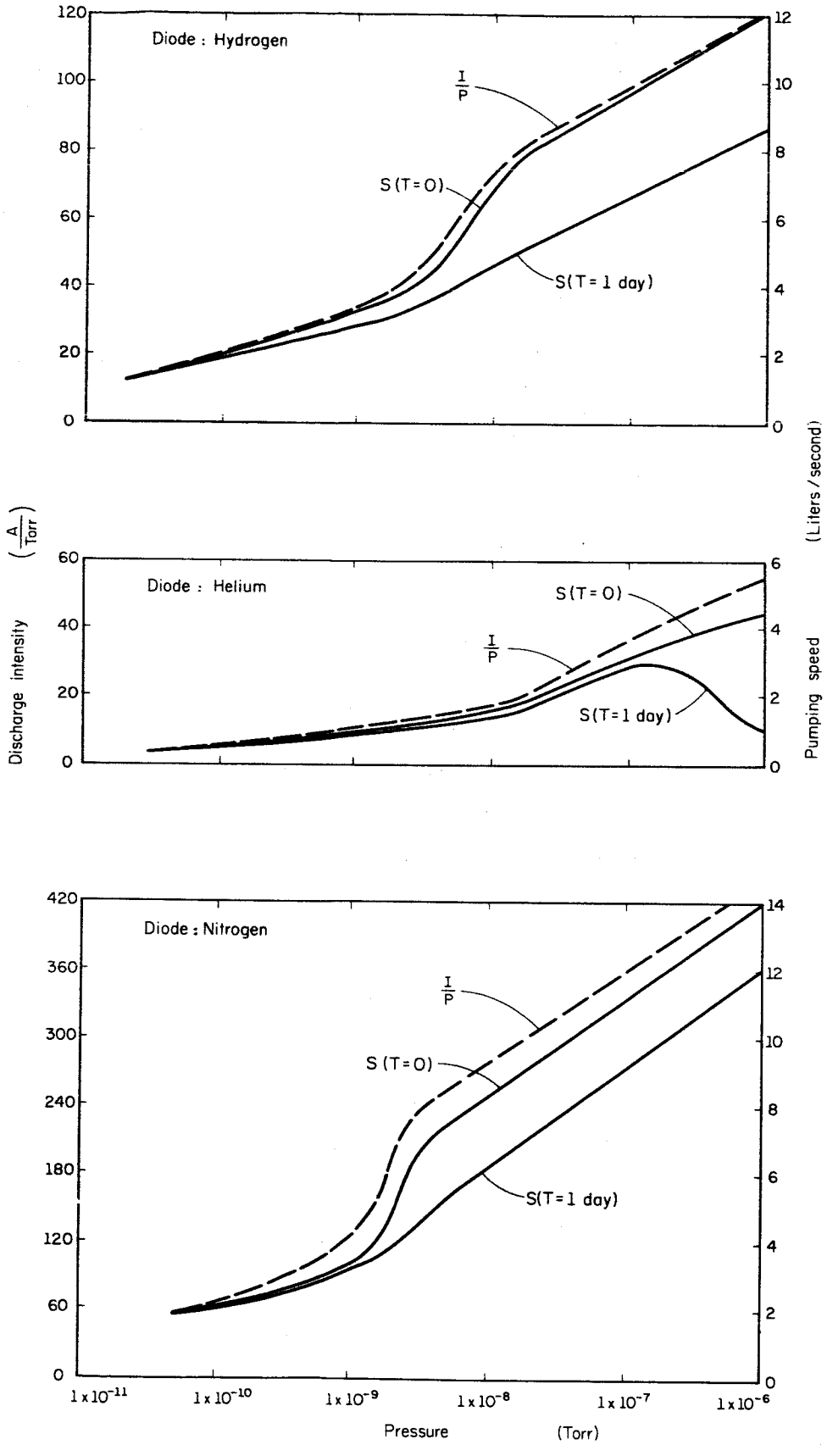

Fig. 4.3. Pumping Speed S and Discharge Intensity I/P vs. Pressure in the Diode Pump for a) Hydrogen, b) Helium, and c) Nitrogen.

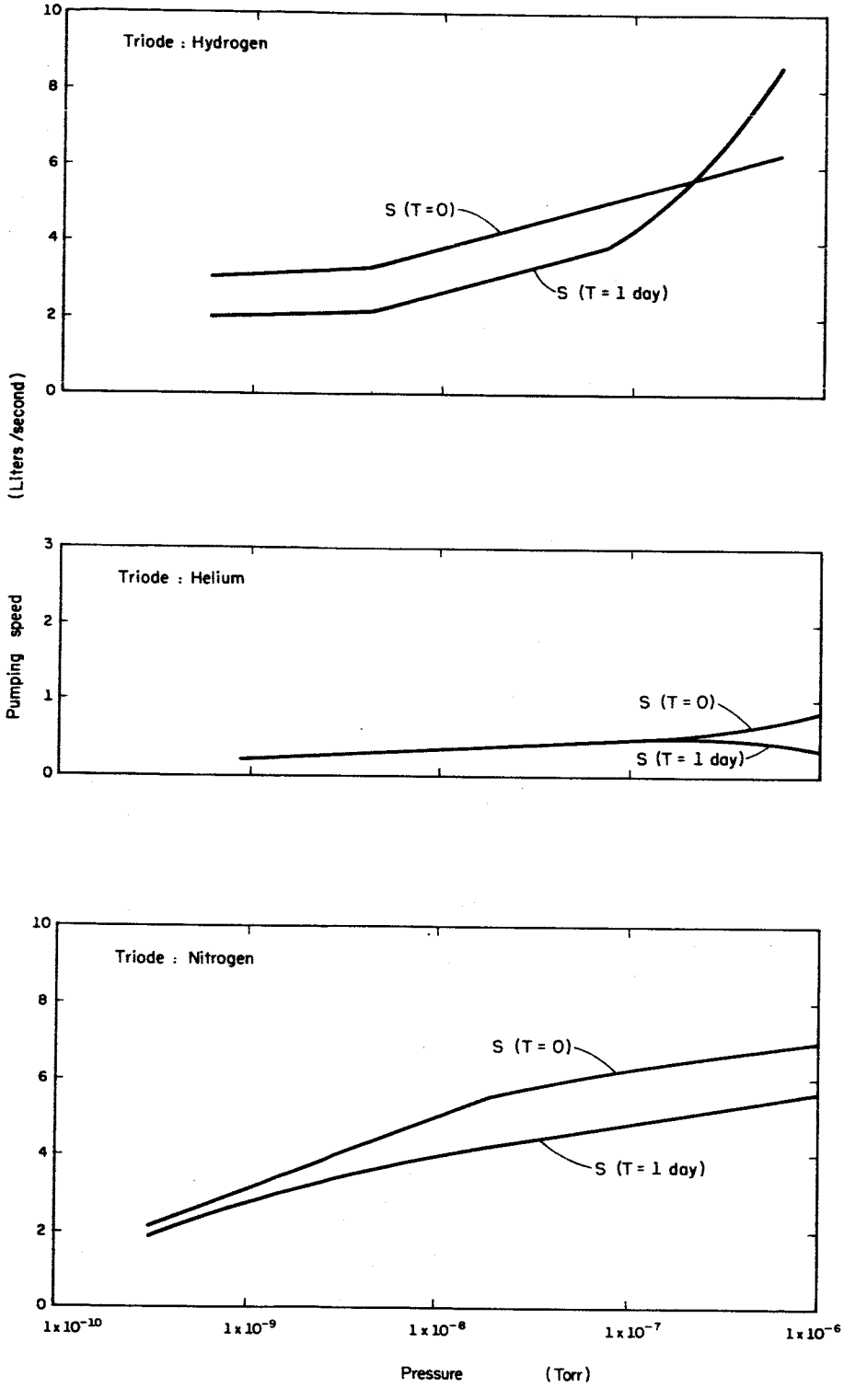

Fig. 4.4. Pumping Speed S vs. Pressure in the Triode Pump for a) Hydrogen, b) Helium, and c) Nitrogen.

4.4 Discussion

In getter-ion pumps, the discharge intensity, I/P, is proportional to pumping speed, S, for different gases and pressures below 10^{-6} Torr for short pumping times. In other words, the number of molecules or atoms pumped per electric charge is pressure independent.

Saturation occurs after pumping times of the order of a day at pressures above 10^{-7} Torr. This saturation is serious only in the case of noble gases. All other gases are pumped for a very long time with a pumping speed which is a large fraction of the initial speed. In the case of hydrogen in the triode, the pumping speed increased with time for many days at pressures above 10^{-7} Torr.

No significant difference in pumping speed or saturation time was found between diode and triode.

5. BAKEOUT PROCEDURES FOR SMALL GLASS ULTRAHIGH VACUUM SYSTEMS. REDUCTION OF O_2 TO CO CONVERSION.

In a recent communication by J. H. Singleton and W. J. Lange[1] it was reported that the main residual gas in their Pyrex glass systems of about two liters volume was CO_2. The lowest stable pressure was $\sim 5 \times 10^{-11}$ Torr when they processed their systems in the following way: a) trap refrigerated, system baked ~10 h at 420°C; b) trap isolated from system and pumped while baked at ~250°C; c) ion gauge outgassed by electron bombardment. It was observed that the lowest pressure was about one order of magnitude higher when between stages b) and c) the system was baked once more. Diffusion pumps giving an effective pumping speed of ~0.5 ℓ/sec at the systems were used with various pumping fluids.

The performance of some very similar systems (see Fig. 5.1) has been examined in the laboratory during the past two years. They were made from Pyrex glass (Corning 7740) and had a volume of one to three liters. Usually a magnetic deflection type mass spectrometer[2] was included for partial pressure measurements. Bayard-Alpert gauges and Schuemann photocurrent suppressor gauges[3] were used for total pressure measurements. An optically dense zeolite trap filled with approximately

---

[1] J. H. Singleton and W. J. Lange, J. Vac. Sci. Technol. 2, 93 (1965).

[2] W. D. Davis and T. A. Vanderslice, Trans. AVS Vac. Symp. 7, 417 (1960).

[3] W. C. Schuemann, Rev. Sci. Instr. 34, 700 (1963).

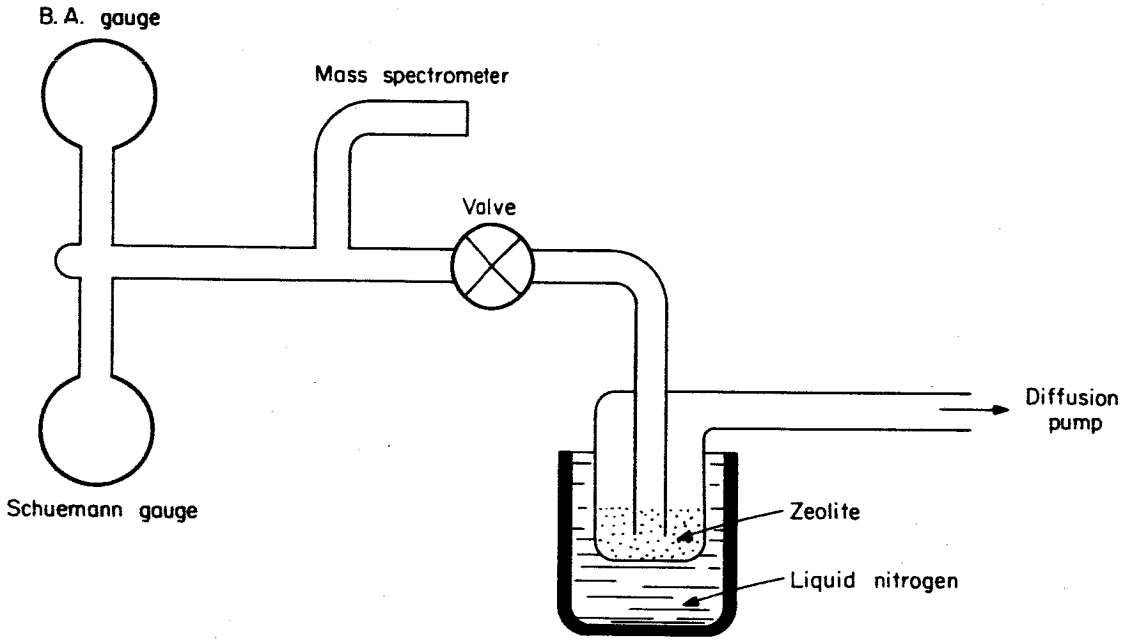

Fig. 5.1. A Schematic View of the Vacuum System.

10 g of Molecular Sieve (Linde 13 X) could be refrigerated at liquid nitrogen temperature. A one-inch valve served to isolate the trap from the system. Two-stage fractionating oil diffusion pumps (CVC GF-20) were used with Monsanto OS-124 oil; the pump was air cooled, and the pumping speed for N_2 at the system was ~0.5 ℓ/sec.

With the following procedures, pressures below 1×10^{-11} Torr were regularly obtained two to three days after exposing the system to atmospheric pressure. a) The system was pumped with a forepump to $\sim 10^{-3}$ Torr (the valve between system and diffusion pump was kept closed with the diffusion pump always running). Then the valve was opened and the system pumped for several hours with the diffusion pump. b) The trap was valved off from the system and baked at ~350°C for four hours; the glass tubing between valve and trap and the valve were kept at ~150°C to prevent oil condensation. c) The valve was opened after the trap had been refrigerated to liquid nitrogen temperature. Then the system was baked at 350°C for ~10 hours. d) Stage b) was repeated. e) The ion gauges were outgassed at 80 W for six hours. f) Stage b) was repeated. If necessary, the cycle c) to f) was repeated.

One of the systems was used for a detailed investigation of partial pressures during system processing. It was repeatedly cycled from atmospheric to very low pressure. It consisted of a Bayard-Alpert gauge WL-5966, a Schuemann photocurrent suppressor gauge of more recent design[4] with a low temperature filament, and a mass spectrometer.[2]

---

[4] W. C. Schuemann, CSL Report R-249 (March 1965).

The main residual gas during bakeout of the system and outgassing of the gauges was CO; CO_2 was always less than CO. H_2 was also present and became the major residual gas when the system was close to room temperature.

To obtain low pressures, the gauges and mass spectrometer had to be outgassed at 50 W (Bayard-Alpert), 120 W (Schuemann) with all metal parts except the filaments connected to the grid, 10 W (ion source of mass spectrometer). Pressures of less than 1×10^{-11} Torr were obtained two days after starting the processing. After three days, the system reached its final pressure in the low 10^{-12} Torr range as measured with the Schuemann gauge. These pressures are in nitrogen equivalent. A further decrease could be observed when the gauges were shut off. Table I gives the dominant partial pressures observed under different conditions. These pressures are actual pressures taking into account the sensitivity of the mass spectrometer for the different gases. Calibrations were made with the Bayard-Alpert gauge in the 10^{-9} Torr region.[5] From a paper by Davis[6] it is known that this mass spectrometer is linear down to the lowest pressures. Helium diffusing through the glass walls is the major component. H_2 is important, too, and very probably arises from the mass spectrometer source region as can be seen from an H_2 increase if the emission current is increased. Davis[6] reports a partial pressure of H_2

---

[5] P. A. Redhead, E. V. Kornelsen, and J. P. Hobson, Adv. Electron. Electron Phys. 17, 323 (1962).

[6] W. D. Davis, Trans. AVS Vac. Symp. 9, 363 (1962).

of 1 to 1.5×10^{-12} Torr due to outgassing of the mass spectrometer source. Our values are slightly higher because the source was operated at a higher emission current (.5 mA compared to .2 mA).

TABLE I. Partial Pressures of Dominant Gases.

Condition	H_2	He	CO
Both gauges on	5.0×10^{-12}	8.0×10^{-12}	6.0×10^{-13}
Bayard-Alpert gauge off	4.0×10^{-12}	6.2×10^{-12}	6.0×10^{-13}
Both gauges off	4.0×10^{-12}	5.3×10^{-12}	6.0×10^{-13}

The valve between system and pump was closed for eight days in an attempt to see how much gas was collected in the system. All filaments were off.

Table II gives the partial pressures after eight days: a) five minutes after turning on the mass spectrometer with the valve closed; b) five minutes and c) five hours after operating the valve. The He influx, Q, was calculated to 2.6×10^{-12} Torr ℓ/sec; from the relation $S = Q/P$ at equilibrium, the pumping speed S at $P = 5 \times 10^{-12}$ Torr was found to be $S = 0.65$ ℓ/sec. The H_2 evolution was much smaller when the mass spectrometer was off. This supports again the assumption that the heating of the mass spectrometer source by the hot filament is responsible to a large extent for the observed H_2 evolution. As one can see from a comparison of Table II with Table I, the system reached its base pressure again only a few hours after opening the valve.

TABLE II. Partial Pressures in Torr after Closing the Valve between System and Pump for Eight Days.

Condition	H_2	He	CO
(a) Valve closed, mass spectrometer on for 5 minutes	2.6×10^{-10}	6.6×10^{-7}	8.0×10^{-12}
(b) Valve opened for 5 minutes	6.0×10^{-12}	5.4×10^{-12}	8.0×10^{-12}
(c) Valve opened for 5 hours	3.4×10^{-12}	5.0×10^{-12}	6.0×10^{-13}

In another experiment, the influence of processing upon CO production under O_2 admission was investigated. Some of the earlier experiments by Schuemann, Segovia, and Alpert[7] were repeated. The main difference was the very small CO production rate observed in this experiment if the system was kept oil-free. It was found that it makes a big difference whether the valve and the glass tubing between valve and trap are kept at ~150°C or at room temperature during bakeout of the trap. In the latter case, there was apparently some oil condensation in the valve and the glass tubing. Oil cracking patterns could be seen immediately after turning on the low temperature filament in the mass spectrometer (Fig. 5.2). Only 15 minutes later, the typical oil cracking pattern had disappeared, and only H_2 and CO could be found in large quantities (Fig. 5.3).

[7] W. C. Schuemann, J. de Segovia, and D. Alpert, Trans. AVS. Vac. Symp. 10, 223 (1963).

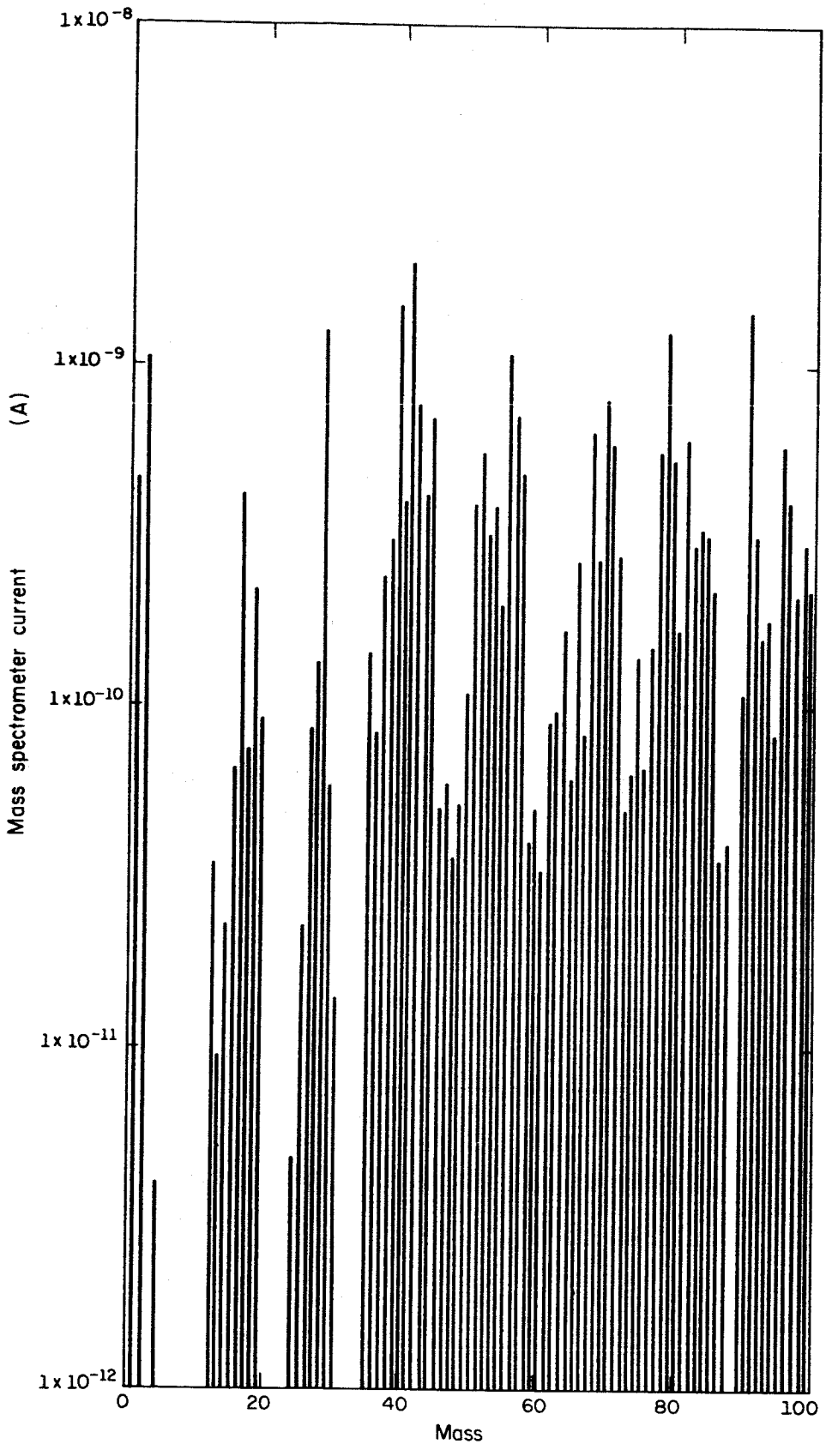

Fig. 5.2. Mass Spectrum with Characteristic Oil Cracking Pattern Taken Immediately after Turning on the Low Temperature Filament in the Mass Spectrometer.

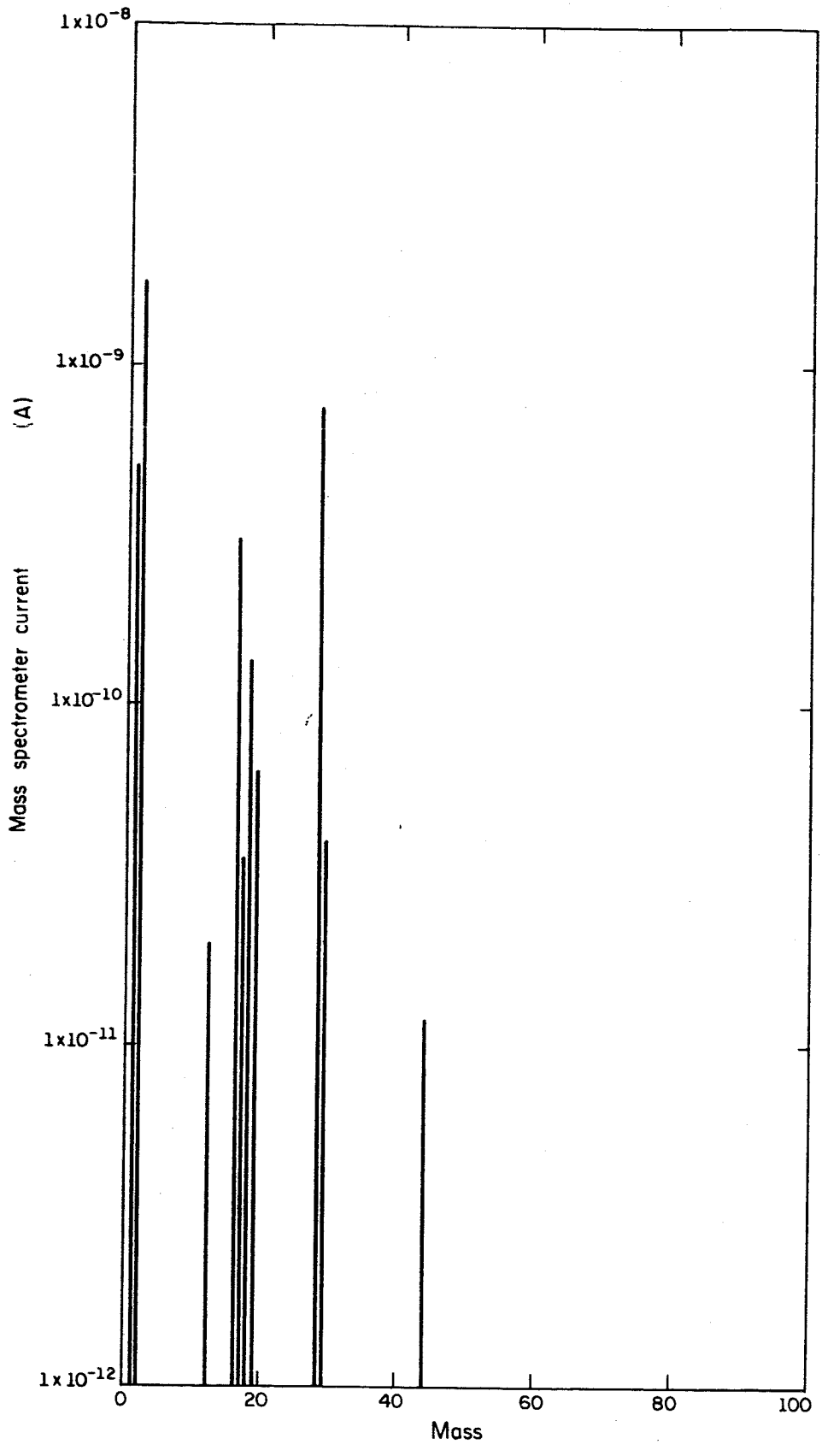

Fig. 5.3. Same Mass Spectrum as in Fig. 5.2, but with the Filament on for 20 Minutes. Note that only hydrogen and CO are left in large quantities. The oil cracking pattern has practically disappeared.

The system still reached pressures in the low 10^{-11} Torr range. In this case, however, the CO pressure reached more than 20 per-cent of the O_2 pressure under equilibrium conditions.

When the processing was done as described earlier, i.e., if valve and glass tubing between valve and trap were kept at ~150°C during bakeout of the trap, the CO pressure was only around 2 per cent of the O_2 pressure under identical conditions. One regular filament in the Bayard-Alpert gauge was replaced by an ultra-pure tungsten filament. With this filament, even lower CO production was observed. In Table III, the CO pressure in percent of O_2 pressure is given under different conditions and for times T = 5 minutes and T = 1 day after O_2 admission.

TABLE III. CO Production (in % of O_2, $P_{O_2} \approx 5\times10^{-7}$ Torr).

Emission Currents: Mass Spectrometer, 1 mA; B.A. Gauge, 10 mA

Conditions	% CO (T = 5 min)	% CO (T = 1 day)
Only mass spectrometer on, low temperature filament, no oil.	.75	.5
Only mass spectrometer on, W filament, no oil	2.0	.9
B.A. gauge on, regular filament, no oil	2.5	2.1
B.A. gauge on, ultra-pure filament, no oil	1.8	.4
B.A. gauge, regular filament, with oil	3.0	25.0

All of our observations are in agreement with results found by Becker, Becker, and Brandes[8] on "Reactions of Oxygen with Pure Tungsten and Tungsten Containing Carbon." Carbon from oil cracking products apparently diffuses into the W filaments. In an oxygen atmosphere, CO is formed on the hot tungsten filament and carbon diffuses out again.

Conclusions

1) Small glass ultrahigh vacuum systems with a zeolite trap between diffusion pump and system are capable of pressures in the low 10^{-12} Torr range (nitrogen equivalent).
2) A valve between trap and system is necessary for system processing.
3) With the technique described in this section, pressures below 10^{-11} Torr may be obtained two days after opening the system to air.
4) Bakeout temperatures of $350^{\circ}C$ are sufficient for glass systems.
5) CO production in the presence of oxygen and a hot filament can be greatly reduced by this technique.

---

[8] J. A. Becker, E. J. Becker, and R. G. Brandes, J. Appl. Phys. 32, 411 (1961).

6. TECHNIQUES

6.1 Non-Magnetic Glass-Molybdenum Feedthroughs

A guarded coaxial feedthrough has been constructed using the high-temperature glass-to-metal sealing techniques developed in this laboratory and is being tested. The feedthrough shown in Fig. 6.1 is made from molybdenum and Corning 1720 alumino-silicate glass; all materials are non-magnetic. Although testing has been insufficient to determine reliability, this feedthrough appears to be useable on ultrahigh-vacuum systems for low current measurement.

6.2 Working Alumino-Silicate Glass

The alumino-silicate glasses offer two advantages over Pyrex glass (Corning 7740) for vacuum work. They can be baked at temperatures as much as 300°C higher than Pyrex, and they offer a substantially lower helium permeation. Unfortunately these glasses are also much more difficult to fabricate. The main problems are strain fractures aggravated by a small working range, and a phenomenon known as "reboil" which causes the surface of the glass to become roughened during glassblowing. Where this glass has been used it has shown promise of allowing much lower pressures to be reached. For this reason skills necessary to fabricate apparatus of Corning 1720 glass have been developed at the Coordinated Science Laboratory.

Reboiling is the most troublesome of these problems, but it can be prevented by paying careful attention to the following details.

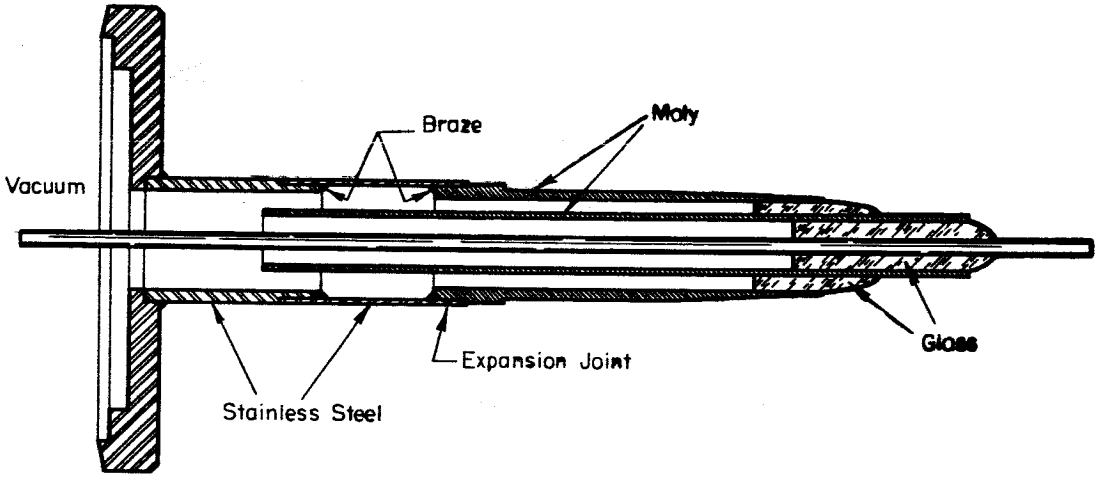

Fig. 6.1. Non-Magnetic Guarded Feedthrough.

(1) Wash and dry the glass carefully before working it.

(2) Use a final rinse with acetone to remove all fingerprints just before heating the glass.

(3) Warm the glass carefully with a bushy flame.

(4) Work in the tip of the flame, far out from the burner, using a reducing flame.

(5) Use hydrogen for fuel rather than gas.

(6) Cut with the flame rather than with the glass knife.

(7) Keep all tools, such as graphite reamer, clean and avoid touching them with the fingers.

Many glassblowers have used additives in the burner flame to retard reboiling. With an additive it is possible to use gas for fuel. Boric acid or ethyl silicate have been used. The best results in our laboratory were from using boric acid with a hydrogen flame. The hydrogen was bubbled through a simple trap filled with a solution of 8 to 10 parts boric acid to 90 parts methyl alcohol. The amount of boric acid in the flame is easily adjusted by changing the liquid level in the trap. After coating the glass with a bushy flame, oxygen could then be added to get a sharp flame and still avoid the reboiling of the glass.

The amount of boron in the flame is controlled by the depth of the liquid in the H_2 chamber of the trap. If mounted in vertical position and the H_2 pressure is zero, the valve can be opened to allow the liquid level to rise in the trap. If there is too much boron in the flame, use the H_2 pressure to force the liquid level down by opening the valve slightly. This system is shown in Fig. 6.2.

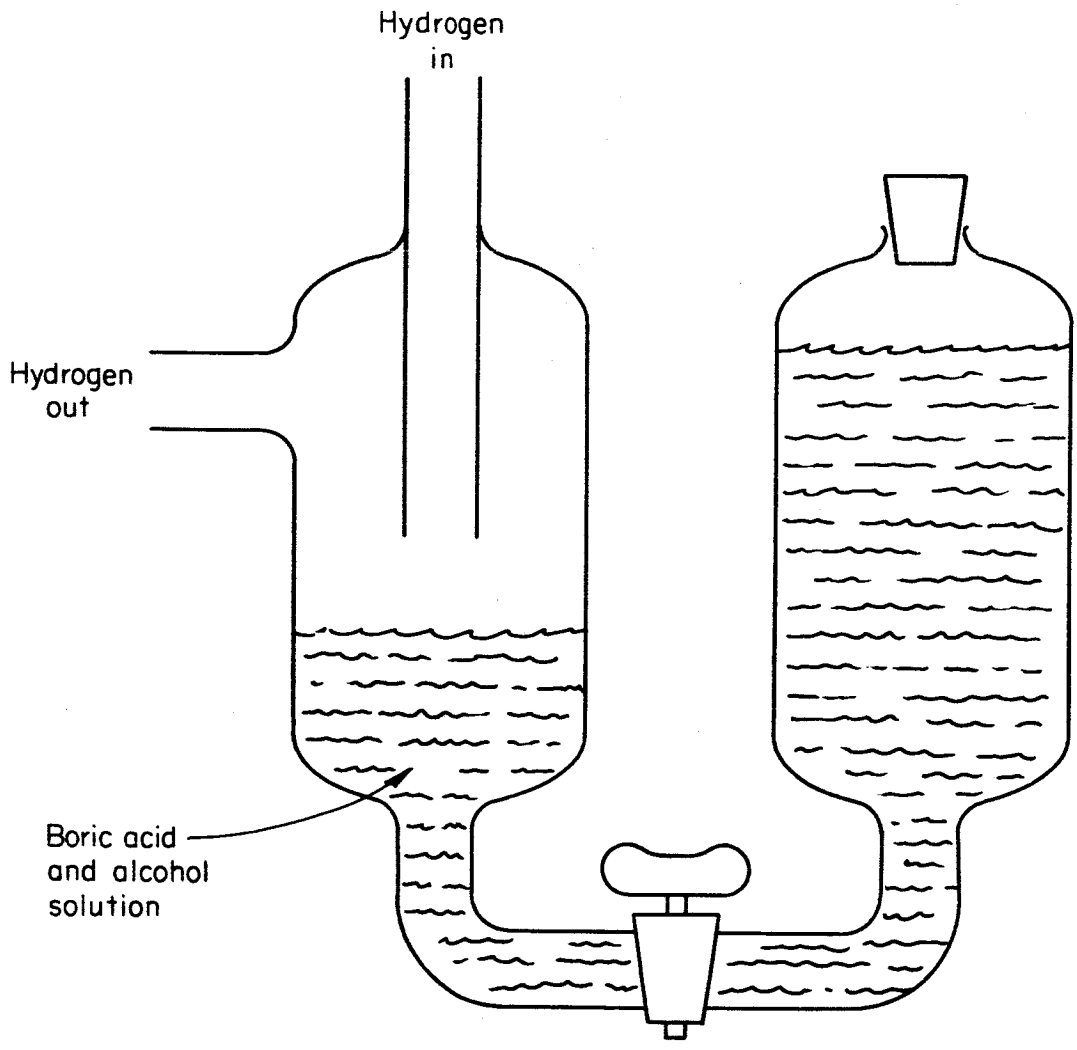

Fig. 6.2. System for Working Alumino-Silicate Glass.

Other suggestions for flame working this glass are as follows.

(1) Keep the glass adjacent to the seal hot during the glassblowing operation.

(2) Apparatus requiring several complicated seals may require doing part of the job, then oven annealing at 715°C, doing another step, annealing, etc.

(3) Molybdenum-to-glass seals require protecting the metal as much as possible; therefore, it is best to seal a thin layer of glass over the molybdenum adjacent to the glass-to-metal seal. This keeps the molybdenum out of the flame.

A diffusion pump has been constructed using these techniques, but it has not yet been tested for improved performance.

6.3 "Fiberfrax" Traps for Diffusion Pump Vapors

A ceramic paper manufactured by the Carborundum Corporation under the trade name of Fiberfrax Ceramic Fiber Paper has been used successfully in the construction of refrigerated and nonrefrigerated traps and baffles for high and ultrahigh vacuum systems.

The paper is manufactured in grades 970-A, -F, and -J and 970-AH, -FH, and -JH. It consists of approximately 51.2 per cent Al_2O_3, 47.1 per cent SiO_2, and small amounts of other materials. The grades 970-A, -F, and -J contain up to 5 per cent organic binder. The paper has a felt-like texture and a large trapping area-to-volume ratio. The Al_2O_3 and SiO_2 are stable and can be fired to high temperatures without

decomposition. Complicated baffles and trap structures can be fabricated using the paper in a simple manner. Also, the walls of pumping tubulation can be converted to effective trapping surfaces by lining them with the paper. Three baffles which can be constructed using this paper are illustrated in Figures 6.3 and 6.4. The method of construction is obvious from the figures. The ceramic paper is prepared for the baffles by firing in air at 1,000-1,200°C for from 5 to 25 minutes.

The performance of two vacuum systems using this material in the traps has been found to be quite good. One system, using a trap similar to that illustrated in Fig. 6.3 and pumped by a glass two-stage oil diffusion pump, has produced pressures of approximately 3 to 5×10^{-12} Torr with the trap cooled to liquid nitrogen temperatures. This same system produced pressures of approximately 1 to 2×10^{-11} Torr with the trap at room temperature. During the time of operation of this system, no increase in pressure was noted due to a saturation of the trapping element.

6.4 UHV Rotary Motion Feedthrough

In order to rotate the Faraday cage and tungsten target for the angular distribution measurement discussed in Section 2.3, an ultra-high vacuum rotary motion feedthrough, or vacuum crank, has been designed. Two such cranks have been constructed in the Coordinated Science Laboratory shop. A schematic of the crank is shown in Fig. 6.5.

The dotted line picture shows the position of the drive shaft and bushing assembly when the crank has been turned through 180° relative

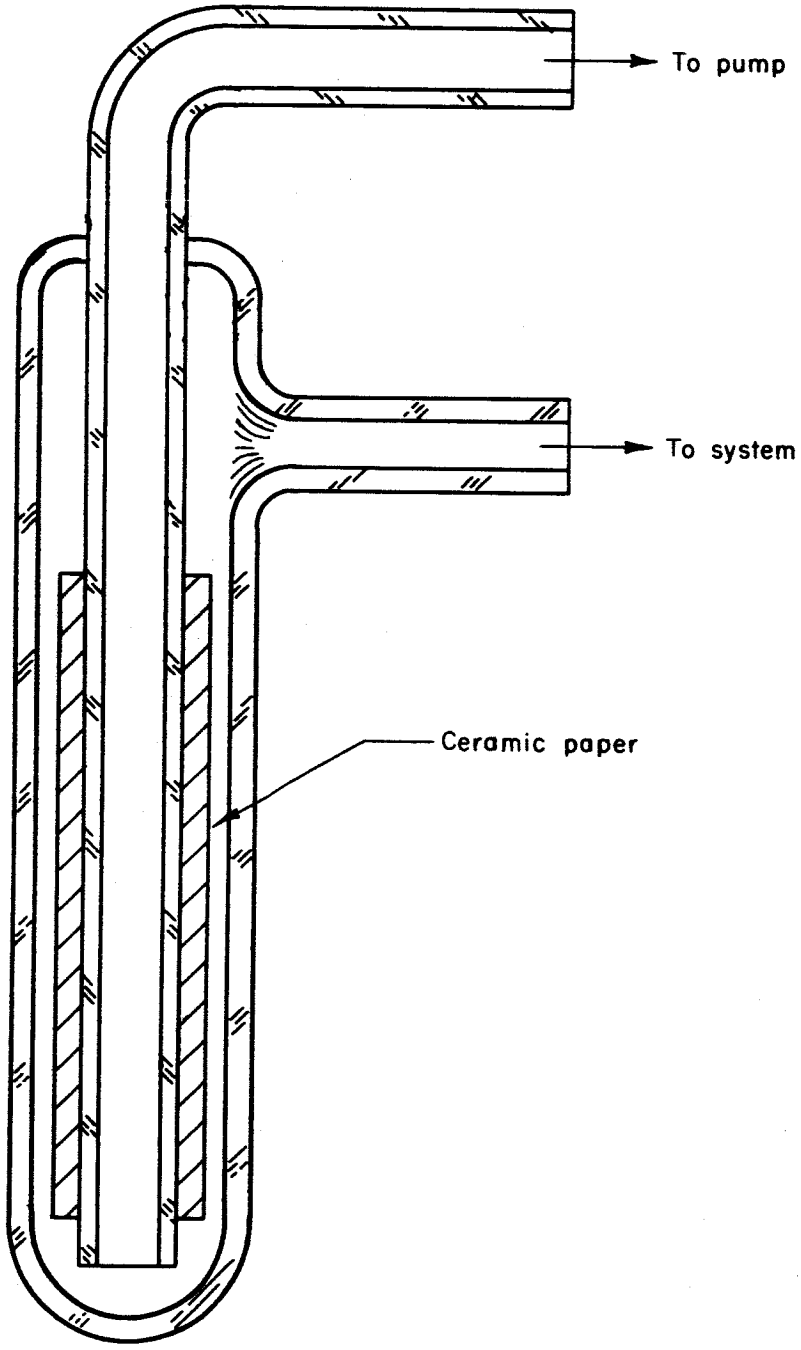

Fig. 6.3. Glass Re-entrant Trap.

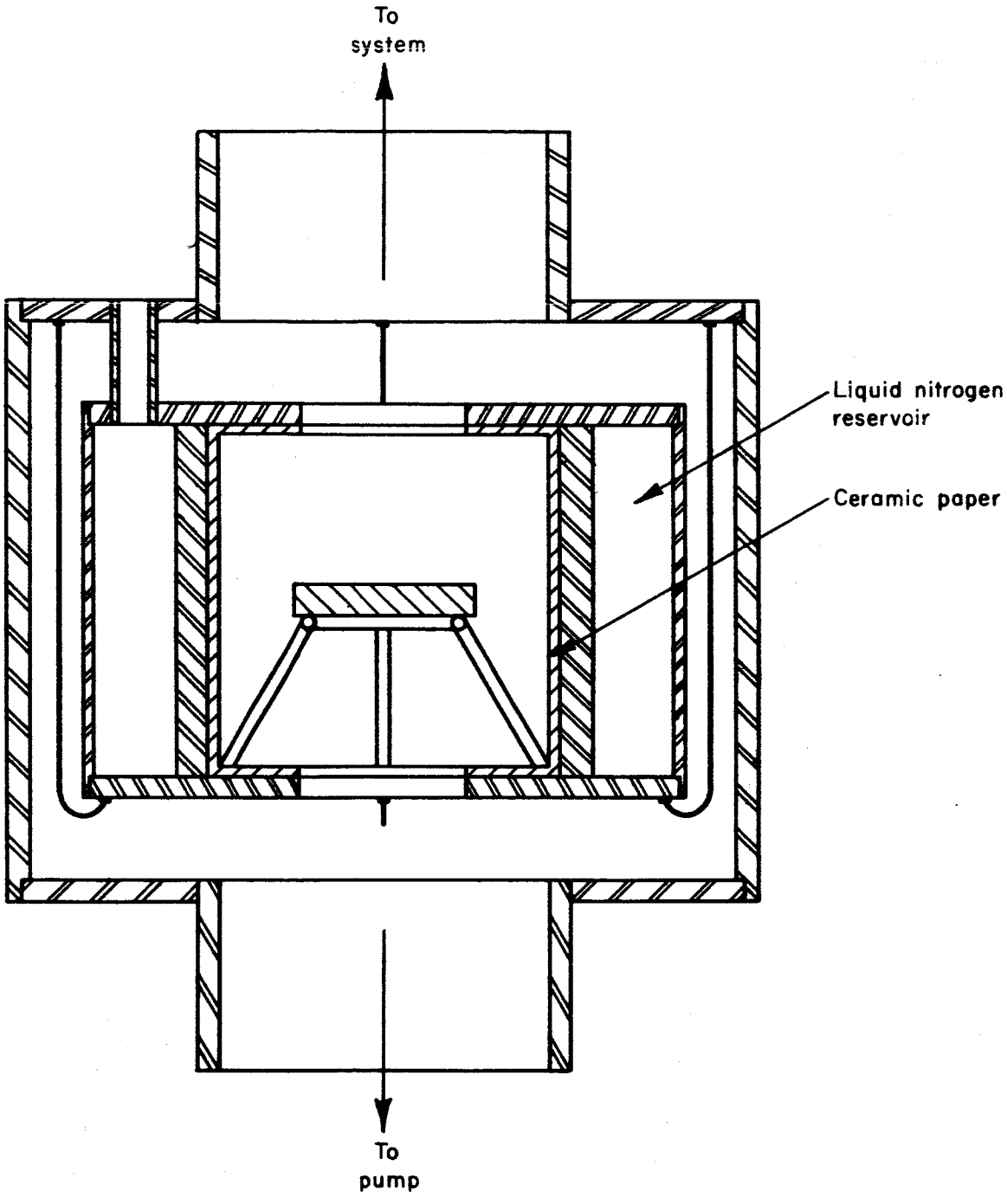

Fig. 6.4. Liquid Nitrogen-Cooled Ceramic Trap.

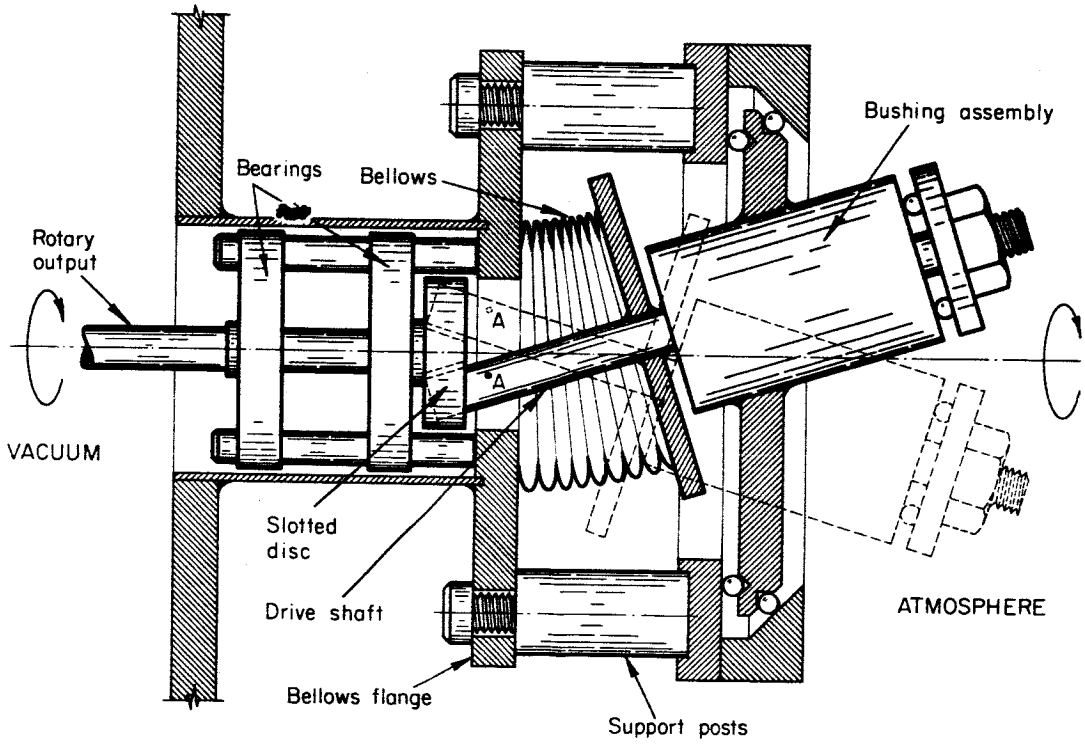

Fig. 6.5. Schematic of Rotary Motion Feedthrough Illustrating Principle of Operation.

to the solid line picture. The point A is fixed on the drive shaft and does not rotate relative to the vacuum system. The drive shaft is free to turn in the bushing assembly and drives the rotary output via a slot in the disk.

For bakeout the entire driving mechanism is slipped off by removing the bolts that hold the support posts to the bellows flange and by removing the nut on the drive shaft. A clamp has been designed to keep the bellows from collapsing due to atmospheric pressure. The crank should allow accurate positioning of counter and target, easy angular calibration, smooth rotary motion, and long bellows life.

PUBLICATIONS

A. Dallos and F. Steinrisser, "Pumping Speeds of Getter-Ion Pumps at Low Pressures" (to be published).

D. Lee, "Modified Bayard-Alpert Gauge with X-Ray Suppression," Rev. Sci. Instr. 34, 816 (1963).

W. C. Schuemann, "Ionization Vacuum Gauge with Photocurrent Suppression," Rev. Sci. Instr. 34, 700 (1963).

W. C. Schuemann, "Final Report on Photo Current Suppressor Gauge Development," Coordinated Science Laboratory Report R-249 (March 1965).

W. C Schuemann, J L. deSegovia, and D. Alpert, "Effects of Electron-Surface Interaction in Ionization Gauges," Coordinated Science Laboratory Report R-180 (August 1963).

RELATED PAPERS

A. Dallos and F. Steinrisser, "Investigations of Ion Getter Pumps at Very Low Pressures," Twenty-fifth Annual Conference on Physical Electronics, Massachusetts Institute of Technology, Cambridge, Massachusetts (March 24-26, 1965).

F. M. Propst, "High Vacuum Symposium--A Series of Three Lectures Concerning the Production and Measurement of High Vacuum," Auburn University, Auburn, Alabama (November 19-21, 1964).

F. M. Propst, "Colloquium--Auger Electron Ejection from Metal Surfaces," Auburn University, Auburn, Alabama (November 20, 1964).

F. M. Propst, "High Resolution Secondary Emission Studies," Third Annual Surface Physics Symposium, Washington State University, Pullman, Washington (May 21-22, 1965).

F. M. Propst, "Opening Remarks," U. S. Army Electronics Command Vacuum Symposium, Fort Monmouth, New Jersey (September 23, 1965).

Security Classification

DOCUMENT CONTROL DATA R&D

(Security classification of title, body of abstract and indexing annotation must be entered when the overall report is classified)

1. ORIGINATING ACTIVITY (Corporate author)

University of Illinois
Coordinated Science Laboratory
Urbana, Illinois 61801

2a. REPORT SECURITY CLASSIFICATION

Unclassified

2b. GROUP

3. REPORT TITLE

FINAL REPORT: THEORETICAL AND EXPERIMENTAL STUDIES OF THE UNDERLYING PROCESSES AND TECHNIQUES OF LOW PRESSURE MEASUREMENT.

4. DESCRIPTIVE NOTES (Type of report and inclusive dates)

5. AUTHOR(S) (Last name, first name, initial)

---

6. REPORT DATE	7a TOTAL NO. OF PAGES	7b. NO. OF REFS.
April 1966	146	60

8a. CONTRACT OR GRANT NO.

DA 28 043 AMC 00073(E)

b. PROJECT NO. 20014501B31F

c. Also National Aeronautics and Space Administration Grant

d. NsG 376

9a. ORIGINATOR'S REPORT NUMBER(S)

R-286

9b. OTHER REPORT NO(S) (Any other numbers that may be assigned this report)

10. AVAILABILITY/LIMITATION NOTICES

Distribution of this report is unlimited.

11. SUPPLEMENTARY NOTES

12. SPONSORING MILITARY ACTIVITY

Joint Services Electronics Program
thru U.S.Army Electronics Command
Ft. Monmouth, New Jersey 07703

13. ABSTRACT

The report relates work done over the past several years in the field of low pressure measurement. Particular emphasis is placed on the development of the suppressor (Schuemann) gauge developed at this laboratory. Other work with total and partial pressure gauges is reported. Related work in surface physics is also discussed in detail. New material not reported in detail in earlier reports includes discussions of 1) pumping speeds of getter-ion pumps at low pressures and 2) bakeout procedures for small glass ultrahigh vacuum systems and reduction of O_2 to CO conversion.

DD FORM 1 JAN 64 1473

Security Classification